Role of Oct4 in pXEN cell differentiation and MET process

Dissertation

zur Erlangung des akademischen Grades

Doctor rerum naturalium

Dr. rer. nat.

Im Fach Biologie

eingereicht an der Lebenswissenschaftliche Fakultät

der Humboldt-Universität zu Berlin

von

Han, Dongjun

Präsidentin der Humboldt-Universität zu Berlin

Prof. Dr. Sabine Kunst

Dekan der Lebenswissenschaftlichen

Prof. Dr. Bernhard Grimm

Gutachter/innen: 1.Prof. Dr. Andreas Kurtz

2.Prof. Dr. Ana Pombo

3.Prof. Dr. Markus Landthaler

Tag der mündlichen Prüfung: Montag, 16.12.2019

To my Family

ABSTRACT

Rat primitive extraembryonic endoderm (pXEN) cell lines appear to represent the committed precursors of the extraembryonic endoderm in the Inner cell mass (ICM) of preimplantation embryos. The pXEN cells maintained in the mesenchymal state can further differentiate to the parietal endoderm and visceral endoderm like-cells *in vitro*. In addition, pXEN cells maintain moderate levels of the ICM marker Oct4, a transcription factor that plays important roles in pluripotency, plasticity, and differentiation. However, the significance of Oct4 in pXEN cell lineage specification is unknown.

Our attempts to knockout Oct4 expression by TALEN technology did not recover colonies, suggesting a role in cell line maintenance. However, we observed that rat pXEN cells show increased Oct4 expression at higher densities, a condition that also promotes their epithelialization (MET) and visceral endodermal (VE) differentiation. In order to elucidate whether the Oct4 expression is causally involved, we modulated the Oct4 levels. Transient knockdown of Oct4 by small interfering RNA molecules tended to reduce the expression of MET/VE-associated genes (such as Dab2, Ihh, Hnf4a, Cdh1, and Zo1); conversely, the doxycycline-induced expression of a human Oct4 transgene promoted MET/VE differentiation and prevented the formation of characteristic duct structures. In the latter case, the MET was preceded by an initial elongation and increased cell motility, thus dividing the process into two stages.

Since GSK3 inhibitor and Activin A also stimulated the MET/VE phenotype, we then asked whether Oct4 acts through the Wnt/β-catenin or TGFβ pathways. IWP2, niclosamide, and 2,4 Diaminoquinazoline, which inhibit different steps of Wnt/β-catenin signaling, did not block the hOct4-induced MET and VE expression. By contrast, Repsox, an inhibitor of Alk5 (TGFBR1), prevented the hOct4-induced MET and the expression of MET and VE genes and rather stimulated the expression of parietal endoderm (PE) genes. Furthermore, the Y-27632, a non-canonical Wnt signaling pathway inhibitor, effectively prevented the MET and reduced the expression of VE-associated genes. However, the effects of the two inhibitors, while overlapping, were not identical.

Taken together, these data indicate a role for Oct4 in MET/VE differentiation via stimulation of TGFβ signaling. Further work is needed to determine how the two MET and VE differentiation processes are distinguished and related within the extraembryonic endoderm lineage.

ZUSAMMENFASSUNG

Primitive extraembryonale Endoderm (pXEN) Stam-Zelllinien der Ratte repraesentieren wahrscheinlich die festgelegten Vorläufer des extraembryonalen Endoderms in der inneren Zellmasse (ICM) von Präimplantationsembryonen. Die im mesenchymalen Zustand gehaltenen pXEN-Zellen können *in vitro* weiter zu parietalen und viszeralen Endoderm-ähnlichen Zellen differenzieren. pXEN-Zellen zusätzlich halten moderate Konzentrationen des ICM-Markers Oct4 aufrecht, einem Transkriptionsfaktor, der eine wichtige Rolle bei der Pluripotenz, Plastizität und Differenzierung spielt. Die Bedeutung von Oct4 in pXEN-Zellen ist jedoch unbekannt.

Wir konnten in Versuchen, die Expression von Oct4 durch die TALEN-Technologie auszuschalten, keine entsprechenden Zell-Kolonien gewinnen, was auf eine Rolle bei der Aufrechterhaltung der pXEN-Zelllinien hindeutet. Bei höheren Zelldichten beobachteten wir jedoch eine erhöhte Oct4-Expression und gleichzeitig eine Tendenz zu Epithelialisierung (MET) und viszeral endodermaler (VE) Differenzierung. Um zu klären, ob die Oct4-Expression kausal beteiligt ist, modulierten wir die Oct4-Konzentration. Transienter Knockdown von Oct4 durch kleine interferierende RNA-Moleküle reduzierte tendenziell die Expression von MET / VE-assoziierten Genen (wie Dab2, Ihh, Hnf4a, Cdh1 und Zo1); umgekehrt förderte die Doxycycline-induzierte Expression eines menschlichen Oct4-Transgens die MET / VE-Differenzierung und verhinderte die Bildung charakteristischer Gang-Strukturen. Im letzteren Fall ging dem MET eine anfängliche Zell-Verlängerung und eine erhöhte Zellmotilität voraus, wodurch der Prozess in zwei Stufen unterteilt wurde.

Da ein GSK3-Inhibitor und Activin A auch den MET / VE-Phänotyp stimulierten, fragten wir uns, ob Oct4 über die Wnt/β-Catenin oder TGFβ Signalwege wirkt. IWP2, Niclosamid und 2,4 Diaminoquinazoline, die verschiedene Schritte der Wnt/β-Catenin Signalgebung hemmen, blockierten die hOct4-induzierte MET- und VE-Expression nicht. Im Gegensatz dazu verhinderte Repsox, ein Inhibitor von Alk5 (TGFBR1), das hOct4-induzierte MET und die Expression von MET- und VE-Genen und stimulierte eher die Expression von parietalen Endoderm (PE) Genen. Darüber hinaus verhinderte der nicht-kanonische Wnt Signalweg-Inhibitor Y-27632 wirksam die MET und reduzierte die Expression von VE-assoziierten Genen. Die Wirkungen der beiden Inhibitoren waren überlappend, jedoch nicht identisch.

Zusammengefasst zeigen diese Daten eine Rolle für Oct4 bei der MET / VE-Differenzierung auf, wahrscheinlich durch Stimulation eines TGFβ Signalweges. Weiterführende Experimente sind erforderlich um zu bestimmen, wie die zwei Prozesse der MET- und VE-Differenzierung innerhalb der extraembryonalen Endoderm-Linie unterschieden und in Beziehung gesetzt werden.

TABLE OF CONTENTS

1. INTRODUCTION

1.1 Early embryonic development

Early embryogenesis is a very dramatic and complex but relatively well-defined process in molecular and morphological detail, including cleavage, morula formation, and gastrulation. The early developmental process involves a tightly regulated series of gene expression, cytokine, and growth factor secretion. These events can be understood in terms of mitosis, migration, differentiation, and lineage specification. And rodents are the most widely used vertebrate species, particularly mice and rats, for understanding the development of the mammalian embryo due to their availability, size, low cost, ease of handling, fast reproduction rate (~3 weeks), and relatively short lifespan (~2-3 years).

1.1.1 Fertilization

Fertilization is the very first and crucial biological step for the birth of a new organism, occurs in the ampulla of the oviduct, and involves a sequence of events (Figure 1). Prior to fertilization, matured mammalian oocytes are arrested at the metaphase of meiosis II.

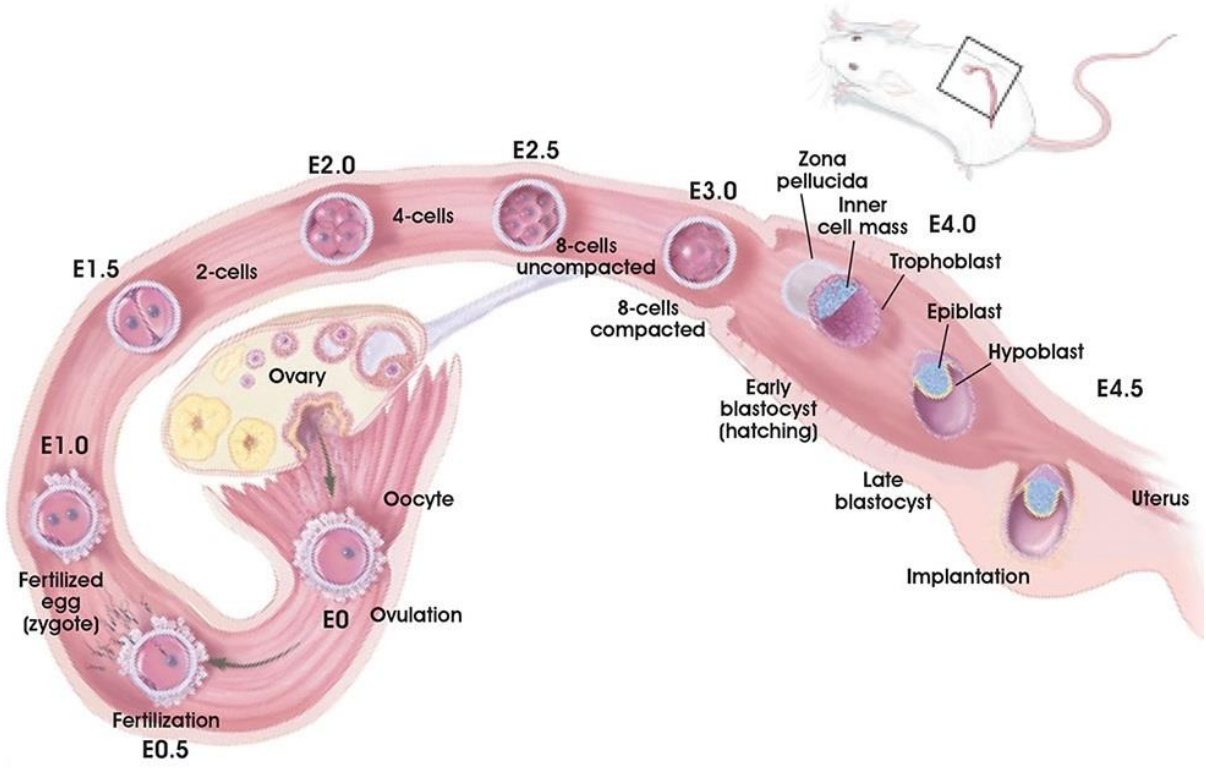

Figure 1: Schematic illustration of early mouse embryo development (Terese Winslow LLC, 2001).

The sperm (spermatozoa fusion) provides a stimulus and reactivates the oocyte's developmental program. Each gamete from a male (sperm) and female (oocyte or egg) meet and fuse to initiate embryonic development. In most species, the development of an organism begins when the fertilizing sperm induces an elevation in the intracellular free Ca^{2+} concentration of the oocyte (Jones et al., 1998). The cell cycle resumption-so called 'egg activation'-is mediated by the phosphoinositide cascade. The fertilizing sperm causes the hydrolysis of PIP2 (Phosphatidylinositol 4, 5-bisphosphate). The sperm-derived factor, Phospholipase C-zeta (PLCζ), is considered the responsible activator during the phosphoinositide cascade (Nomikos et al., 2005). PLCζ cleaves PIP2 to IP3 (1, 4, 5-trisphosphate), and DAG (Diacylglycerol). The generated IP3 binds its receptor and leads to the release of Ca^{2+} from the smooth endoplasmic reticulum of the oocyte. In response to this Ca^{2+} oscillation, the fertilized oocyte completes meiosis and initiates the process of further embryogenesis.

1.1.2 Cleavage and Morula formation

Approximately 24 hours after fertilization, male and female gametes fuse to form a zygote. It begins with the first division step, referred to as cleavage, a series of spatial and temporal mitotic cell divisions. These early divisions produce separate cells (or cleavage-stage cells) are called blastomeres, have the same set of chromosomes as the zygote, and retain totipotency. The primary mechanism of mitosis is highly conserved. However, cleavage is quite different from other patterns of cell division. One remarkable feature of cleavage in mammalian (and nematodes; *i.e.,* holoblastic cleavage) is its synchronies of nuclear division and cytokinesis. However, the mechanisms of mitotic synchrony during the cleavage step still remain to be elucidated. Three regulatory mechanisms have been suggested for the mitotic synchrony (reviewed by (Ogura and Sasakura, 2017)), (i) biochemical switches (Chang and Ferrell, 2013, Deneke et al., 2016), (ii) the variation of nucleo-cytoplasmic (N/C) ratio (Wang et al., 2000, Collart et al., 2013, Brauchle et al., 2003, Arata et al., 2014), (iii)

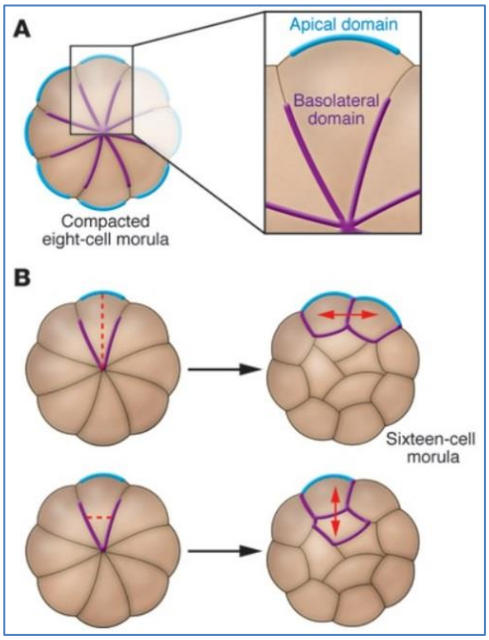

Figure 2: Polarity in the mouse preimplantation embryo. (A) At the 8 cell stage, all cells polarize along the axis of cell contact. Outward: Apical domain; Inward-facing: Basolateral domain. (B) Cell division parallel to the inside-outside axis produce two polar cells (upper); Cell division perpendicular to the inside-outside axis produce one polar (outside) and one non-polar cell (inside) (lower) (Modified from (Cockburn and Rossant, 2010)).

the combination of transcription factors (Ogura and Sasakura, 2016, Momen-Roknabadi et al., 2016). Cleavage continues rapidly and synchronous without cell cycle arrest or cell growth and ranges from the 2-cell stage to the compacted morula composed of 8-16 cells. The subsequent cleavage undergoes an increase in intercellular adhesion. Together with the relocation of microfilaments and microtubules, catenin-mediated anchoring of protein kinase C (PKC), E-Cadherin, and transmembrane calcium-dependent cell adhesion glycoprotein to the cytoskeleton accelerate the compaction process. As a result, the morula forms a compacted spheroid (Pey et al., 1998). This compaction further causes the morula to adopt a more flattened morphology and intracellular polarity. During the 8-32 cell stage embryo, the inheritance of the polarized state is influenced by the orientation of the cleavage plane of the blastomere (Figure 2). Hence, the embryo has two separate cell populations. From the 32-cell stage onward, these two cell populations have distinct cell fates (Cockburn and Rossant, 2010).

1.1.3 Blastocyst

At approximately the 32-cell stage (~E3.5 in the mouse), an outer layer surrounding the blastomere give rise to the trophectoderm (TE), while inside cells contribute to the inner cell mass (ICM) formation. ICM is a heterogeneous population, pluripotent epiblast (Epi) and primitive endoderm (PrE or hypoblast) (Figure 3). The TE formation is the first morphogenetic event and the first emerging of a fully functional epithelial cell type during the developmental process (Marikawa and Alarcon, 2012). Soon after forming a tight junction between TE cells, it becomes a structural and chemical barrier to the embryo from the outer environment. Na^+/K^+ ATPases (Watson and Barcroft, 2001) and aquaporins (Barcroft et al., 2003) in TE play an essential role in trans-epithelial fluid movement. In a process called cavitation, fluids from the external environment are transported across the TE layer and accumulate internally. As a result, blastocoel is formed. Once the blastocoel has appeared, the embryo is referred to as a blastocyst. At this point, the blastocyst is composed of three different cell types and becomes an organism with an external and internal environment rather than just a collection of cells. The rat blastocyst of day 5 is roughly spherical, ranging in size from 60 – 85 μm and surrounded by a 2.5 – 3 μm thick zona pellucida (Schlafke and Enders, 1963).

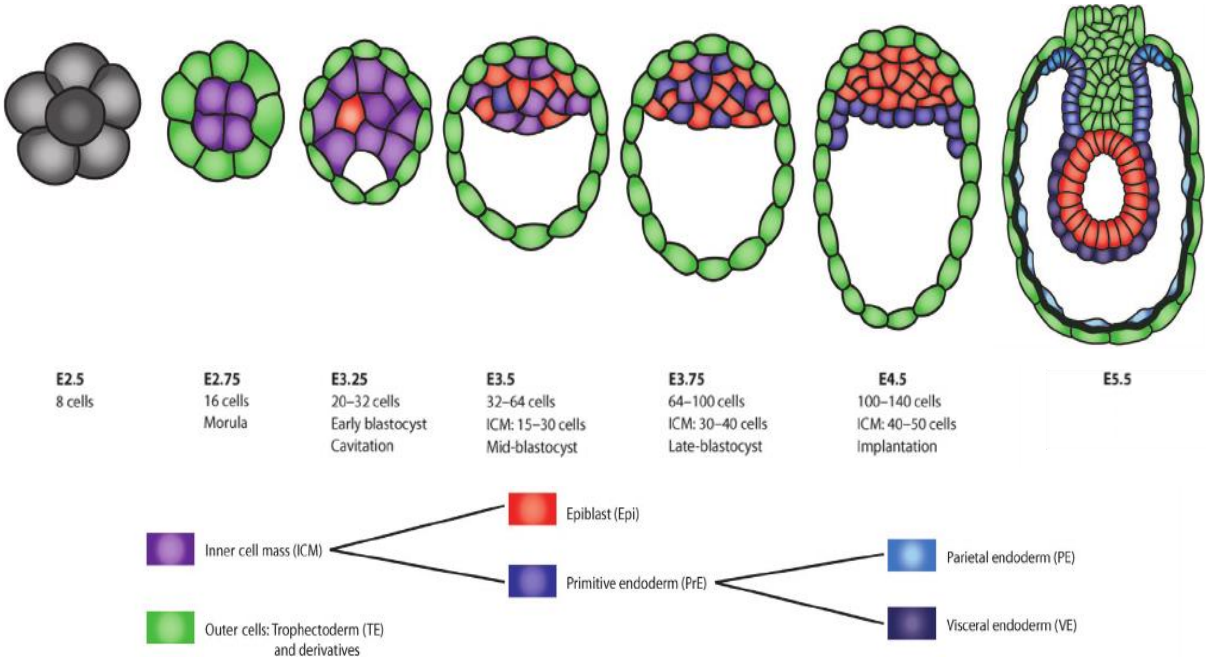

Figure 3: Overview of preimplantation stage blastocyst development and lineage segregation in mouse (Modified from (Bassalert et al., 2018)

It is widely established that differential gene expression pattern controls cell fate decisions, and many of these genes have been identified as TFs (transcription factors). Oct4 and Cdx2 have reciprocal inhibition effects on TE development (Niwa et al., 2005). By E3.5, caudal-related homeobox TF Cdx2 expression becomes restricted to the TE cells, while ICM shows a random ‘‘salt and pepper’’ gene expression pattern of homeobox TF Nanog and zinc-finger TF Gata6. A Nanog knockout experiment shed light on the early-stage cell fate decision. Frankenberg et al. demonstrated that impaired Nanog expression leads to an upregulation of PrE-related genes such as Gata4, Gata6, and Sox17 (Frankenberg et al., 2011). Indeed, Nanog and Gata6 TF network play essential roles in this Epi/PrE segregation. Nanog can bind to Gata6 promoter and repress its expression (Singh et al., 2007). Conversely, in the absence of Gata6, all ICM cells adopted an Epi lineage and lost the ability to form PrE lineage (Bessonnard et al., 2014). At E4.5, Oct4 and Gata6 genes are clearly separated to Epi and PrE, respectively (Chazaud et al., 2006) (Figure 3). After the implantation stage (~E8.5 in mouse), PrE cells start to segregate into two different cell types-parietal endoderm (PE) and visceral endoderm (VE). PE cells distally migrate along with the TE layer of blastocyst through the epithelial-mesenchymal transition (EMT) process, while VE cells covering the Epi and extraembryonic ectoderm (Perea-Gomez et al., 2007). Later, TE contributes to the placenta, and PrE gives rise to the yolk sac as well as the gut tube of the fetus (Kwon et al., 2008), and Epi contributes to the fetus.

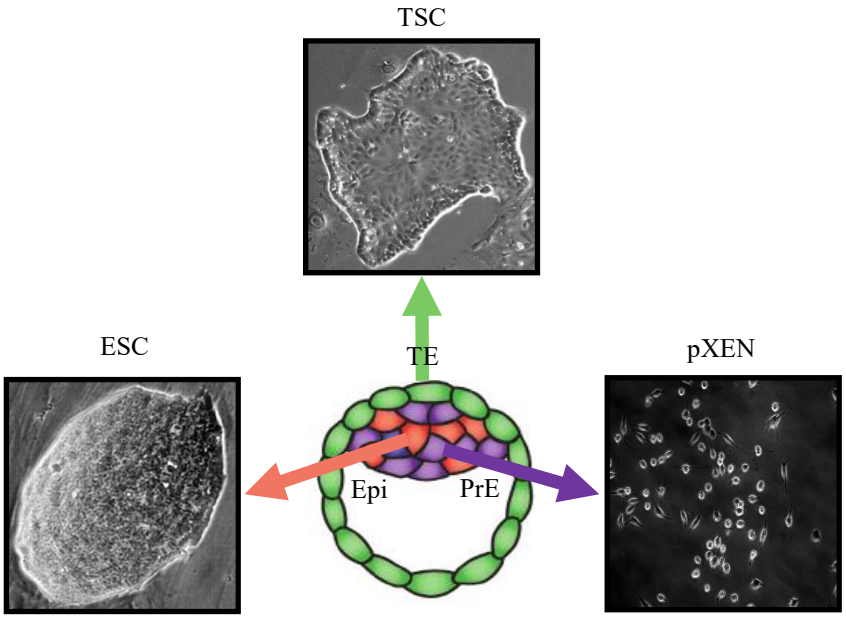

Figure 4: Isolation of stem cell lines from blastocyst. TOP, TSC (image from (Quinn et al., 2006)): Trophoblast stem cells derived from TE (Tanaka et al., 1998). *BOTTOM-LEFT*, ESC (image from (Nichols and Smith, 2011)): Embryonic stem cells derived from Epi (Evans and Kaufman, 1981). BOTTOM-RIGHT, pXEN: Primitive extraembryonic endoderm cells derived from PrE (Debeb et al., 2009).

Nowadays, each of these three different cell types-Epi, TE, and PrE-can be isolated from the blastocyst and cultured as stem cell lines-ESC, TSC, and pXENC, respectively. (Figure 4). All three cell lines provide enormous benefits for the understanding of the early developmental process and molecular mechanism.

In 1981, Evans and Kaufman reported a derivation of undifferentiated (or pluripotent) embryonic stem cell lines directly from mouse blastocysts (Evans and Kaufman, 1981). ESCs are the *in vitro* equivalent of the epiblast of the blastocyst and show self-renewal and pluripotency. Austin Smith and colleagues demonstrated that inhibition of MEK1/2 and GSK3β combined with activation of STAT3 signaling by LIF (2i/LIF) is sufficient to promote the pluripotency of ESCs from rodents (Buehr et al., 2008, Buehr and Smith, 2003). In recent years, a wide range of molecular markers has been elucidated, especially from humans. Membrane proteins or cell surface markers are most important for recognizing ESCs. Several stage-specific embryonic antigens (*i.e.,* SSEA1, 3, and 4) and a cluster of differentiation antigens (CD9, 24, 29, 59, etc.) are suggested ESC-specific markers. However, most of these markers are overlapped with carcinoma or tumor cells (SSEAs, CD96, 133, etc.) (Zhao et al., 2012). While, TFs such as Oct4, Nanog, KLF, Sox family regulate numerous gene expression directly involved with maintaining stemness and stem cell self-renewal. In addition,

intracellular signaling pathways including LIF-STAT3, BMP-SMAD, TGFβ (Activin/Nodal), and Wnt/β-catenin are considered as the core elements for pluripotency.

Meanwhile, TSCs possess the capacity to differentiate into all trophoblast subtypes (cytotrophoblast, extravillous cytotrophoblast, and syncytiotrophoblast) of the placenta. The placenta is multifunctional and essential tissue for the development of the fetus after implantation. It facilitates metabolic and gas exchange between the fetus and pregnant mother. Mouse TSCs were first derived from the blastocyst and the extraembryonic ectoderm (Tanaka et al., 1998). In contrast to ESCs, TSCs express Cdx2, Eomes, and Gata3 and can be cultured indefinitely in the presence of FGF4 and Activin (Latos and Hemberger, 2016). More recently, human TSC lines have been isolated directly from blastocyst by activation of Wnt and EGF and inhibition of HDAC, Rock, and TGFβ signaling pathway (Okae et al., 2018).

More details about the pXEN cells will be discussed in the following section.

1.2 Primitive extraembryonic endoderm cell

1.2.1 pXEN cell: New sibling of the embryonic stem cell

As previously mentioned, in 1981, ESCs are initially derived from the ICM of the mouse blastocyst. (Evans and Kaufman, 1981). More than a decade later, Thomson et al. finally isolated human ESCs from a blastocyst (Thomson et al., 1998). Both cell lines can be cultured indefinitely *in vitro* and contribute to all three germ layers: endoderm, mesoderm, and ectoderm *in vivo*. Because of their broad developmental potential, embryonic stem cells are considered as one of the most promising approaches expected to become a major source of biomedical therapy and regenerative medicine.

In recent years, two main versions of rodent extraembryonic stem cell lines have been isolated from pre-implantation stage blastocysts: Extraembryonic endoderm (XEN) cells, isolated from mouse only (Kunath et al., 2005), and pXEN cells, isolated from both mouse and rat (Debeb et al., 2009; Zhong et al., 2018). Rat pXEN cells are Oct4-expressing stem cell type cells like ESCs and show extraembryonic lineage restriction *in vivo,* but *in vitro*, pXEN cells exhibit lineage plasticity and multipotency (Lo Nigro et al., 2012). More specifically, pXEN cells maintained in the mesenchymal state can further differentiate to the PE and VE-like-cells *in vitro* (Zhong et al., 2018, Debeb et al., 2009). Superficially, these pXEN cell lines look similar to previously described mouse XEN cell lines (Kunath et al., 2005) in terms of incorporation into the ICM and show the full XEN differentiation potential. However, pXEN cells also share a similar phenotype with bone marrow-derived multipotent adult precursor cells (MAPCs) (Lo Nigro et al., 2012).

pXEN cells show a unique gene expression signature sharing some of the characteristics of ESCs, trophoblast stem cells (TSCs), and XEN cells. Both mouse XEN and rat pXEN cell lines express the pancreatic endoderm marker Gata6. However, in addition to PE markers (Lamb1 and Sparc, typical of mouse XEN cell markers), the rat pXEN cell lines more highly express VE markers such as Dab2 and Foxa2. Most importantly, rat pXENC but not mouse XENC lines also show ES-like features that expression of crucial pluripotency markers Oct4, Rex1, and SSEA1, although the other ES markers Nanog, Fgf4, and Sox2 are missing. The placental lineage markers Cdx2 and placental lactogen were absent from both rat pXEN and mouse XEN cells (Debeb et al., 2009, Kunath et al., 2005). In addition to that, rat pXEN cells exhibit cytokine LIF-dependency.

1.3 Oct4: A master regulator of pluripotency

The Oct4 is known as a critical player in lineage specification during the developmental process. The Oct4 belongs to a family of DNA-binding POU domain which was discovered in 1990 (Okamoto et al., 1990). This protein is a homeodomain-containing transcription factor that can bind to octamer sequence ATGCAAT, which was first found in the promoters of immunoglobulin genes (Falkner and Zachau, 1984). Oct4 is expressed in unfertilized oocytes, ICM of the blastocyst, primordial germ cells (Scholer et al., 1989), and naïve and primed pluripotent stem cells, including iPSCs (Takahashi and Yamanaka, 2006). According to Boyer et al., Oct4 has 623 target promoters that dominantly encode transcription factors and collaborate with other pluripotency genes such as Sox2 and Nanog to form core transcriptional regulatory circuitry in human ES cells (Boyer et al., 2005). As we described above, Oct4 (also known as Pou5f1 or Oct43/4) represents Epi state pluripotent cells but also expressed in pXEN cells.

Nowadays, Oct4 is one of the best-known transcription factors for its key role in the lineage specification and maintenance of pluripotency during early development, stem cell self-renewal, and establishment of pluripotency. Besides, it has become apparent that the Oct4 plays a pivotal role in stem cell differentiation. By virtue of its versatility, encompass *in vivo* and *in vitro*, the Oct4 is a well-studied transcription factor in this context. The major discoveries regarding the functions of Oct4 are as follows:

1.3.1 Lineage specification

Cell fate during development is a tightly regulated process dependent upon the coordination of multiple signaling pathways, molecular switches, and gene transcriptional responses. Oct4 has been denoted to be a key transcription factor controlling early embryo development.

In 1998, Nichols et al. addressed that Oct4 is required for establishing the ICM. The Oct4-deficient embryos are arrested around E4.5 or committed to the extraembryonic trophoblast lineage in the mammalian embryo (Nichols et al., 1998). In the same context, Velkey and O'Shea found that Oct4 knockdown via RNA interference induces trophectodermal differentiation (Velkey and O'Shea, 2003). While, overexpression of Oct4 promotes primitive endodermal and mesodermal differentiation in mouse ESCs (Niwa et al., 2000). Besides, it has been shown that Oct4 is also required for the extraembryonic primitive endoderm development and acts in a cell-autonomous manner via FGF4/MAPK pathway (Frum et al., 2013). (Plachta

et al., 2011). A recent study demonstrated that Oct4 deficient human blastocysts exhibit downregulation of preimplantation ICM stage genes such as Nanog, Gata4 and Gata2 correspond to epiblast, PrE, and TE, respectively (Fogarty et al., 2017). After implantation, Oct4 also acts as a crucial organizer for proper axis formation and epithelial-mesenchymal transition (EMT) process in the post-implantation stage (Mulas et al., 2018). Lineage tracing study reveals that cells with slower Oct4 kinetics tend to be ICM lineage, while with faster Oct4 kinetics give rise to extraembryonic lineage. Taken together, Oct4 has been denoted to be a key transcription factor controlling early embryo lineage specification through gene dosage effect (Stefanovic and Puceat, 2007).

1.3.2 Pluripotency

Pluripotency refers to the ability that can form all the cell types in a body except the extraembryonic tissue, such as the yolk sac and placenta. This ability can be established through a fine-tuning of the gene expression network.

In 2006, Yamanaka and his group opened a new era of the stem cell research field. By introducing just four transcription factors (*i.e.,* Yamanaka factors; Oct4, Sox2, Klf4, and c-Myc) into somatic cells, they established induced pluripotent stem cells (iPSC) from murine fibroblast (Takahashi and Yamanaka, 2006). About a year later, Yu et al. reported generation of iPSCs from human fibroblasts, but with a different combination, three transcription factors (Oct4, Sox2, and Nanog) and Lin28 encodes a LIN28 family RNA-binding protein (Yu et al., 2007). It has been announced that the ectopic expression of Oct4 is sufficient to generate pluripotent stem cells from mouse neural stem cells (Kim et al., 2009a). After these innovative findings, many researchers were dedicated to understand the molecular mechanisms of Oct4 during the reprogramming process. Li et al. reported that Oct4 activates caspase 3 and 8 to regulate apoptotic cascades (Li et al., 2010a) and reactivates silenced pluripotency genes by cooperating with Sox2 and Klf4 during the iPSC generation process (Sridharan et al., 2009). More importantly, Oct4 and Sox2 facilitate the mesenchymal-epithelial transition (MET) process by repressing EMT mediator gene Snai1 in the earliest reprogramming phase (Li et al., 2010b).

Comprehensive epigenetic approaches include chromatin reorganization, DNA demethylation, re-activation of the silenced X chromosome, and resetting of post-translational modifications also have yielded the mechanisms of reprogramming. Notably, the treatment of somatic cells with small molecules that affect epigenetic modification, including histone methylation inhibitors, dramatically enhances the reprogramming efficiency (Huangfu et al., 2008).

Furthermore, a specific small molecule combination including valproic acid (HDAC inhibitor), tranylcypromine (H3K4 demethylation inhibitor), CHIR99021 (GSK3 inhibitor), and Repsox (TGFβ inhibitor) is sufficient to generate iPSCs from mouse fibroblasts in the presence of Oct4 (Li et al., 2011). Although the precise mechanism of reprogramming and maintaining stemness has not been fully elucidated yet, Oct4 has been proposed as an essential coordinating factor for the generation and maintenance of pluripotent stem cells.

1.3.3 Induction of differentiation

Robust and continuous Oct4 expression is widely considered a central determinant and maintenance of the pluripotent state. However, additional vital roles in lineage plasticity and differentiation have emerged (Sterneckert et al., 2012).

Paradoxically, Oct4 has also been invoked in triggering differentiation. Efe et al. showed that overexpression of the Yamanaka factor with cardiomyocyte formation condition can convert mouse embryonic fibroblast into cardiomyocytes (Efe et al., 2011). Thier et al. also demonstrated that trans-differentiation of neural stem cells from mouse fibroblast by strictly limited Oct4 expression during the initial reprogramming phase (Thier et al., 2012). Furthermore, ectopic Oct4 expression induces reactivation of hematopoietic transcription factor, results in differentiation of human fibroblasts toward blood progenitor cells (Szabo et al., 2010). A recent study also revealed that Oct4 mediates cardiac lineage differentiation by epigenetic modification in bone marrow-derived mesenchymal stem cells (MSCs) (Yannarelli et al., 2017).

The Oct4 mediated trans-differentiation of somatic cells into a different cell lineage suggested that reprogramming to the pluripotent stage may not necessary. However, relatively little is known about regulation in the context of differentiation factors that govern this “non-classical” expression. One regulatory element, which is involved in mesodermal and cardiac differentiation, has been identified and is located within Region 1 (Niwa et al., 2000, Zeineddine et al., 2006). According to recent research, Oct4 expression is stage-specifically regulated by the repressive histone marks and DNA methylation in different enhancer regions during embryonic and germ cell development (Choi et al., 2016).

Hence, identifying the role of Oct4 in different cell types can teach us about a fundamental understanding of embryonic development, lineage specification, stem cell reprogramming, and differentiation.

1.4 Wnt signaling pathway

Since the first discovery of the Wnt-1 as a proto-oncogene about three decades ago (Nusse and Varmus, 1982), the Wnt signaling pathway has emerged as a critical signaling transduction pathway controls the body axis patterning, growth control, carcinogenesis, cell migration, and cell fate specification. Wnt originates from a fusion of the name of the *wingless* gene and *integration-1* gene (Wodarz and Nusse, 1998). WNTs are highly conserved lipid-modified glycoproteins. The O-acyltransferase porcupine (Porc) is required for this lipid modification in the endoplasmic reticulum (ER) (Takada et al., 2006), and 19 genes encode WNT in the mouse and human genome (Willert et al., 2003). Wnt proteins are ~40 kDa, range in length about 350-400 amino acid, and contain many conserved cysteines (Nakatani et al., 2002). The Wnt signal triggers several intra-cellular cascades: the canonical Wnt/β-catenin pathway and the β-catenin independent non-canonical pathway further branched into several subtypes. There are at least two non-canonical pathways: The Planar cell polarity (PCP) pathway and the Wnt/Ca^{2+} pathway (Kikuchi et al., 2011). Also, Wnt pathways act in both paracrine and autocrine manner.

Oct4 is a direct target of β-catenin, especially -875/-881 upstream region of the Oct4 promoter site is vital for β-catenin/TCF-mediated transcriptional regulation. Furthermore, it has been shown that glycogen synthesis kinase 3 (GSK3) inhibitor treatment increases Oct4 expression in HepG2 cells (Li et al., 2012).

1.4.1 Canonical Wnt signaling pathway

The key feature of the canonical Wnt pathway is the stabilization, accumulation, and translocation of the cytoplasmic β-catenin protein into the nucleus. WNT1, WNT3A, and WNT8 are commonly involved in the canonical pathway (Kikuchi et al., 2011). The Wnt receptor and co-receptor signals are mainly mediated by intracellular phosphorylation. In the canonical pathway, Wnt signaling is triggered by Wnt ligands that pass signals into a cell through the seven-transmembrane spanning receptor Frizzled (7TM) (Bhanot et al., 1996) and its co-receptor, lipoprotein receptor-related protein (LRP) 5/6 (Wehrli et al., 2000). After binding the Wnt ligand to the receptor complex, GSK3 and Casein kinase 1 (CK1) mediate phosphorylation of the cytoplasmic tail of LRP 5/6 (Zeng et al., 2005). This dual phosphorylation activates LRP 6 and promotes translocation of scaffolding protein Axin-a member of β-catenin destruction complex (Axin, Adenomatous polyposis coli (APC), CK1, and GSK3)-to the receptors (Mao et al., 2001). Another cytoplasmic scaffolding phosphoprotein Disheveled (Dvl), binds to the cytoplasmic tail of the Frizzled and forms LRP 6-signalosomes,

which in turn triggers LRP 6 phosphorylation (Bilic et al., 2007). Simultaneously, Dvl then becomes a hyper-phosphorylated state on Ser/Thr residues, and its DIX and PDZ domains inhibit the activity of the GSK3 (Wallingford and Habas, 2005). GSK3 and CK1 phosphorylate the N-terminal of β-catenin, resulting in its subsequential ubiquitination mediated by E3 ubiquitin ligase, β-TrCP (beta-transducin repeat-containing protein). As a result, the β-catenin undergoes proteasomal degradation (MacDonald et al., 2009). Thus, a combination of GSK3 inactivation and dislocation of the destruction complex components (Gordon and Nusse, 2006) leads to cytoplasmic β-catenin stabilization, accumulation, and trans-localization to the nucleus. Eventually, accumulated β-catenins associated with T cell factor (TCF) (Molenaar et al., 1996) and lymphoid enhancer-binding factor (LEF) (Behrens et al., 1996) to regulate the Wnt target genes. In the absence of Wnts, β-catenin is targeted by the destruction complex and continuously degraded by proteasomes (Stamos and Weis, 2013).

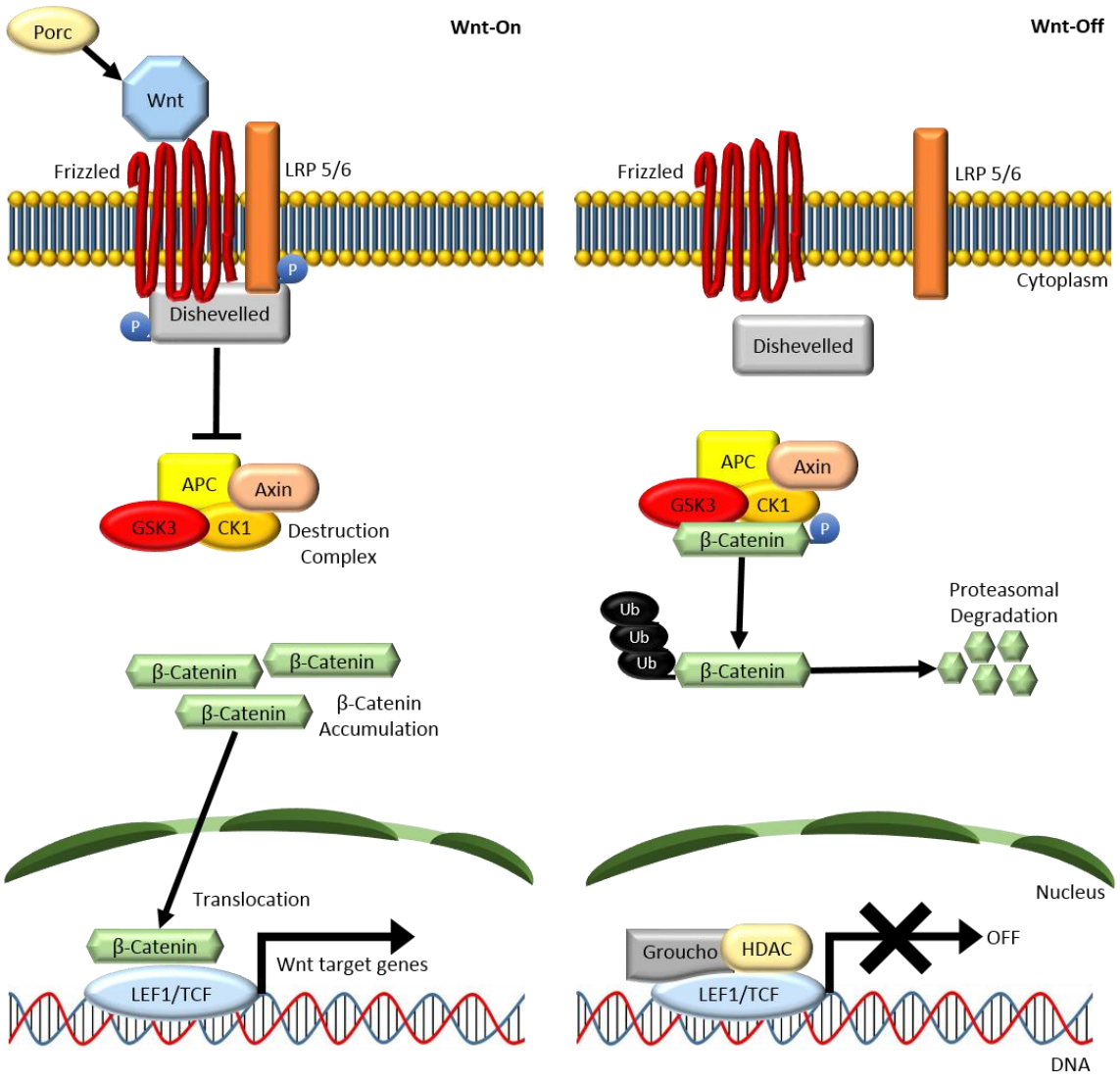

Figure 5: Schematic illustration of canonical Wnt signaling pathway.

1.4.2 Non-canonical Wnt signaling pathway

In contrast to the canonical pathway, the non-canonical pathway encompasses that β-catenin-TCF/LEF module independent signaling. WNT5a and WNT11 are well known as non-canonical signaling ligands. The non-canonical pathway also regulates crucial embryonic developmental events as well as cytoskeletal protein formation and rearrangement.

1.4.2.1 PCP pathway

PCP pathway is the best-characterized non-canonical pathway initially identified in Drosophila (Boutros et al., 1998). PCP pathway uses RAR-related orphan receptor (ROR) and protein tyrosine kinase (PTK) as co-receptors instead of LRP5/6 in the canonical pathway. Like the canonical pathway, PCP signaling ligand activates Frizzled/Dvl complex. However, the downstream of the Dvl pathway consists of small GTPases of the Rho family, Rho-associated kinase (ROCK), and the c-Jun N-terminal kinase (JNK)-type MAPK (Yang and Mlodzik, 2015). Activation of the non-canonical Wnt pathway leads to actin polymerization and microtubule stabilization responsible for the cell shape. Ultimately, it regulates cell polarity and morphogenetic movement during embryogenesis, neural tube formation as well as inner ear cell development (Kikuchi et al., 2011, Simons and Mlodzik, 2008, Qian et al., 2007).

1.4.2.2 Wnt/Ca^{2+} pathway

The non-canonical Wnt/Ca^{2+} pathway was initially described in zebrafish and *Xenopus* (Slusarski et al., 1997), also influences both the canonical and PCP pathways. Wnt/Frizzled interaction with its co-receptor Ror1/2 mediates activation of Dvl via heterotrimeric G protein. Subsequently, the heterotrimeric G protein also activates membrane-associated enzyme PLC. As a result, membrane-bound phospholipid PIP2 is hydrolyzed into IP3 and DAG. The newly formed IP3 interacts with calcium ion channels present on the ER resulting in the release of Ca^{2+}. It activates the Ca^{2+}-calmodulin-dependent protein kinase II (CamKII), calcineurin, and PKC (Kuhl et al., 2000, Sheldahl et al., 1999). Both CamKII and PKC activate nuclear transcription factors such as nuclear factor-kappa B (NFκB) and cAMP-response element-binding protein (CREB). On the other hand, calcineurin activates the nuclear factor of T cells (NFAT) via dephosphorylation. Finally, NFκB, CREB, and NFAT translocate to the nucleus and regulate gene expression, controlling cell fate and cell migration (Hogan et al., 2003, Feske et al., 2003).

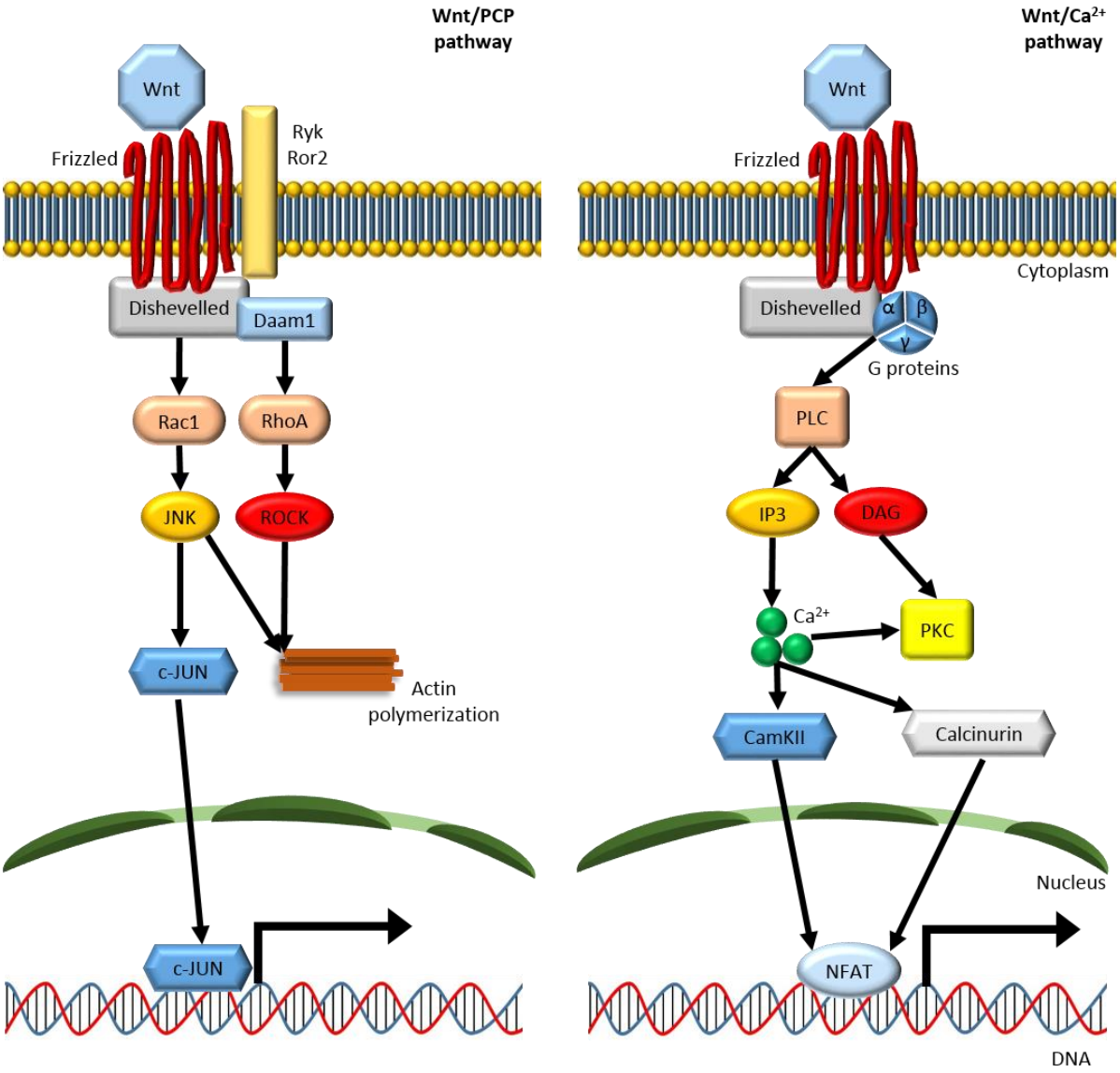

Figure 6: Schematic illustration of non-canonical Wnt signaling pathway.

1.5 TGFβ signaling pathway

The transforming growth factor β (TGFβ) superfamily signaling pathway plays versatile roles such as developmental regulation, cellular homeostasis, cell growth, apoptosis, and epithelial-mesenchymal transition (EMT) process. There are diverse TGFβ ligands, including TGFβ themselves, BMPs, Nodal/Activin, growth and differentiation factors (GDFs), and others (Pauklin and Vallier, 2015). While three different types of receptors exist, TGFβR I (or activin receptor-like kinase (ALK)), II and III (or β-glycan). In general, the signaling cascades begin with the binding of TGFβ ligands to constitutively activated TGFβR II. The TGFβR II is a Ser/Thr receptor kinase, which recruits and trans-phosphorylates the Gly/Ser domain of TGFβR I (Wrana et al., 1994). This hetero-tetrameric receptor complex, composed of two TGFβR I and TGFβR II receptors, then activates cytoplasmic signaling molecules such as Smads or TGFβ-activated kinase-1 (TAK1) by phosphorylation (Kim et al., 2009b). Especially, Smads are a control tower for the canonical pathway for a fine-tuning of TGFβ signaling cascade. Massive researches have described the molecular mechanism of TGFβ signaling, and as a result, it has been highly advocated. To date, central signaling cascades have been identified, including Smad-dependent canonical TGFβ/Nodal/Activin and BMP signaling pathways and Smad-independent non-canonical pathways such as MAPK, PI3K, p38, JNK, and RhoA/Rock pathway. Downstream of the cascades can induce or suppress the target genes by interaction with other transcriptional cofactors or direct binding to the target gene promoter region depending on the signal intensity or cell types (Vander Ark et al., 2018).

1.5.1 Nodal/Activin pathway

Nodal/Activin is a member of the TGFβ superfamily bind to TGFβR I (ALK4/7) and II (Acvr2 A/B) Ser/Thr kinase receptors. Activated TGFβR I by TGFβR II, phosphorylates receptor-regulated Smads (r-Smads)-Smad 2/3-results in the formation of the transcriptional regulator Smad complex, coSmad-Smad4 (Baker and Harland, 1997). The Smads mediated pathway is involved in axis formation, carcinogenesis, and stem cell pluripotency maintenance (Gaarenstroom and Hill, 2014).

Nodal was first reported as a lethal embryonic gene in the mouse by retroviral mutagenesis study (Conlon et al., 1991). Nodal is expressed in the epiblast and visceral endoderm, which is also considered an indispensable component in gastrulation and extraembryonic tissue differentiation (Pauklin and Vallier, 2015). The Nodal triggers anterior visceral endoderm (AVE) differentiation, which facilitates anterior-posterior axis specification results in primitive

streak formation as well as neural patterning and meso-/endoderm specification (Beddington and Robertson, 1999, Waldrip et al., 1998, Shen, 2007).

Meanwhile, Activins are disulfide-linked homo-(Activin A and B) or hetero-(Activin AB) dimeric proteins and were initially discovered as gonadal proteins that stimulate follicle-stimulating hormone secretion (Vale et al., 1986). Like Nodal, Activins are also multifunctional secreting proteins but mainly involved in the development of reproduction organ, immune cell maturation as well as lineage specification. Many studies demonstrated that Activin promotes proliferation in different cell types, including smooth muscle and Sertoli cells (Buzzard et al., 2003, Cho et al., 2003). Besides, Activin A treatment leads to morphological changes and mast cell differentiation in murine bone marrow-derived progenitor cells (Cho et al., 2003). Activin A also induces differentiation of human ESCs toward pancreatic β cells and definitive endoderm lineage (D'Amour et al., 2005, Yao et al., 2006).

Paradoxically, Activins also play critical roles in the maintenance of pluripotency and stemness. Activin A treatment is able to culture human ESCs in the undifferentiated state absence of the LIF and feeder cells (Beattie et al., 2005). About a year later, Xiao et al. addressed that Activin A induces pluripotency markers-such as Oct4 and Nanog- as well as Nodal, Wnt3, and FGF, while reduces BMP expression in human ESCs (Xiao et al., 2006).

1.5.2 BMP pathway

The first discovery of BMPs was in 1965, and the name was originated from their ability to induce bone formation or osteogenesis by auto-induction (Urist, 1965). In contrast to the Nodal/Activin signaling, the BMP pathway is mainly mediated by different sets of R-Smads (Smad1/5/8) and TAK1. Nowadays, more than 15 BMPs have been identified, and the signaling is known to play crucial roles in embryo patterning, vasculogenesis, ocular/kidney development, and EMT process (Dudley et al., 1995, McCormack et al., 2013, Yoshimatsu et al., 2013). In Xenopus, BMP2 and BMP4 regulate ventral mesodermal patterning during gastrulation (Hemmati-Brivanlou and Thomsen, 1995). And Levet et al. reported that BMP9 knockout in adult mice results in abnormal lymphatic vessel patterning and the functional deficiency (Levet et al., 2013). In the EMT context, BMP4 suppresses E-cadherin expression while increases motility in epithelial cells (McCormack et al., 2013).

How stem cells escape from pluripotent state to differentiation is an important issue in the developmental process and cell fate decision. This mechanism lays on the road in a complex

interaction among those signaling pathway networks. For instance, the interplay between Nodal/Activin signaling from the epiblast and BMP signaling from extraembryonic ectoderm induces distal visceral endoderm (DVE) differentiation (Brennan et al., 2001, Waldrip et al., 1998). Furthermore, Nodal and Wnt pathway inhibitors such as Lefty and Dickkopf-related protein 1 (Dkk1) negatively regulate primitive streak-inducing signals and contribute anterior-posterior axis formation (Mukhopadhyay et al., 2001, Perea-Gomez et al., 2002). As we mentioned above, the proper functioning of a fine-tuned signaling pathway is critical to development. Nonetheless, the molecular mechanisms that regulate the spatial-temporal expression of Nodal/Activin and BMP during the developmental process and lineage specification are poorly understood.

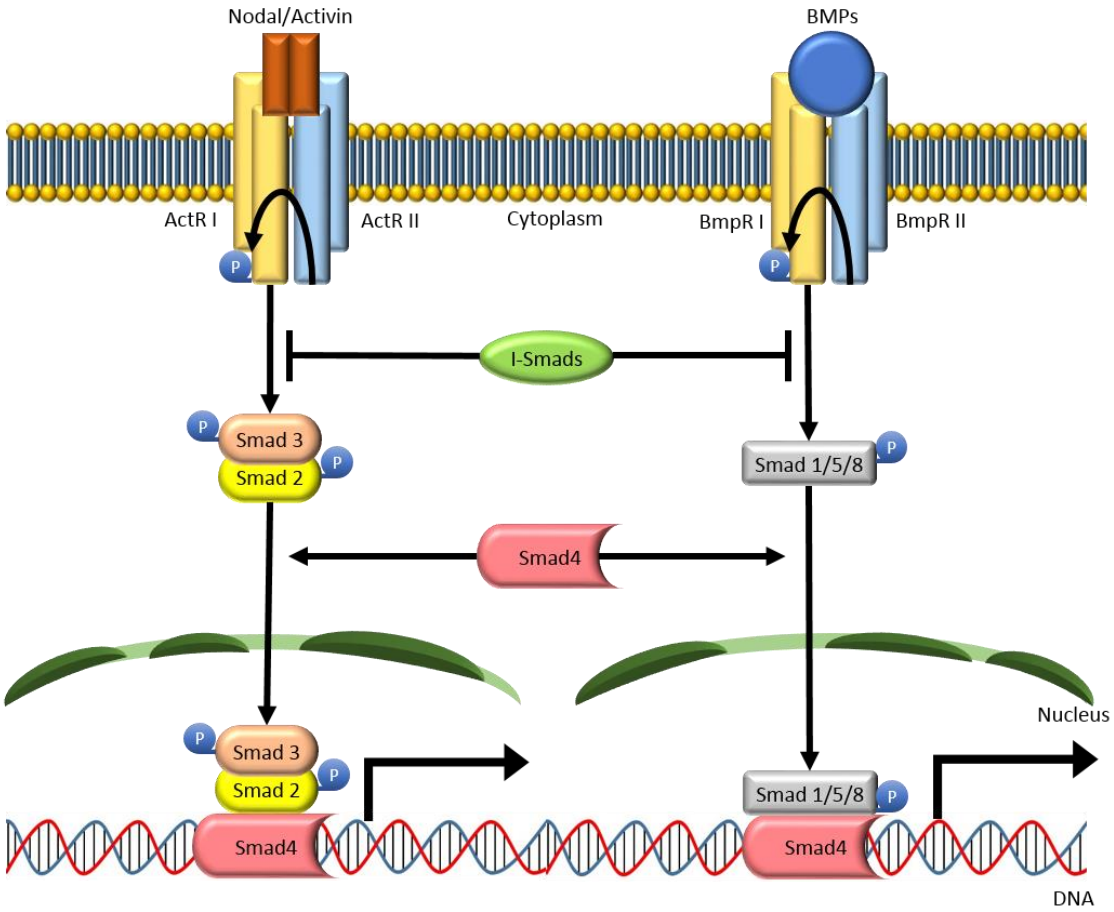

Figure 7: Schematic illustration of Nodal/Activin and BMP signaling pathway.

1.6 Preliminary result: Oct4 dynamics and differentiation in pXEN cells

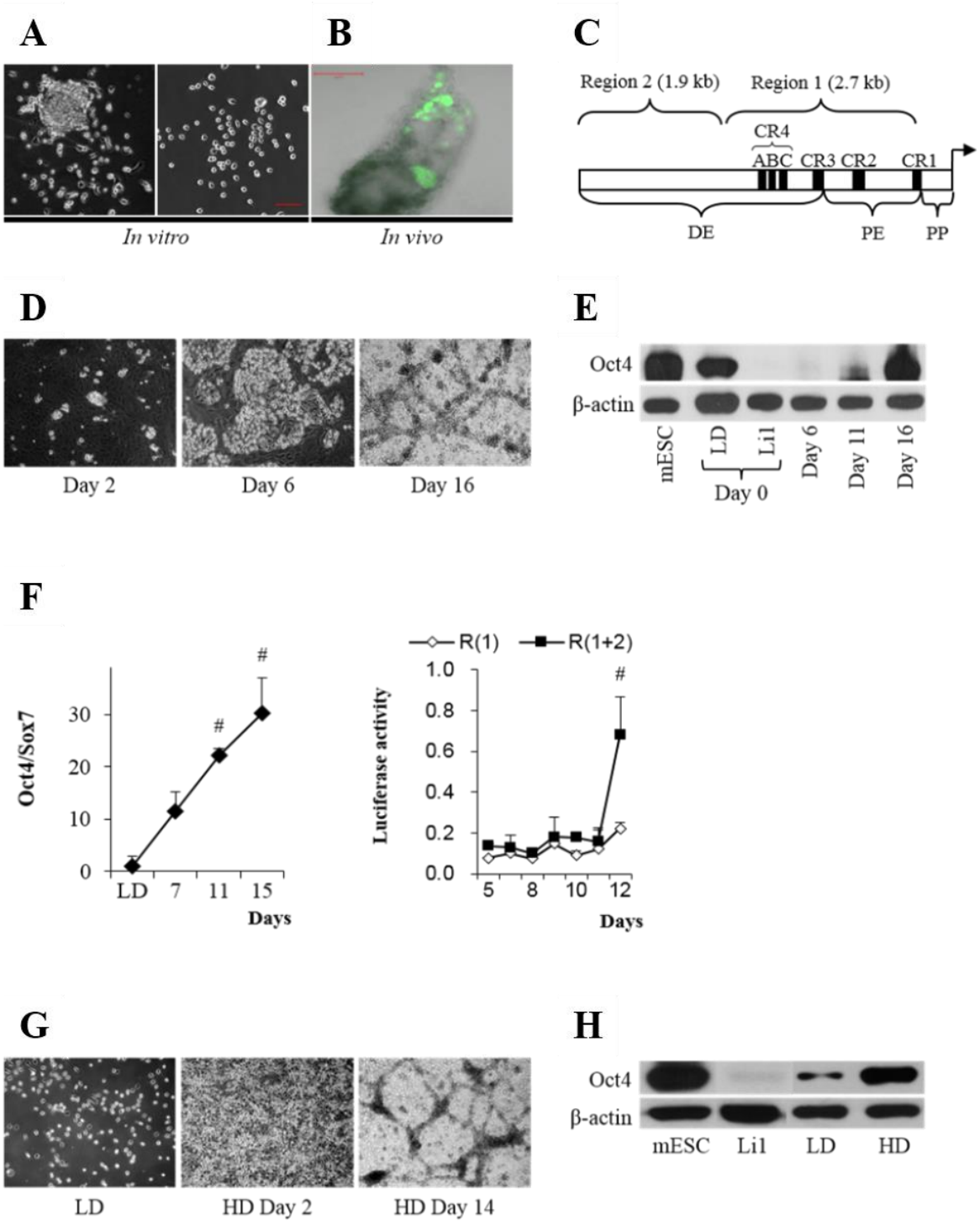

Figure 8: Characteristics of rat pXEN cells. (A) Isolation of pXEN cells from rat blastocyst. (B) Fluorescence image demonstrating visceral endoderm contributions of injected GFP-labelled rat pXEN cells *in vivo*. (~7 dpc mouse, adapted from (Debeb et al., 2009)) (C) Relation of regions 1 and 2 with previously defined regions: Region 1, ~2.7 kb upstream of PP containing CR 1-4 (conserved regions 1-4) (Nordhoff et al., 2001); Region 2, ~1.9 kb upstream of Region 1 (partial DE); A, B and C, conserved motifs within CR4 (Chew et al., 2005). PP, proximal promoter; PE, proximal enhancer; DE, distal enhancer (Yeom et al., 1996). (D) Phase-contrast image of pXEN cell colonies 2, 6, and 16 days after seeding onto mitomycin C-treated Li1. Magnification: 100x. (E) Western blot for Oct4 protein expression of pXEN cells cultured on feeder cells. mESC, Mouse ES-like cells (HM1); Li1, Rat embryonic fibroblast feeder cell. (F) *LEFT,* Time course of the ratio of Oct4/Sox7 mRNA levels (set =1 for LD). #, P<0.05 (Day 15 vs. Day 11 or Day 11 vs. Day 7). *Right,* Luciferase reporter expressions driven by Region 1 or Regions (1+2). #, P<0.05 (R(1+2) vs. R(1)). (H) Representative phase-contrast images of pXEN cells under low density (LD) or high density (HD). Magnification: 100x. (I) Western blot for Oct4 2 days after seeding the pXEN cells at LD VS. HD. Figures 8A, 8D, and 8H were performed by Dongjun Han, Figure 8E, 8F, and 8I were performed by Minjin Jeong. All preliminary experiments were conducted under the supervision of Prof. Bert Binas (former PI of Dongjun Han and Minjin Jeong) at Hanyang University, Ansan, South Korea.

When pXEN cells are maintained at low to medium density and without feeder cells, these cell lines are mesenchymal by morphology (Figure 8A) and PE-like by gene expression profile (Kunath et al., 2005, Lo Nigro et al., 2012, Zhong et al., 2018). When injected into preimplantation embryos, the observed chimerism appears to reflect the in vitro phenotypes. That is, mouse XEN and rat pXEN cells maintained in the mesenchymal state contribute efficiently to the PE but poorly to VE (Kunath et al., 2005; Lo Nigro et al., 2012). However, on feeder cells, upon stimulation with BMP4 (Bone morphogenetic protein 4), after treatment with the Wnt agonist CHIR99021, or at a higher density, they can also form VE-like cells that are epithelial by morphology (Debeb et al., 2009, Kruithof-de Julio et al., 2011, Artus et al., 2012, Paca et al., 2012, Chuykin et al., 2013, Bangs et al., 2015). Additionally, rat XEN cells pretreated with Nodal contributed efficiently to the VE (Kruithof-de Julio et al., 2011), and rat pXEN cells cultured on the feeder (resulting in a mix of epithelial and mesenchymal pXEN cells) contributed to both PE and VE (Figure 8B) (Debeb et al., 2009).

According to our preliminary results, during pXEN cells endothelial trans-differentiation, their Oct4 expression was further increased by activating a previously unknown enhancer. It has not yet been precisely defined but is located within the 1.9-kb "Region 2" that ends ~2.5 kb upstream of the transcription start site of the Oct4 gene (Figure 8C). We also studied the evolution of Oct4 gene expression when culturing the pXEN cells on the feeder. When starting with low density, the pXEN cells first formed flat epithelial colonies, which were self-limiting in size. Besides, the cells eventually piled up on the epithelial colony and then also resolved

into chord/duct-like structures (Figure 8D *RIGHT*). While it is known that the epithelial cells (unlike the round, undifferentiated pXEN cells located on the colony fringes) do not express Oct4 (Debeb et al., 2009), we detected an increased Oct4 expression in aging colonies, *i.e.,* after cells started piling up on top of the epithelium (Figure 8E). This increase was not due to simply an increasing number of undifferentiated pXEN cells relative to the number of feeder cells, as indicated by a growing ratio of the Oct4 mRNA to the pXEN cell marker Sox7 mRNA (Figure 8F *LEFT*) and activation of the Region 2 enhancer (Figure 8F *RIGHT*).

We then wondered whether the feeder cells were necessary for inducing this phenomenon. To investigate this hypothesis, we seeded the pXEN cells at a "High density (HD)" which far exceeded the maintenance density. In this condition, cells in the deeper layers tended to adopt an epithelial morphology, but round cells were also abundant (Figure 8G). Simultaneously, we observed a parallel increased production of Oct4 protein that approached the level seen in ES cells (Figure 8H). It is thus clear that the novel differentiation-associated Oct4 gene expression was not related to the previously described (Debeb et al., 2009) extraembryonic endodermal differentiation of the early colony stage. Instead, the late emergence of duct-like structures showed a temporal correlation with Oct4.

Over the past several years, diverse roles and novel molecular mechanisms of Oct4 in different contexts are revealed. Meanwhile, genome-wide analysis and epigenetic studies significantly expand the scope of fundamental understanding associated with the TGFβ and Wnt pathway during the developmental process and lineage specification as mentioned above. Nevertheless, the molecular mechanisms of PE/VE lineage specification and correlations to density-dependent-Oct4 expression dynamics together with Wnt and TGFβ signaling pathway in pXEN cells remain largely unknown.

1.7 Aim of the study

Recently discovered primitive extraembryonic endoderm (pXEN) cells are closely related to embryonic stem cells (ESC). And the pXEN cells are similar to the ICM-stage extraembryonic endoderm precursor and, most importantly, express Oct4.

The transcription factor Oct4 is a central regulator of pluripotency, which is the ability of certain cell types can give rise to all other cell types. However, it remains unknown which cells are affected, how Oct4 is regulated during the early lineage specifications. Therefore, it is clear that the level, location, and timing of the Oct4 expression need to be tightly controlled. Furthermore, it is indicated that at least more than one mechanism regulates Oct4 levels precisely. Eventually, an understanding of this exquisite machinery that regulates Oct4 levels is vital for expanding our knowledge about pluripotency and early differentiation.

Our preliminary results suggest that at low-density culture condition, rat pXEN cells express Oct4 but at only ~10% level compared to ESCs. However, at high-density culture, the Oct4 expression was increased to a level comparable with ESCs together with dramatic morphological changes. In summary, the pXEN cell is an ideal model for investigating the role of Oct4 in PE/VE lineage specification, EMT/MET process, and a morphogen.

This study shows that induced Oct4 in rat pXEN cells promotes visceral endodermal differentiation and the MET process while suppresses parietal endoderm gene expression. On this basis, it is argued that the role of Oct4 in pXEN cells will be beneficial for the understanding of pluripotency and stem cell plasticity. So we study the density-induced Oct4 gene expression and correlation between Oct4 and Wnt/TGFβ signaling pathway in terms of endodermal differentiation and MET of pXEN cells. Specifically, we investigate the following questions.

1. What is the identity of the cells showing increased Oct4 gene expression?

- Are they more or less differentiated than pXEN cells?

2. What is the significance of the increased Oct4 expression?

- Is Oct4 affecting differentiation, proliferation, or morphogenesis?

3. Which are the core mechanisms mediating the Oct4 dynamics

- Canonical or non-canonical TGFβ / Wnt signaling pathway or another novel model for Oct4 regulation?

2. MATERIALS

2.1 Chemicals and buffers

Table 1: List of chemicals and buffers used in this study.

Chemicals	Company	Cat. #
2,4-Diaminoquinazoline	Sigma-Aldrich	CDS001152
4′,6-diamidino-2-phenylindole (DAPI)	Dianova	SCR-038448
Agarose	Carl Roth	T 846
Ampicillin	Carl Roth	HP62
Blasticidin	Invivogen	Ant-bl-05
Bromophenol blue	AppliChem	A1120
CHIR99021	Tocris	4423
Coelenterazine	Biosynth	C-7001
Cristal violet solution	Sigma-Aldrich	HT901-8FOZ
Dimethyl sulfoxide (DMSO)	Sigma-Aldrich	D2650
D-luciferin	Sigma-Aldrich	L9504
Doxycycline	Sigma-Aldrich	D9891
Ethanol	Carl Roth	5054
Ethidium bromide (EtBr)	AppliChem	A1152,0100
Ethylenediaminetetraacetic acid (EDTA)	Carl Roth	8040
Fibronectin	Harbor Bio-Products	2008
Forskolin	Tocris	1099
Glycerol	Carl Roth	3783
Glycine	Carl Roth	3908
IWP2	STEMCELL Technologies	72122
Lenti-X Concentrator	Takara	631232
Lipofectamine RNAiMAX	Thermo Fisher	13778030
Mitomycin C	Sigma-Aldrich	M4287
Niclosamide	Cayman Chemical	10649
NP-40	Fluka	74385
Polyethylenimine (linear, MW: 40,000)	Polysciences	24765-1
Puromycin	Invivogen	Ant-pr-1
Repsox	Sigma-Aldrich	R0158
SB431542	Abcam	ab120163
Sodium chloride	Carl Roth	9265
Tris	Carl Roth	A411
TrypLE Select	Gibco	12563-029
Trypsin/EDTA (0.05%)	Gibco	25200-056
Trypsin/EDTA (0.25%)	Gibco	25300-054
Tween 20	Carl Roth	9127
Y-27632	Wako	253-00513
Activin A	Peprotech	120-05ET
BMP4	Peprotech	120-05ET

Buffers	Company	Cat. #
BD Cytofix™ fixation buffer	BD Biosciences	554655
BD Perm/Wash™ buffer	BD Biosciences	554723
NuPAGE MOPS SDS running buffer (20x)	Thermo Fisher	NP0000102
Odyssey blocking buffer	Licor	927-40000
RIPA buffer	Sigma-Aldrich	R0278
Roti® Block blocking buffer	Carl Roth	A151.2
Smart ladder	Eurogentec	MW-1700-10
DNA loading buffer	Tris-HCl (pH 7.5) 60 mM EDTA 60 mM Glycerol 60 % Bromophenol blue 1x	
Wet transfer buffer	Tris 25 mM Glycine 192 mM Methanol 20 %	
TE buffer	Tris (pH 8.0) 10 mM EDTA 1 mM	
TAE buffer	Tris-HCl 10 mM EDTA 1mM	
TBS buffer	Tris-Cl (pH 7.6) 50 mM NaCl 150 mM	
TBS-T buffer	Tris-Cl (pH 7.6) 50 mM NaCl 150 mM Tween20 0.05 %	
FACS buffer	PBS BSA 2 % EDTA 2 mM	
SDS loading buffer	Tris-HCl (pH 6.8) 100 mM SDS 4 % Glycerol 20 % EDTA 25 mM β-mercaptoethanol 2 % Bromophenol blue 0.04%	
Cell lysis buffer	PBS NP-40 0.25 %	
Luciferase reaction buffer	Glycylglycine 25 mM $MgSO_4$ 15 mM	

2.2 Consumables

Table 2: List of consumables used in this study.

Product	Company	Description
Cell culture plates/dishes	TPP/ BD Biosciences	Cell culture
Conical tubes (15, 50 mL)	BD Biosciences	General experiment
Filtertips (10, 100, 200, 1000 p)	Eppendorf	RNA work
MicroAmp™ Optical 384-Well Reaction Plate	Applied Biosystems	qRT-PCR
Microcentrifuge tubes (0.5, 1.5, 2.0 mL)	Eppendorf	General experiment
NuPAGE Bis-Tris precast gel (4-12 %)	Thermo-Fisher	Precast polyacrylamide gel
PCR tubes (0.2 mL)	Eppendorf	General PCR
Roti®-PVDF membrane	Carl Roth	Western blot membrane
Round bottom polystyrene tubes (5 mL)	BD Biosciences	FACS analysis
Serological pipettes (5, 10, 25, 50 mL)	BD Biosciences	General experiment
Syringe (0.5 mL)	BD Biosciences	Filtration
Syringe filters (0. 35, 0.45 µm)	Millipore	Filtration
Whatman blotting paper	Sigma	Western blot
Glass capillaries with filament	Narishige	Single-cell picking

2.3 Molecular biology kits

Table 3: List of molecular biology kits used in this study.

Product	Company	Cat. #
BCA protein assay kit	Pierce	23227
Lipofectamine™ RNAiMAX	Invitrogen	13778030
NucleoBond Xtra Midi	Macherey-Nagel	740410.100
NucleoSpin Gel and PCR Clean-up	Macherey-Nagel	740609.250
NucleoSpin Plasmid	Macherey-Nagel	740588.250
NucleoSpin Tissue	Macherey-Nagel	740952.250
RNeasy Mini Kit	Qiagen	74106
RT² SYBR® Green ROX™ qPCR Mastermix	Qiagen	330523
SuperScript III	Invitrogen	18080093

2.4 Primers and oligos

Table 4: List of primers and oligos used in this study.

Gene	Forward	Reverse
Adam8	CAA GTT TTC ACC CTG CAC CT	TCC TCC ACC TCA GAG CCA TT
Afp	ACC TGA CAG GGA AGA TGG TG	GCA GTG GTT GAT ACC GGA GT
ApoE	CTG GTT CGA GCC GCT AGT G	CCT GTA TCT TCT CCA TTA GGT TTG C
Cdh1	TGG AGA GAG GCC ACA TCC TG	CCG TTT GAC TGT GAT GAC GCC
Cdx2	GCG AGG ACT GGA ATG GCT AC	TCC TTG GCT CTG CGG TTC
Cited1	CAA AGA GGA CCA GAC GCG A	GTG CAG GCC TCG ACA TAG TT
Dab2	CCA CAG GAC AAC CTG CAG TC	GCC ACA GAT GTG GTA GGA CAC
Endoglin	TGC AGA AAG AGT CGG TTG TG	TCT CAG TGC CAT TTT GCT TG
Eomes	TGT TCG TGG AAG TGG TTC TG	TTG CCC TGC ATG TTA TTG TC
Fgf4	TCT ACT GCA ACG TGG GCA TC	TGG TCC GCC CGT TCT TAC
FoxA2	AGC CCC AAC AAG ATG CTG AC	TGG TTG AAG GCG TAA TGG TG
Gapdh	AAG GGC TCA TGA CCA CAG TC	GGA TGC AGG GAT GAT GTT CT
Gata6	GCC GGG AGC ACC AGT ACA	GTG ACA GTT GGC ACA GGA CAG
Hnf4α	ATT CTT CAG GAG GAG CGT GA	TGA GCC TGC AGT AAC GAC AC
hOct4	GTG AAG TGA GGG CTC CCA TA	GAA GGA TGT GGT CCG AGT GT
Ihh	GAG CTC ACC CCC ACC TAC AA	TGA CAG AGA TGG CCA GTG AG
Lamb1	ACT ACA CCA CGG GCC ACA AC	GCC CAG GTA ATT GCA GAC ACA C
Lyve1	AGG TGT CCT GAT TTG GAA CG	GCA GAC GTT GTG GAG TCT GA
Nanog	TAT CCC AGC ATC CAT TGC AG	GTC CTC CCC GAA GTT ATG GAG
Nodal	CTT CTC CAA ACC TGC TGG AC	AGT TCT GCC CAG TCA CAT CC
Ocln	GGC CTT TTG AGA GTC CAC CT	AAA GAG TAT GCC GGC TGA GA
Pdpn	CCA GCC ACT CCA CGG ACA AG	GGG TCA CTA CAG CCA AGC CAT C
Pecam1	AAC GGA AGG CTC CCT TGA TG	AAT TGG ATG GCT TGG CCT GA
Prox1	GAA CCC AGT CAT CAG CAT CAC	TCG AAG GTT CTG GTT CAC C
Pth1r	AGA GAA GGC ATC GGG AAA GT	TAC TGC CAC CAC TTC ACC TG
Rex1	TGG AGT ACA TGA CAA AGG GGA C	GCA GCC ATC AAA AGG ACA CAC
rhβ-Actin	GGA AAT CGT GCG TGA CAT TA	AGG AAG GAA GGC TGG AAG AG
rOct4	GGT GGA GGA AGC TGA CAA CAA C	GGC AAT GCT AGT GAT CTG CTG C
Snai1	CCT TGC GTC TGC ACG ACC TG	GGG AGC AGG AGA AAG GCT TC
Sox17	GGG GAC GTA AAG GTG AAA GG	TCC AGG ATT TGC CTA GCA TC
Sox2	CCA AGA CGC TCA TGA AGA AGG	CTG ATC ATG TCC CGG AGG TC
Sparc	ATT GCA AAC ATG GCA AGG TG	GCC AGT GGA CAG GGA AGA TG
T	TAC CCC AGC CTC TGG TCT GT	AAG GCT TTG GGC TGT GTC AT
Thbd	GCA GGG ACA TTT GAT GAC AG	GGA GCT GTA AAC CGA TCC AG
Vcam1	ACA GCT CCT CTC GGG AAA TG	AGC ACA TGT CAG AAC AAC GG
VE-Cad	GGC CAA CGA ATT GGA TTC TA	GTT TAC TGG CAC CAC GTC CT
Vegf3	CTC CAA CTT CTT GCG TGT CA	ACA AGG TCC TCC ATG GTC AG
Vil1	CTA AGG CTG CAC TCA AGC TG	GCT GAG CAA GTC CTG TGT GA
Vim	TCA GCT CAC CAA TGA CAA GG	GAA TGA CTG CAG GGT GCT CT
vWF	CTG CTG GAT CTC GTC TTC CTC	CTC TCC ATC GTA CCC ACC AC
Zeb1	TGG GAA AGC GTT CAA GTA CAA A	TTG GTT TAC AGA AAG CGG TTC TT
Zo1	GCG GGC TAC CTT ATT GAA TG	GTC ATG GGA GCG AAC TGA AT

Gene	Forward	Reverse (Continued)
αSM	TCC AGA GTC CAG CAC AAT ACC AG	AAT GAC CCA GAT TAT GTT TGA GAC C
β-Cat	ACT CCA GGA ATG AAG GCG TG	GAA CTG GTC AGC TCA ACC GA

Cloning	Forward	Reverse
TRE-CMV-hOct4	AAA GGA TCC GGT ACA GTG CAG GGG AAA GA	GGG CCA CAA CTC CTC ATA AAT GTA CAA AA
Sequencing	GGA TGG AGT GGG ACA GAG AA	CCA AAA GAC GGC AAT ATG GT

siRNA	Oligo 1	Oligo 2
s148663	UGAAUAUUCCCAACGAGAATT	UUCUCGUUGGGAAUAUUCAAT
s148664	GUUCGAGUGUGGUUCUGUATT	UACAGAACCACACUCGAACCA
s220720	GAGAUAUGCAAAUCGGAGATT	UCUCCGAUUUGCAUAUCUCCT

Oct4 KO	L1-DAS	R1-RR
TALEN	TTC AGA GGT GCT GGG GAT CT	TCC ACA GAA CTC GTA TGC TG
Reporter	TTC AGA GGT GCT GGG GAT CTC CCC GTG TCC CCC AGC ATA CGA GTT CT GT GGA	

2.5 Plasmids

Table 5: List of plasmids used in this study.

Product	Source	Description
FUW-tetO-hOct4	Addgene #20726 (Hockemeyer et al., 2008)	Tet-responsive human Oct4 expression
mPB transposase	From Werner. J (AG Gossen) (Cadinanos and Bradley, 2007)	PiggyBac transposase
PL-SIN-EOS-C(3+)-EiP	Addgene #21313 (Hotta et al., 2009)	Lentivirus backbone for TOP cloning
pMD2.G	Addgene #12259 gift from Didier Trono	Lentiviral packaging (VSV-G Glycoprotein)
pPB-hEF-GFP-Puro	Cloning (AG Gossen)	hEF1a driven GFP reporter (PiggyBac transposon)
pPB-hEF-mcs-Puro	From Hofsttäter. M (AG Gossen)	PiggyBac transposon backbone
pPB-hEF-tdTomato-Puro	Cloning (AG Gossen)	hEF1a driven tdTomato reporter (PiggyBac transposon)
pPB-TRE-mcs-hEF-M2rtTA-IRES-Bsd	From Werner. J (AG Gossen)	hEF1a driven tet reverse *trans*-activator (PiggyBac transposon)
psPAX2	Addgene #12260 gift from Didier Trono	Lentiviral packaging (gag/pol)
pTRE-d2EGFP	From Werner. J (AG Gossen)	Tet-responsive d2EGFP reporter
pUHC131-T6	From Reuter. C (AG Gossen)	Constitutively activated tet-responsive luciferase reporter

2.6 Enzymes

Table 6: List of enzymes used in this study.

Product	Company	Cat. #
PWO Master polymerase	Roche	03 789 403 001
T4 Quick DNA ligase	New England BioLabs	M2200S
Taq DNA polymerase	Invitrogen	10342-020
Restriction enzymes	New England BioLabs	

2.7 Antibodies

Table 7: List of antibodies used in this study.

Product	Host Clone Isotype	Company	Cat. #
Cited1	Rabbit Polyclonal IgG	Thermo-Fisher	PA1-22469
E-Cad (Cdh1)	Mouse Monoclonal IgG	BD Biosciences	610181
GSC	Goat Polyclonal IgG	R&D systems	AF4086
Oct4 (C-10)	Mouse Monoclonal IgG	Santa Cruz	SC-5279
Oct4 (N-19)	Goat Polyclonal IgG	Santa Cruz	SC-8628
Pdpn	Rabbit Polyclonal IgG	Biorbyt	Orb215007
T (Brachyury)	Goat Polyclonal igG	R&D systems	AF2085
Vcam1	Goat Polyclonal IgG	R&D systems	BBA19
vWF	Rabbit Polyclonal IgG	Abcam	ab9378
Zo-1	Rabbit Polyclonal IgG	Biorbyt	orb340146
β-Actin	Mouse Monoclonal IgG	Sigma	A5441
β-Catenin	Rabbit Monoclonal IgG	Cell signaling	9582S
IRDye® 680RD	Goat anti-Mouse IgG	Abcam	ab216776
IRDye® 800CW	Goat anti-Mouse IgG	Abcam	ab216772
Alexa Fluor™ 488	Donkey anti-Mouse IgG (H+L)	Thermo-Fisher	A21202
Alexa Fluor™ 488	Donkey anti-Goat IgG (H+L)	Thermo-Fisher	A11055
Alexa Fluor™ 488	Donkey anti-Rabbit IgG (H+L)	Thermo-Fisher	A21206
Alexa Fluor™ 647	Donkey anti-Goat IgG (H+L)	Thermo-Fisher	A21447
Alexa Fluor™ 647	Donkey anti-Rabbit IgG (H+L)	Thermo-Fisher	A31573

2.8 Cell lines

Table 8: List of cell lines used in this study.

Product	Species	Description
293T	Human	HEK (human embryonic kidney), transformed with large T antigen.
HM1	Mouse	ES-like cell line
IMR90	Human	Human iPSC line
iOX1	Rat	Doxycyclin-Inducible human Oct4 transgenic MX10 clone #1 cell line
iOX1-GFP	Rat	GFP expressing transgenic iOX1 cell line
Li1	Rat	Embryonic fibroblast cell line
MX10	Rat	Wild type pXEN cell line
MX10-tdTomato	Rat	tdTomato expressing transgenic MX10 cell line
Stbl3	*E. Coli*	Competent bacterial cell line
TOP10F	*E. Coli*	Competent bacterial cell line

2.9 Media and supplements

Table 9: List of media and supplements used in this study.

Product	Company	Cat. #
Luria-Bertani (LB) medium	Carl Roth	X964.1
B27 Supplement	Gibco	17504-044
BSA	Gibco	15260-037
Dexamethasone	Sigma-Aldrich	D2915
DMEM (High glucose)	Gibco	31966-021
DMEM (Low glucose)	Gibco	10567-014
DMEM/F12	Gibco	12634-010
EGF	PeproTech	AF-10015
FBS	Biochrom	S0115
Glutamax™	Gibco	35050-061
ITS	Gibco	41400-045
LA-BSA	Sigma-Aldrich	L9530
L-ascorbic acid	Sigma-Aldrich	A4034
LIF	Miltenyi Biotec	130-095-778
MCDB 201	Sigma-Aldrich	M6770
N2 Supplement	Gibco	17502-048
NEAA	Gibco	11140-035
Neurobasal	Gibco	21103-049
Opti-MEM	Gibco	31985-047
PD0325901	Miltenyi Biotec	130-103-923
PDGF-BB	R&D systems	520-BB-050
Penicillin/Streptomycin	Gibco	15140-122
β-mercaptoethanol	Sigma-Aldrich	M6250

pXEN medium	For 100 mL
DMEM (Low glucose)	60 mL
MCDB 201 (pH 7.2)	40 mL
FBS	2 mL
LA-BSA (100x)	1 mL
ITS (100x)	1 mL
L-ascorbic acid (10 mM)	1 mL
Dexamethasone (250 µM)	20 µl
β-mercaptoethanol (50 mM)	200 µl
LIF (10^6 units/mL)	100 µl
PDGF (10 µg/mL)	100 µl
EGF (10 µg/mL)	5 µl
Penicillin/Streptomycin (100x)	1 mL

1i medium	For 100 mL
Neurobasal	50 mL
DMEM/F12	50 mL
Glutamax™	1 mL
B27 Supplement (50x)	1 mL
N-2 Supplement (100x)	0.5 mL
10 % BSA	0.5 mL
1-Thioglycerol (1.19 M)	12.6 µl
PD0325901 (1 mM)	100 µl
LIF (10^6 units/mL)	100 µl
Penicillin/Streptomycin (100x)	1 mL

pXEN on feeder medium	For 100 mL
DMEM (High glucose)	100 mL
FBS	15 mL
NEAA (100x)	1 mL
LIF (10^6 units/mL)	100 µl
Penicillin/Streptomycin (100x)	1 mL

Feeder medium	For 100 mL
DMEM (High glucose)	100 mL
FBS	15 mL
NEAA (100x)	1 mL
Penicillin/Streptomycin (100x)	1 mL

2.10 Equipment

Table 10: List of equipment used in this study.

Product	Company	Description
Accuri C6 Flow Cytometer	BD Biosciences	FACS analysis
Avanti J-26 XP	Beckman Coulter	High-Speed centrifugation
Axio Observer Z1	Zeiss	Microscope
Centrifuges (5417R, 5810R)	Eppendorf	Centrifugation
CO_2 incubator (Hypoxia, 5%)	Thermo	Cell culture
CO_2 incubator (Normoxia)	Binder	Cell culture
DM-IL	Leica	Microscope
Eclipse Ti-U	Nikon	Microscope
Electrophoresis gel chamber	PeqLab	Agarose gel electrophoresis
FIREBOY	Integra Bioscience	Bunsen burner
Gel documentation system	Berthold Technologies	Gel imaging
Hemocytometer	Reichert	Cell counting
Incubator (Bacteria)	Memmert	Bacterial cell culture
Innova 44 Incubator shaker	New Brunswick Scientific	Bacterial cell culture
Laminar flow hood	Thermo Scientific	Cell culture
Mastercycler ep gradient S	Eppendorf	PCR
Micropipettes	Eppendorf	General experiment
Mithras LB 940	Berthold Technologies	Microplate reader
Mr. Frosty cell freezing container	Nalgene	Cell freezing and storage
Nanodrop 1000	PeqLab	DNA/RNA measurement

Product	Company	Description (Continued)
Odyssey imaging system	LI-COR Biosciences	Infrared fluorescence imaging
PC-10	Narishige	Glass needle puller
PowerPac™ 300	Bio-rad	Power supply
QuantStudio 6 Flex Real-Time PCR System	Applied Biosystems	qRT-PCR
Refrigerator (4/-20 °C)	Liebherr	Sample/chemical storage
SDS XCell SureLock™	Invitrogen	SDS PAGE
TE 22 Mighty Small Transfer Tank	Amersham Biosciences	Gel-membrane transfer
Thermomixer comfort	Eppendorf	General experiment
Vacusafe™ comfort aspirator	Integra Bioscience	General experiment
Vortexer	VWR	General experiment
Water bath	GFL	General experiment
TransferMan® 4r	Eppendorf	Single-cell picking
CellTram® vario	Eppendorf	Single-cell picking

2.11 Software

Table 11: List of software used in this study.

Product	Company	Description
NIS-Elements BR 4.51 software	Nikon	Microscope imaging
AxioVision SE64 Rel. 4.9	Zeiss	Microscope imaging
SnapGene Viewer	SnapGene	Plasmid mapping, primer designing
GraphPad QuickCalcs	GraphPad	p-value calculation
ImageJ	Open-source	Image processing and analyzing
MS Office 2016	Microsoft	General documentation
SerialCloner 2.5	SerialBasics	Plasmid mapping, primer designing
Primer3 v. 0.4.0	Open-source	Primer designing
EndNote X7	Clarivate Analytics	Bibliography management
BD Cflow Plus 1.0	BD Biosciences	FACS analysis
Firecam	Leica	Microscope imaging

3. METHODS

3.1 Cloning procedure

3.1.1 Bacteria culture

Stbl3 *Escherichia coli (E. coli)* cells were cultured with Luria-Bertani (LB) medium in an orbital shaking incubator at 37 °C, 200 rpm overnight. For long-term storage, 500 µl of Stbl3 (non- and transformed) suspension was mixed with 500 µl of 50 % glycerol and stored at -80 ℃ deep freezer.

3.1.2 Transformation

The classical Heat-shock method (42 ℃, 90 sec, followed by ice-incubation for 2 min) was used for transformation using 50 µl of competent Stbl3 with 10 – 50 ng of each target plasmid. Transformed Stbl3 cells were cultured in 5-100 mL of antibiotics containing LB medium in the shaking incubator at 37 ℃ for 24 hours.

3.1.3 Isolation of plasmids from *E. coli*

The principal of plasmid purification is anion exchange chromatography. Plasmid preparation was performed by purification kits (NucleoSpin Plasmid and NucleoBond Xtra Midi kits) according to the manufacturer's instructions.

3.1.4 Measuring plasmid DNA and RNA concentration

The concentration and purity of plasmid DNA or total RNA were measured using the Nanodrop 1000. 1.0 µl of samples were loaded onto the Nanodrop 1000 and measured after the normalization step with TE buffer or D.W.

3.1.5 PCR

For the tet-on human Oct4 system, the TRE-CMV-hOct4 fragment was amplified by the PWO polymerase (with proofreading activity) from the FUW-tetO-hOct4 plasmid. BamHI/BsrGI site was added upstream/downstream of the TRE/hOct4 site respectively by 5' end overhanging primer set. For the pPB-hEF-tdTomato-Puro construct, the tdTomato fragment was amplified from the pcDNA3-tdTomato plasmid by the PWO polymerase.

The primers for the cloning step are listed in Table 4.

pPB-hEF-tdTomato-Puro construct The primer sequences for the tdTomato segment amplification are listed in Table 4. PCR was performed in the Mastercycler ep gradient S thermal cycler.

Reaction mixture

dNTPs (10 mM)	1 µl
Primers (10 µM)	4 µl (2 µl of Forward + 2 µl of Reverse)
Template DNA	10 ng
Pwo Master	25 µl
D.W.	Up to 50 µl

The reaction mixture was gently vortexed to mix. After spin down, the following PCR conditions were employed:

Initial denaturation	94 ℃	2 min	
Denaturation	94 ℃	30 sec	┐
Annealing	57 ℃	30 sec	┘ 30 cycles
Elongation	72 ℃	2 min	
Final elongation	72 ℃	5 min	
Termination	4 ℃	∞	

3.1.6 Agarose gel electrophoresis

The classical agarose gel electrophoresis was performed to separate, confirm, and isolate the target amplicon or plasmid DNA. Briefly, 0.8 - 1.0 % agarose gel was prepared in EtBr (0.5 µg/mL) contained 1x TAE buffer. The samples were mixed with a loading buffer and loaded into the wells. By applying 100 volts for 1 hour, the DNA migrates through the agarose gel from cathode to anode. The DNA fragments were detected and documented by a UV-trans illuminator and imaging system.

3.1.7 DNA isolation from agarose gel

The target amplicons or plasmids with correct sizes were cut out with a scalpel and transferred to a 1.5 mL microcentrifuge tube. Gel elution kit (NucleoSpin Gel and PCR Clean-up kit) was used to purify target amplicon after PCR reaction and electrophoresis according to the manufacturer's instructions.

3.1.8 Restriction enzyme reaction

In general, restriction enzymes recognize and hydrolysis specific hexanucleotide sequences of double-strand plasmid or genomic DNA. According to the manufacturer's instructions, appropriate restriction enzymes and reaction buffers were used to cut target fragments or generate insertion sites from target plasmids. 1.0 μg of target plasmids or amplicons were incubated with restriction enzymes for 1 hour at 37 ℃. For double digestion, the compatible buffer was added to the reaction mixture.

Reaction mixture

Target plasmid DNA or amplicon	1 μg
Restriction enzyme	1 μl (20 units/μl)
10x Restriction enzyme buffer	5 μl
D.W.	Up to 50 μl

3.1.9 Ligation

The amplicons were ligated by using the Quick ligase and manufacturer’s instructions. The molar ratio between insert and backbone was 1:3. The amplified TRE-CMV-hOct4 fragment was introduced into the BamHI/BsrGI sites of PL-SIN-EOS-C(3+)-EiP. The tdTomato amplicon was inserted into the KpnI/XhoI site of the pPB-hEF-mcs-Puro plasmid.

Reaction mixture

Plasmid mixture (insert+backbone)	4.5 μl
Quick DNA ligase buffer	5.0 μl
T4 Quick DNA ligase	0.5 μl
Total	10.0 μl / reaction

3.1.10 Plasmid sequencing

TOP construct cloning was confirmed by the Microsynth Seqlab (Göttingen, Germany) using the Sanger sequencing method. 1μg of TOP plasmids were prepared by purification kit (NucleoSpin Plasmid) and mixed with 1.5 μl of each sequencing primers (10 μM stock; Seq F and Seq R). The sequencing primers are listed in Table 4. The lentiviral vector containing the TRE-CMV-hOct4 fragment was named TOP.

3.2 Cell culture

3.2.1 Isolation of pXEN cell line and maintenance

Wild type pXEN cell line, MX10, was isolated from rat blastocyst (F344×BN, male) as previously described (Lo Nigro et al., 2012). Cells were seeded onto fibronectin (FN)-coated cell culture plates and cultured in pXEN medium (Table 9). Cells were routinely cultured under hypoxia conditions (5 %). Cell passaging was done by trypsinization with 0.05% trypsin/EDTA solution and replated every 2-3 days at a density of 1.0×10^3 / cm^2.

3.2.2 Low- (LD) and High-density (HD) culture condition

Seeding cell densities of ~$1.0\text{-}1.25 \times 10^3$ cells / cm^2 were considered "low density (LD)"; note that while this seeding density was within the range of densities used for cell line maintenance.

Seeding densities of ~8.0×10^4 cells /cm^2 were considered "high density (HD)"; this exceeded cell line maintenance density already at the time of seeding and required frequent medium changes (1 mL, every 24 hours).

3.2.3 Transfection and transposition

Oct4 siRNA transfection The Silencer® select negative control #1 siRNA (4390843) and the Pou5f1 silencer® select siRNAs (Table 4) were purchased from Invitrogen (Carlsbad, CA, USA) and dissolved in DEPC-treated water at a concentration of 2 pmoles/µL. The RNA interference experiments were performed in feeder-free culture conditions at HD. For the HD version, 6 pmol of RNAi duplex (two out of three siRNAs) were diluted in 91 µL of serum-free Opti-MEM medium in each well of a 24-well culture plate. Then, 6 µL of Lipofectamine™ RNAi MAX Transfection Reagent were added, and after an incubation of 15 min at room temperature, the cells were seeded. From the next day on, the medium was changed daily.

Oct4 knockout TALEN transfection The TALEN (L1-DAS and R1-RR) and surrogate reporter plasmids were co-transfected with a ratio 1: 1: 2 (TALEN-Left (L1-DAS): TALEN Right (R1-RR): Reporter) by Polyethylenimine (PEI) method (Reed et al., 2006). PEI contains one nitrogen per monomer ethylenimine subunit. Ionic interactions between the nitrogen and phosphate in the nucleic acid backbone result in DNA-PEI complex formation. The linear DNA-PEI complexes are taken up into target cells degraded by endosomes and lysosomes, and

then the plasmid DNAs were released in the target cell cytoplasm. The amount of PEI was determined as follows:

$$PEI\ (\mu l) = \frac{Plasmid\ DNA\ (\mu g) \times 3\ \left(nmol\frac{Phosphorous}{DNA\ (\mu g)}\right) \times R}{7.5\ \left(nmol\frac{Nitrogen}{PEI\ (\mu l)}\right)}$$

- R: Ratio of nitrogen (PEI) to phosphorous (DNA)

The optimal R-value for pXEN cell is 15 and determined by pcDNA-Tn-hEF-eGFP plasmid control transfection. 50 µl of NaCl (150 mM) mixed with 1µl of plasmid (1 µg/µl)

Tube 1 (1.5 ml tube)

NaCl (150 mM)	50 µl
Plasmid DNA	1 µl

Tube 2 (1.5 ml tube)

NaCl (150 mM)	50 µl
PEI (7.5 mM)	6 µl

Two tubes were combined into a 1.5 mL tube together and mixed by vortexing. After the incubation step for 10 min at RT, the mixture was added dropwise to target cells.

rtTA/GFP/tdTomato transfection The rtTA, GFP, and tdTomato expressing pXEN cell lines were produced by a transposition approach. To this end, piggyBac transposon (pPB) containing plasmids (pPB-TRE-mcs-M2-IRES-BSD or pPB-hEF-GFP-Puro or pPB-hEF-tdTomato) were co-transfected with piggyBac transposase (mPB). 2.5×10^4 wild type MX10 cells per well were seeded into a 6-well plate, and 24 hours later, pPB and mPB were transfected (1 µg of pPB plasmid and 0.1 µg of mPB plasmid) by PEI as previously described. The medium was changed 24 hours after transfection and supplemented with selection drugs (1.0 µg/mL Puro or 10.0 µg/mL BSD). 48 hours later, selection drug-resistant colonies were collected with a glass capillary or cloned by limiting dilution. Then the cells were transferred into 24-well plates and expanded under continued selection for more than two passages.

3.2.4 Lentiviral transduction

2.5 µg of pMD2.G and psPAX2, together with 5.0 µg of the TOP construct, were co-transfected into 293T cells with the PEI method in a 100 mm cell culture dish. 5 hours later, the medium was changed, and viral supernatant was collected after subsequent 48 hours of cultivation. And

the supernatant was filtrated through 0.45 μm filters and then concentrated with Lenti-X Concentrator (1:3 ratio, 3 mL of concentrator + 9 mL of viral supernatant). The mixture was incubated for 1 hour at 4 °C and then centrifuged (3,000 g; 4 °C; 45 min). After the centrifugation, the concentrated virus was resuspended in 1 mL of PBS.

1.0×10^4 rtTA-pXEN cells in a well of 6-well plate were seeded 2 days before viral infection. The rtTA-pXEN cells were infected with 10 μl of polybrene (8 μg / μl) and 1 μl of viral supernatant (MOI: 1) on day 2. The medium was changed into 1.0 μg/mL doxycycline contained pXEN cell culture medium. 48 h later, the infected cells were split into a 6-well plate at 1:6 ratio and selected by adding 1.0 μg / mL of Dox and puromycin for 2 days. The puromycin-resistant clones were recovered by limiting dilution. After the expansion step, transgenic clones' identities were confirmed using a panel of pXEN-specific primer pairs. The primers for the pXEN-specific genes are listed in Table 4.

3.2.5 Co-culture experiment

Equal numbers of GFP-expressing non-Oct4-transgenic pXEN cells (green color) and tdTomato-expressing hOct4-transgenic pXEN (iOX1) cells were mixed, seeded at intermediate density (10^4 cells total/well) into 12-well plates, and cultured with 1i medium in the absence or presence of Dox (1.0 μg/mL) for 6 days.

3.2.6 Cryopreservation

Cells were detached from the culture dish by trypsinization and collected by centrifugation (300g, 5 min). After removing the supernatant, the cells were resuspended in 1 mL of ice-cold cell freezing medium and transferred into a cryovial. The cryovial was placed in a Mr. Frosty cell freezing container and stored at -80 ℃ deep freezer. The next day, the cryovial was transferred to the LN_2 tank for long-term storage.

3.3 Analytical methods

3.3.1 Cell migration assay

1.0×10^4 iOX1 cells per well were plated into a 12-well-plate and cultured for 2 days. The cell monolayer was slowly scratched with a sterile 200p pipette tip across the center of the wall. After scratching, the cells were gently washed once with PBS ($+Ca^{2+}/+Mg^{2+}$) to remove the debris and replenished with 1 ml of fresh medium (with or without Dox). The gap closure was photographed again after 24 hours. The increment of the covered area (24 h area – 0 h area) was calculated using Image J software (Cormier et al., 2015), and the recovered area of the +Dox condition was set as 100%.

3.3.2 Luciferase assay

2.5×10^4 rtTA integrated pXEN cells were seeded in a well of 6-well plate 2 days before transfection. 1 µg of pUHC131-T6 (Firefly) and 0.1 µg of pRL tk (Renilla) plasmids were co-transfected using the PEI method. 24 hours later, cells were lysed in 200 µl of lysis buffer and incubated for 10 min on ice. After centrifugation (11,000g, 1 min), 10 µl of supernatant were added mixed with 90µl of 5 mM ATP contained reaction buffer. D-luciferin (final concentration: 200 µM) and coelenterazine (final concentration: 4 µM) were separately mixed with substrate buffers (50 µL/sample) and placed into separate injectors of Mithras LB 940 microplate reader. 10 µl of mixed reaction buffer into a luciferase assay plate. Luciferase activities determined in a Mithras LB 940 microplate reader. After the measurements, results were calculated as the ratio of the activities of firefly/renilla.

3.3.3 Flow cytometry

1.0×10^4 rtTA-pXEN cells in a well of 6-well plate were seeded 2 days before pTRE-d2EGFP plasmid transfection. The medium was replaced with 1.0 µg/mL Dox contained pXEN cell culture medium before transfection. 1.0 µg of plasmid was used for PEI transfection. 48 h later, the transfected cells were harvested by trypsinization. Then the cells were resuspended in FACS buffer and filtered through a 35 µm FACS tube with a nylon mesh cap. The Dox-induced GFP expression was analyzed using the Accuri C6 Flow Cytometer and the BD Cflow Plus software.

3.3.4 Western blot

5.0×10^4 cells were seeded into a 100 mm dish, cultured for 4 days in the absence or presence of Dox, and then lysed in 100 µL of RIPA buffer. The lysate was centrifuged (11,000 x g, 10 min, 4 ℃), and the supernatant was transferred to a fresh tube for further analysis. The protein concentrations of the samples were measured using the BCA protein assay kit. The lysates were boiled at 95 °C for 10 min, separated by SDS-PAGE, and blotted onto PVDF membranes. After a 1-hour blocking step with Odyssey blocking buffer at room temperature, the membranes were incubated overnight at 4°C with mouse anti-Oct4 and mouse anti-β-Actin at a dilution of 1:1,000 and 1:5,000, respectively. Goat anti-Mouse IgG IRDye® 800CW and 680RD were used as the secondary antibody to detect Oct4 and β-Actin, respectively. The signals were visualized using the Odyssey imaging system.

3.3.5 Immunocytochemistry

5.0×10^3 iOX1 cells/well were seeded into a FN-coated 24-well-plate and cultured with or without Dox (1.0 µg/mL) for 2 or 4 days. Cells were washed with ice-cold DPBS (with Ca^{2+}/Mg^{2+}) and fixed in BD Cytofix™ fixation buffer for 10 min at RT. The fixed cells were washed three times with DPBS, incubated with permeabilization buffer for 10 min at RT, and rewashed three times with DPBS for 5 min. Following blocking in Roti®-Block solution for 30 min at RT, cells were incubated overnight at 4 °C with the primary antibodies (1:1,000 dilution). After washing with DPBS (3 times, for 5min each wash), cells were incubated at room temperature for 1 hour with the secondary antibodies (1:10,000 dilution) and DAPI, washed, and mounted for viewing with a microscope.

3.3.6 qRT-PCR

Total mRNA was isolated using the RNeasy Mini Kit. 1.0 µg of total RNA was used for cDNA synthesis. Reverse transcription reaction was performed using the SuperScript™ III according to the manufacturer's instructions. All the primers used were listed in Table 4. qRT-PCR was performed in a QuantStudio 6 Flex Real-Time PCR System using a reaction mixture with RT² SYBR® Green ROX™ qPCR Mastermix.

Reaction mixture

SYBR Green master mix	5 µl
Forward primer (10 µM)	1 µl
Reverse primer (10 µM)	1 µl
D.W.	Up to 10 µl

The qRT-PCR cycle parameters were as follows:

PCR cycle

Initial activation	50 ℃	2 min	
Initial denaturation	95 ℃	10 min	
Denaturation	95 ℃	15 sec	] 40 cycles
Annealing	60 ℃	1 min	
Melting curve analysis	95 ℃	15 sec	
Melting curve analysis	60 ℃	15 sec	
Melting curve analysis	95 ℃	15 sec	
Termination	4 ℃	∞	

All the PCR amplification was performed in at least duplicated and repeated in three independent experiments. The relative expression levels of each gene were normalized to Gapdh (or β-actin). The relative expression level is displayed in arbitrary units ($2^{-\Delta Ct}$ or $2^{-\Delta\Delta Ct}$), and the values are the means ± S.D. of triplicate samples. The statistical analyses were performed with Student's t-test using the GraphPad QuickCalcs t-test calculator online software, and $P < 0.05$ was considered statistically significant.

3.3.7 Microscopy

Phase-contrast microscopy To assess cell morphology, motility, and proliferation rate, the Nikon Eclipse Ti-U or the Leica DM-IL was used. The Nikon DS-Qi2 camera was connected to the Eclipse Ti-U microscope, and NIS-Elements BR 4.51 software was used for image acquisition.

Stereo microscopy To assess cell colony formation (plating assay), cells were fixed with methanol for 10 min at RT. After washing step with PBS (with Ca^{2+}/Mg^{2+}), cells were stained with Crystal violet for 1 hour at RT. Then the cells were washed three times with the PBS. Leica DFC420 camera connected Leica M165C stereomicroscope and Leica Firecam software were used for stereo microscopic image acquisition.

Fluorescence microscopy To assess fluorescence signal (immunostaining, plasmid transfection, GFP, or tdTomato expressing cell line), the Axio Observer Z1 or the Nikon Eclipse Ti-U microscope was used. The AxioCam MRm was connected to the Axio Observer Z1 microscope for image acquisition using the AxioVision SE64.

4. RESULTS

4.1 High-density culture condition induces VE/MET-associated gene expression

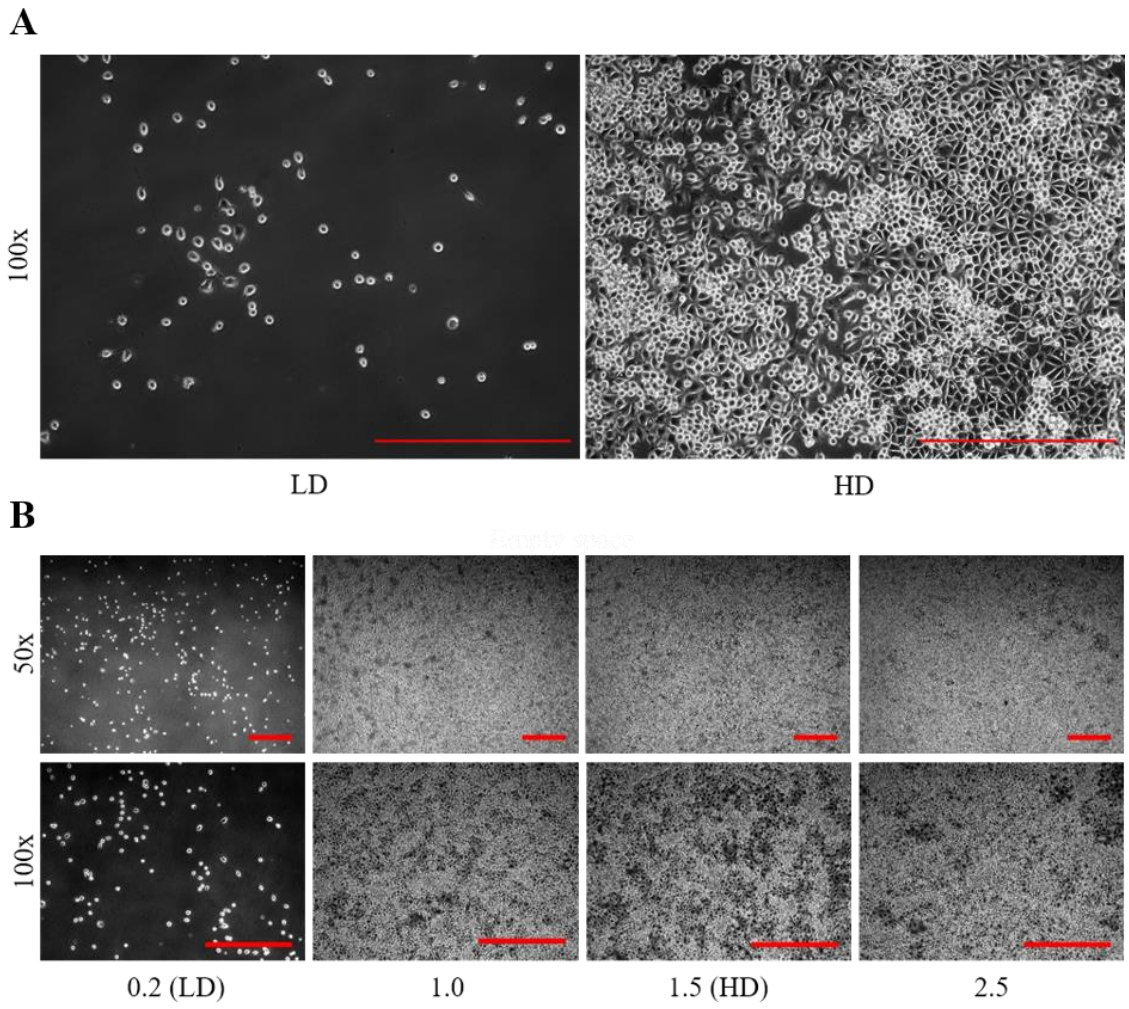

Figure 9: High density causes morphological changes in the MX10 cell line. (A) Representative phase-contrast images of MX10 cells in LD and HD conditions. MX10 cells show round and spindle-shaped in LD or maintain culture condition while in HD culture, the cells were differentiated to flattened and angulated epithelial-like cells 2 days after seeding. (B) MX10 cell image cultured in different densities. The cells were cultured for 2 days with indicated density. Scale bar: 500 µm

Rat pXEN cell lines are maintained at low to intermediate densities, either

(i) with a low-serum medium without feeder cells (Lo Nigro et al., 2012)) or

(ii) with a high-serum medium on feeder cells (Debeb et al., 2009); in both cases, they express Oct4 at moderate levels and require LIF.

Under the feeder-free maintenance condition, pXEN cells exhibit a mesenchymal morphology. When the cells are seeded at high density (HD), they piled up and started to form VE-like angulated flattened cells (Figure 9) that eventually resolved into aggregates and duct-like structures (See Figure 8G).

Under this high-density culture condition, we observed a significant increase of Oct4 mRNA compare to low-density (LD) or maintain culture condition (Figure 10A) within 2 days. In parallel with the increased endogenous Oct4 expression, some well-established markers associated with epithelialization and tight junction (Cdh1, Zo1) were increased (Figure 10B *UPPER*). In contrast, some (Vim, Zeb1) but not all (Snai1) mesenchymal markers went down (Figure 10B *LOWER*). Simultaneously, some VE markers (Dab2, Ihh, ApoE, Cited1) were remarkably increased (Figure 10B *UPPER*). While the PE markers Pth1r and Sparc were not decreased, Sparc was even significantly increased (Figure 10B *LOWER*).

A

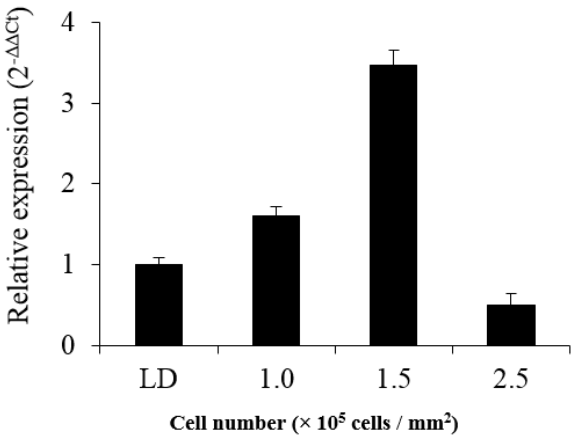

B

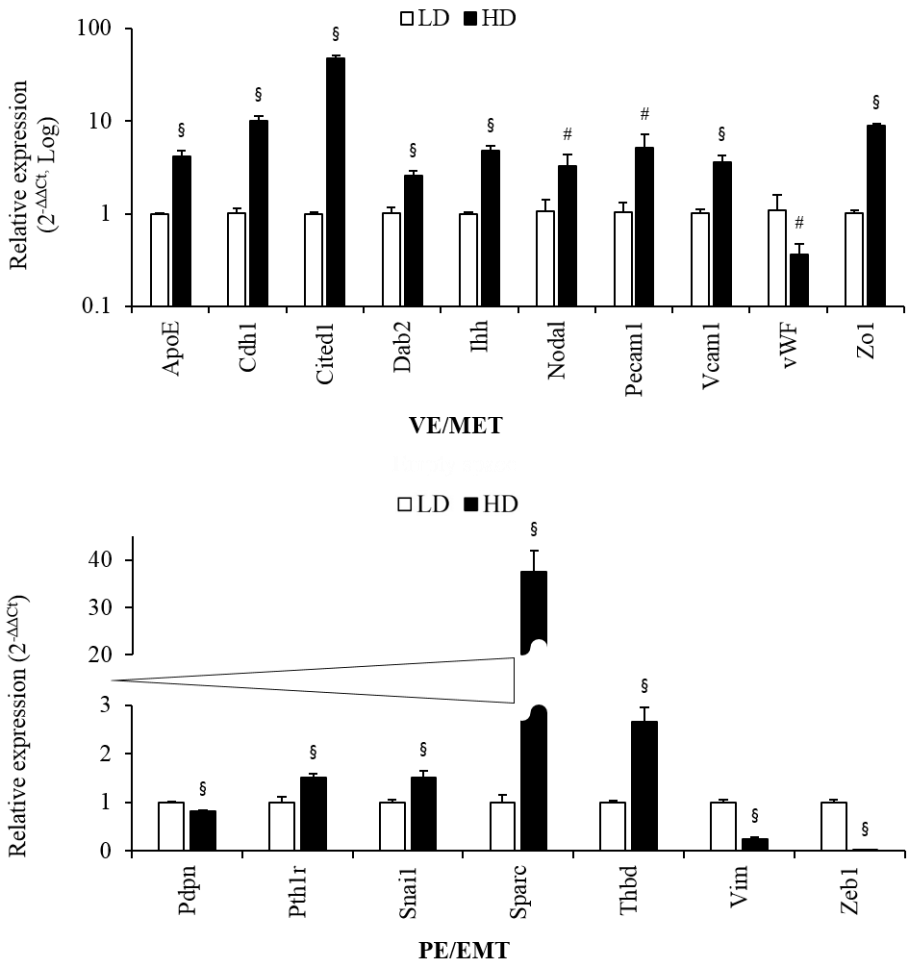

Figure 10: HD culture condition induces Oct4 and VE/MET-associated gene expression in MX10 cell line. (A) Density-dependent endogenous Oct4 expression regulation. (B) Expression of VE/MET or PE/EMT-associated genes in LD and HD condition (Day 2). Gene expression was normalized to Gapdh levels, and average $2^{-\Delta\Delta Ct}$ values of the LD condition were set as 1. #, P<0.05; §, P<0.001.

4.2 Oct4 knockdown induces epithelial genes while downregulates mesenchymal genes expression

To investigate the correlation between the Oct4 upregulation and the density-related epithelialization or aggregation/duct-like morphogenesis, we blunted the HD-induced Oct4 mRNA/protein in the feeder-free system via oligonucleotide-mediated RNA interference.

Compared to the mock, the siRNA transfection reduced the Oct4 mRNA levels down to ~63.5 % (Figure 11B *RIGHT*). Moreover, Oct4 knockdown by siRNA transfection resulted in a remarkable morphological effect: The RNAi appeared to accelerate the aggregation of the piled-up cells, *i.e.,* the beginning of the duct-like morphogenesis (Figure 11 *LEFT*).

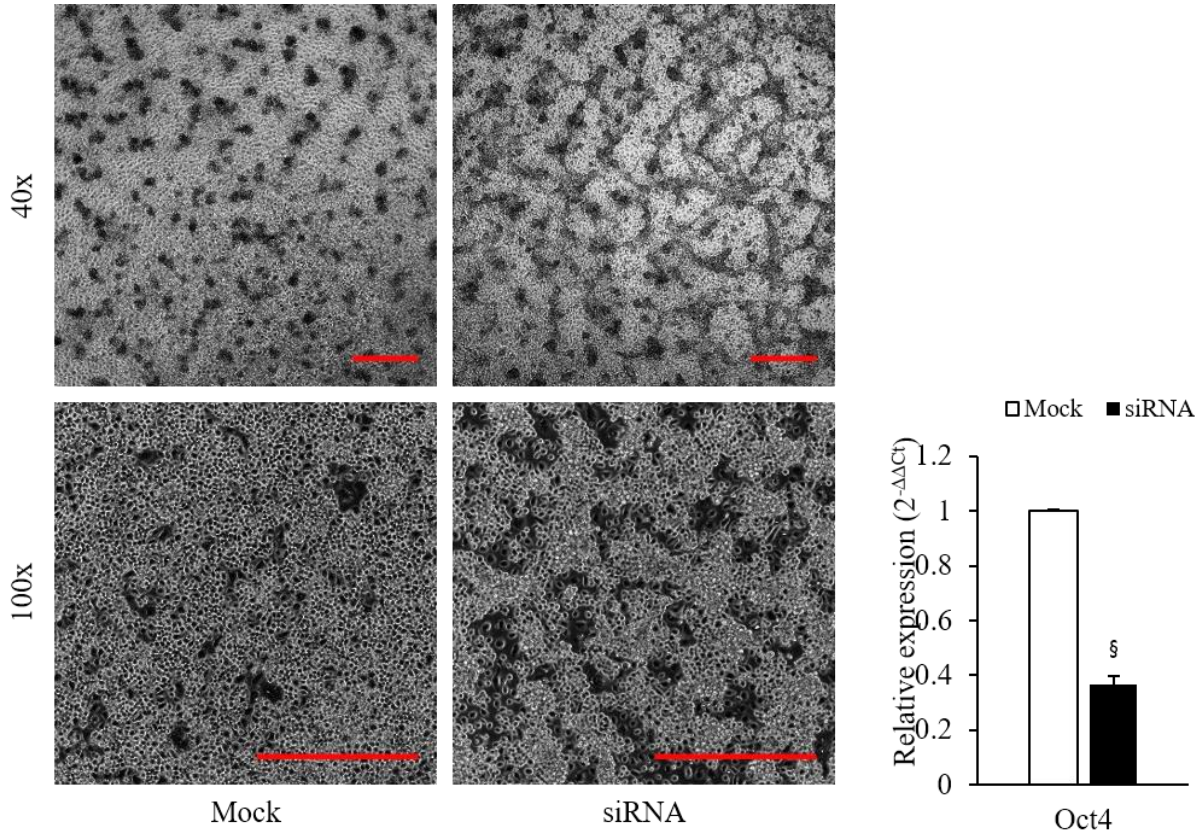

Figure 11: Oct4 targeted siRNA oligo transfection facilitated aggregated cell formation. *LEFT*, Representative phase-contrast photos of Mock and siRNA transfected wild type cells in HD culture condition (Day 2). Scale bar: 500 µm, *RIGHT*, Endogenous Oct4 expression 2 days after siRNA transfection. Gene expression was normalized to Gapdh levels, and average $2^{-\Delta\Delta Ct}$ values of the Mock transfection were set as 1. §, P<0.001.

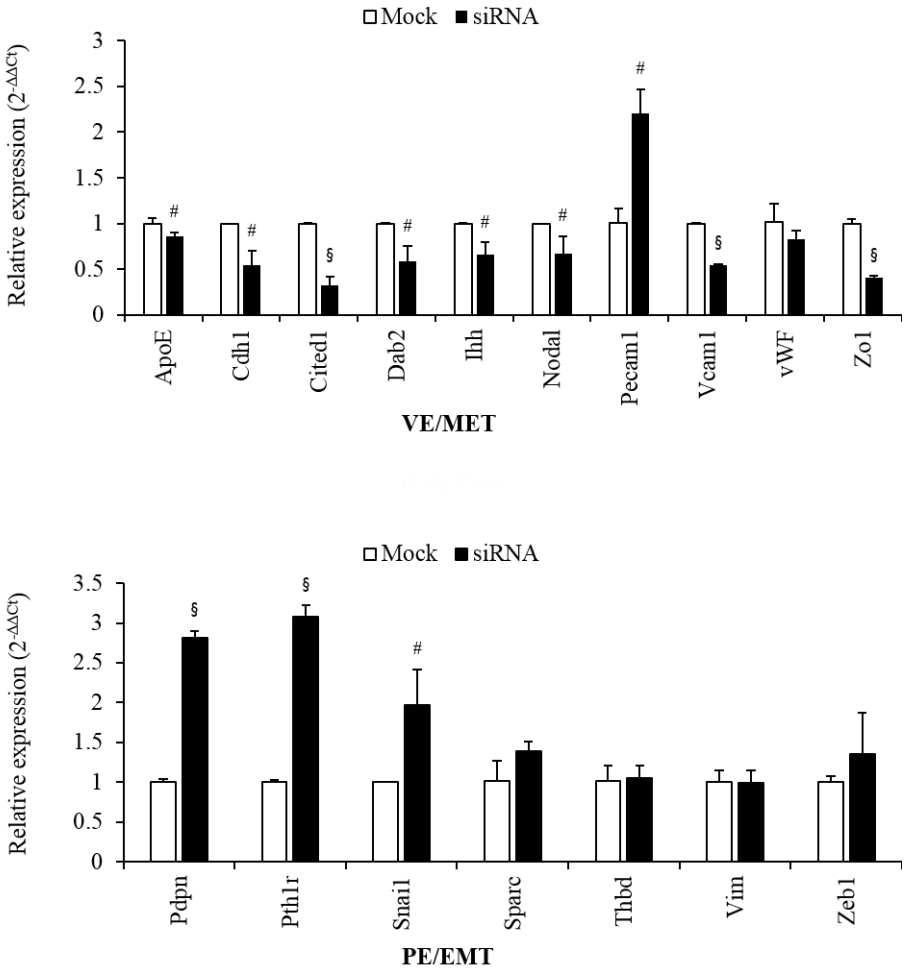

Figure 12: Effect of Oct4 knockdown on marker gene expression, determined by qRT-PCR 2 days after transfection. Representative results obtained with a mix of two siRNA pairs (s148663 and s220720) are shown. Gene expression was normalized to Gapdh levels, and average $2^{-\Delta\Delta Ct}$ values of the Mock transfection were set as 1. #, P<0.05; §, P<0.001.

Besides, expression of the epithelial (Cdh1, Zo1) and VE (ApoE, Dab2, Ihh) markers were significantly reduced (Figure 12 *UPPER*), while some PE and mesenchymal (Pth1r, Snai1, Zeb1) markers were increased (Figure 12 *LOWER*). The HD-induced upregulation of the PE marker Sparc, although not reversed, was prevented (Figure 12 *LOWER*). This result indicates that the HD-mediate gene expression changes were blunted, albeit with minor exception: The RNAi increased rather than decreased the endothelial marker Pecam1 expression (Figure 12 *UPPER*).

4.3 Doxycycline induced Oct4 effect in transgenic pXEN cells

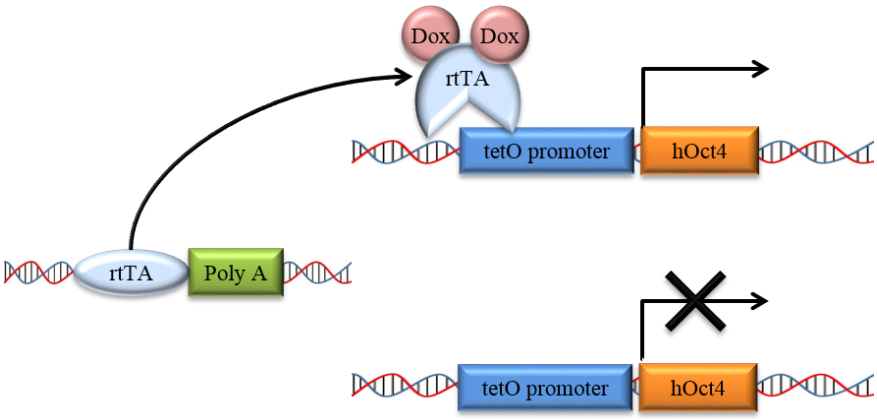

Figure 13: Schematic illustration of Tet-On system. rtTA, Reverse tetracycline transactivator; Dox, Doxycycline; tetO, Tetracycline operator; hOct4, Human Oct4.

The Tet-On/Off system is originated from a tetracycline-resistance operon in bacteria. It has extensively broad applications in biological research especially, in the stemcell field. Nowadays, it is widely used for the analysis of gene function in eukaryotic cells. This system is controlled by binding the effector (tetracycline or its derivatives, *e.g.*, doxycycline) to the tetracycline regulatory element (TRE). The TRE comprises 7 repeats of a tetO sequence and a minimal promoter. In the presence of the effector, the reverse tetracycline transactivator (rtTA) undergoes a conformational change then recognizes the tetO sequence in the TRE. The binding of the effector and rtTA complex to tetO recruits transcription machinery thereby enhances transcription activity, in our case, Oct4 (Figure 13) (Gossen et al., 1995).

4.3.1 Establishing doxycycline-inducible Oct4 system in pXEN cells

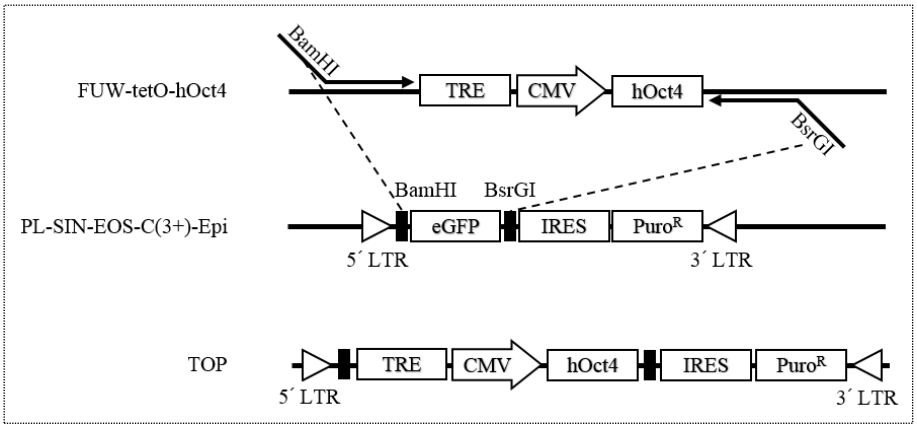

Figure 14: Schematic illustration of generating TOP construct for the establishment of inducible human Oct4 system.

To confirm the proposed role of Oct4 directly, we generate a transgenic pXEN cell line that is expressing Oct4 under the control of doxycycline (Dox) (Figure 14). The cell line was established in two steps as follows.

In the first step, we used PiggyBac transposon and transposase-mediated approach to integrate the rtTA cassette into the pXEN cell genomic DNA. The integration of the rtTA cassette was validated by transfection of the pTRE-d2EGFP construct. In the presence of doxycycline, rtTA-integrated cells expressed GFP within 24 hours (Figure 15). Through FACS analysis and dual luciferase assay, we screened the Cl.3 for further genetic manipulation process. Due to the lowest background and highest GFP positive population in the absence and presence of doxycycline, respectively (Figure 16A, 16B)

In the second step, a Dox-dependent human Oct4 expression cassette was introduced by lentiviral transduction into the rtTA Cl.3. The rtTA and TRE-hOct4-Puro^{R} cassette inserted transgenic pXEN cells named iOX.

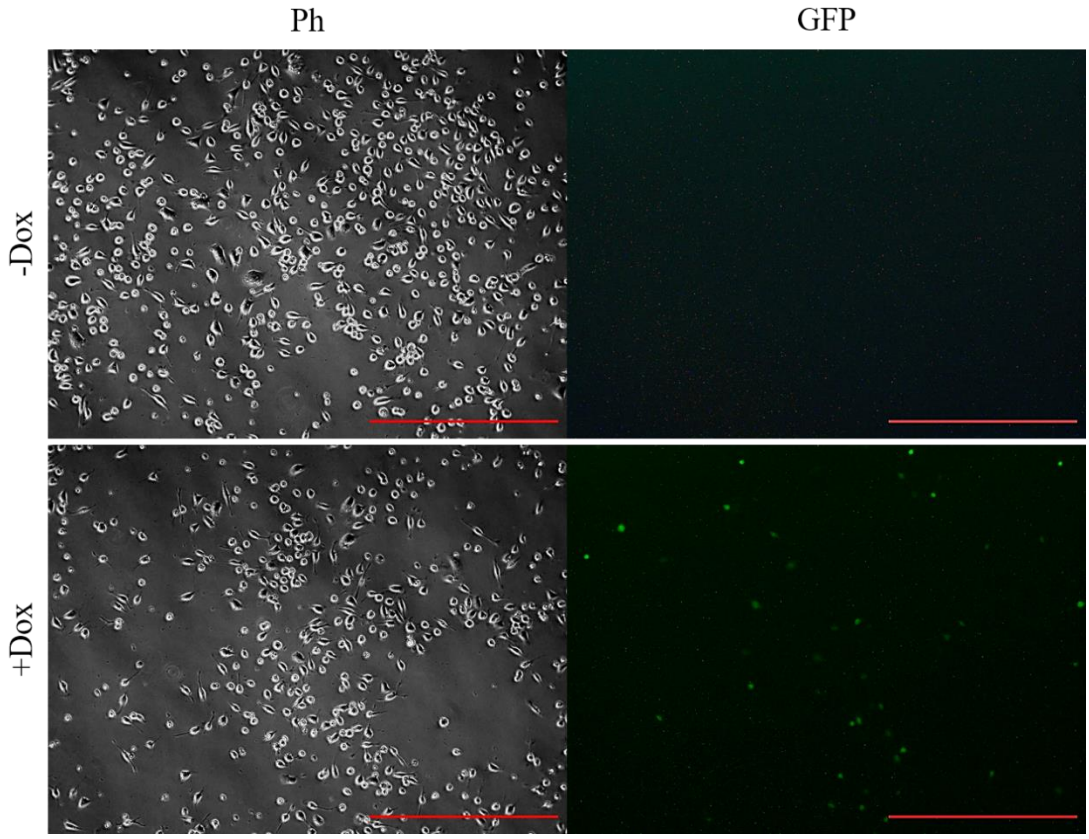

Figure 15: Validation of rtTA-integrated pXEN cells (Cl.3). Phase-contrast and fluorescent (GFP) images of pTRE-d2EGFP plasmid transfected rtTA-pXEN clone 3 on Day 3. 2.5 × 10^4 cells were seeded in a 6-well on Day 0. pTRE-d2EGFP transfection was performed on Day 2. The cells were then cultured with (1.0 µg/mL) and without Dox for 24 hours (Day 3). Scale bar: 500 µm, Magnification: 100x.

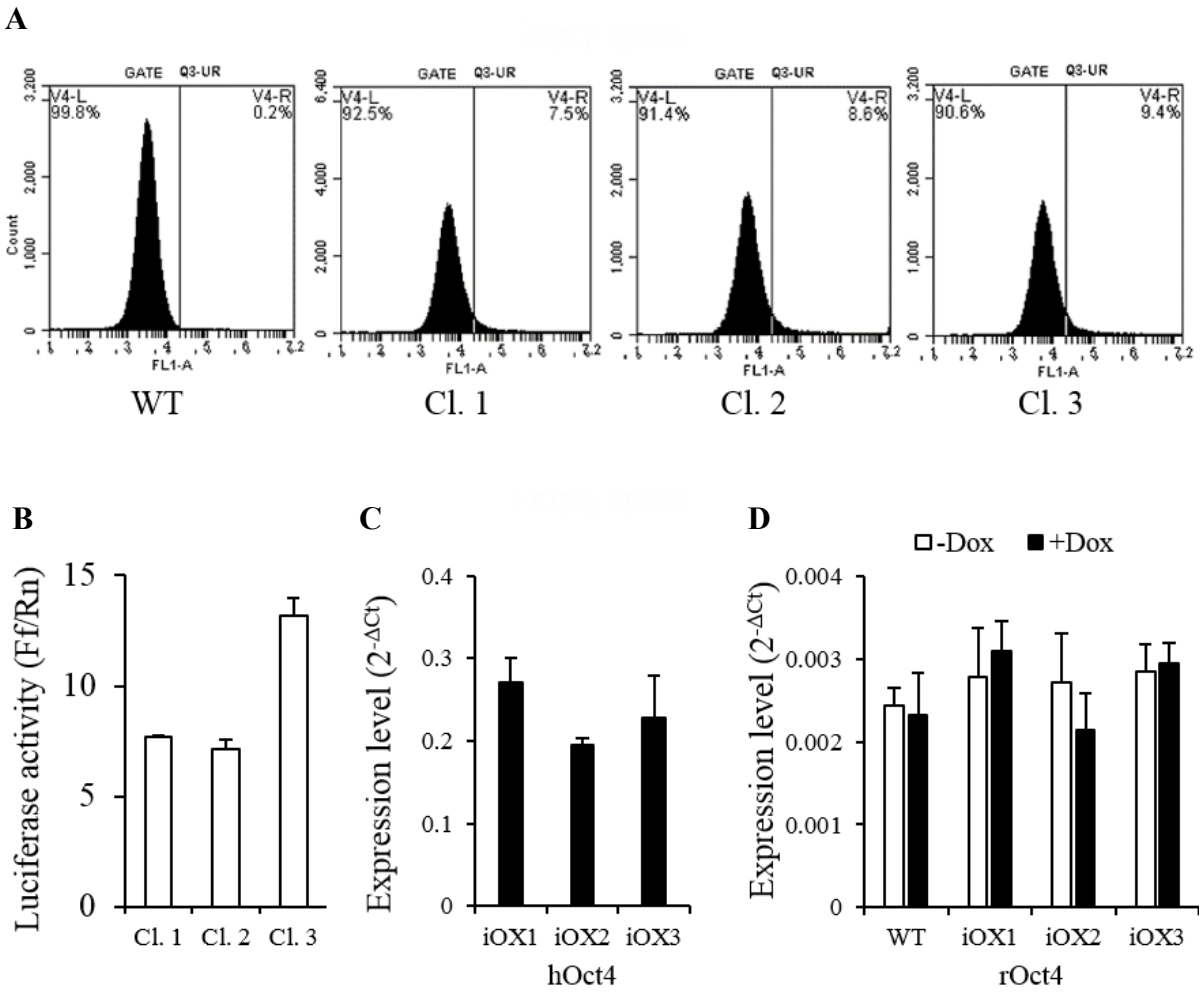

Figure 16: Validation of rtTA- and TRE-hOct4 integrated clones. (A) FACS analysis of pTRE-d2EGFP construct transfected rtTA clones in the presence of Dox (1.0 µg/mL) (B) Dual-luciferase assay. The rtTA clones were transfected with reporter plasmid in the presence of Dox. Ff, Firefly; Rn, Renilla. (C) qRT-PCR analysis of Dox-induced human and (D) rat endogenous Oct4 expression level in iOX clones. Oct4 expressions were normalized to Gapdh levels and average $2^{-\Delta Ct}$ value. The data represent three independent experiments, each performed in duplicate. The values are the means ± S.D. of duplicate samples.

In the presence of Dox, three puromycin-resistant iOX clones were recovered by limiting dilution. After the expansion step (Figure 17), the Dox-induced human Oct4 mRNA level was verified by qRT-PCR (Figure 16C). We also confirmed that the Dox treatment (1 µg/mL) for two days did not alter the endogenous Oct4 level in the iOX clones and wild-type cell line (Figure 16D). Even though there were no significant differences among those iOX clones, the iOX1 cells showed the most stable phenotype in the Dox response aspect (the lowest background expression with the highest Dox-induced Oct4 expression). Thereby we decided to use the iOX1 cell line for further study (Figure 16C, 16D).

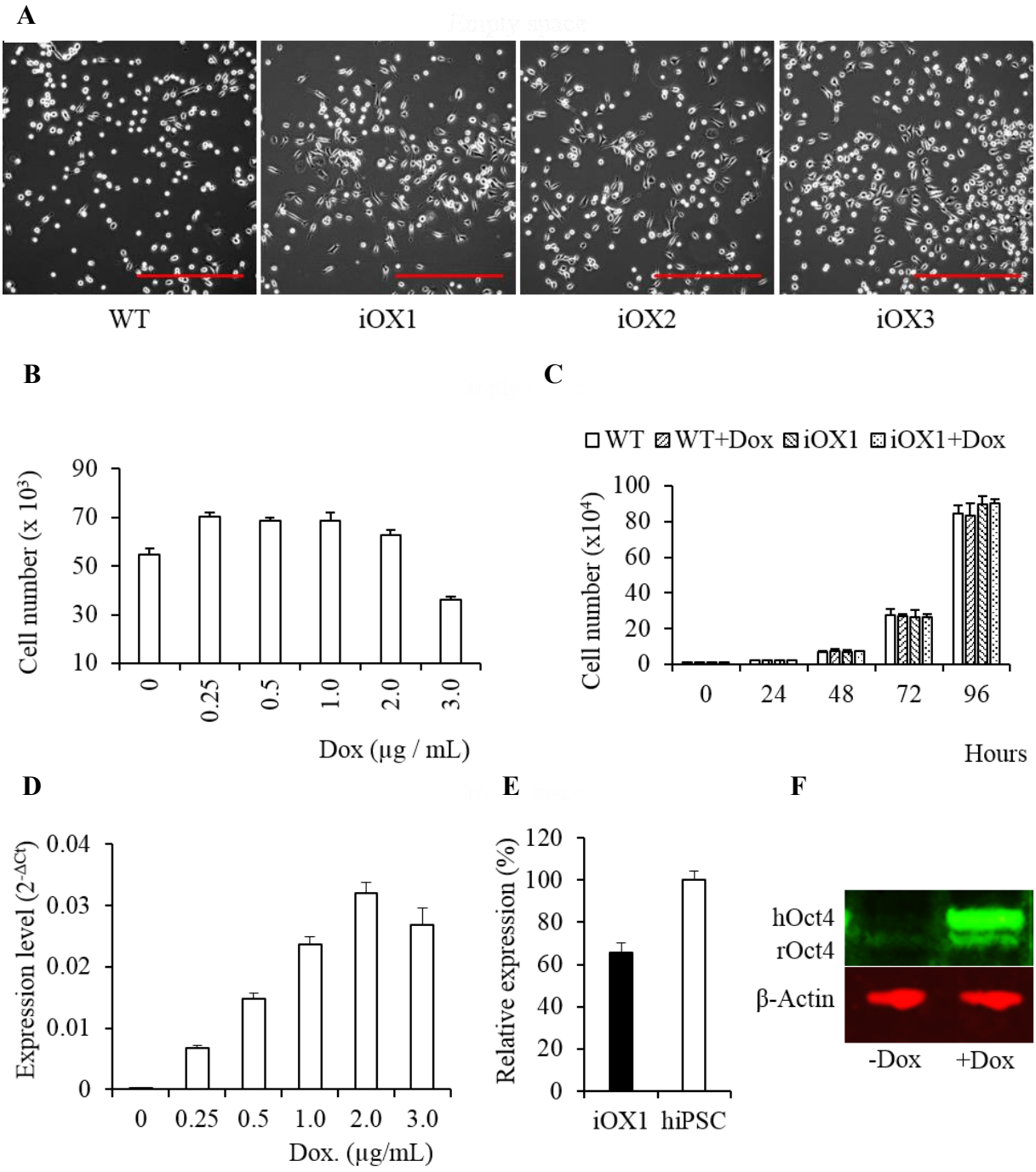

Figure 17: Establishment of transgenic pXEN cell lines. (A) Phase-contrast images of wild type (MX10) and iOX cell lines after the limiting dilution and the expansion step. Scale bar: 500 µm, Magnification: 100x. (B) High concentration (>2.0 µg/mL) of Dox. administration showed cytotoxicity after 2 days. (C) Dox-induced human Oct4 expression did not affect the cell proliferation rate. (D) Determination of effective Dox concentration in iOX1 line by dose-response test ($2^{-\Delta CT}$ ± S.D., normalized to Gapdh). (E) Direct comparison of human Oct4 mRNA level in iOX1 and hiPSC. Human Oct4 expression was normalized to β-actin (by rat and human dual specific β-actin primer) levels, and the average 2-ΔCt value of the hiPSC was set 100 %. hiPSC, human induced pluripotent stem cell (IMR90). The data represent three independent experiments, each performed in duplicate. (F) Western blot for Oct4, 4 days after seeding.

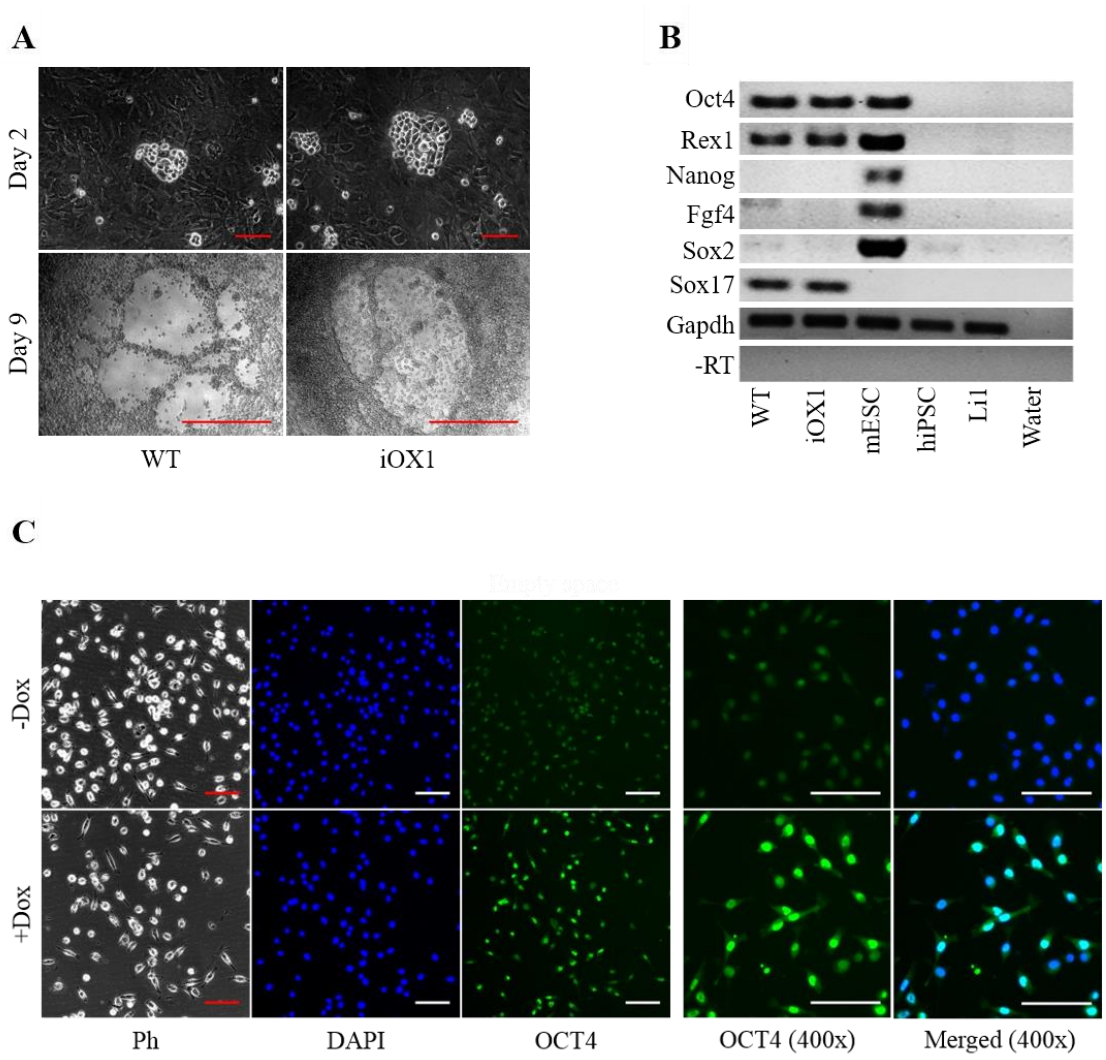

Figure 18: Establishment of transgenic pXEN cell line iOX1 exhibiting Dox-inducible Oct4 expression and maintaining pXEN cell identity. (A) Duct formation assay on feeder cells (B) RT-PCR of wild type and transgenic iOX1 cells for selected marker genes. mESC, mouse ES cells (positive control for Nanog, Fgf4 and Sox2, negative control for Sox17); hiPSC, human induced pluripotent stem cell line (negative control for rat Oct4); Li1, rat feeder cell line (fibroblast, negative control for all lineage markers). (C) Oct4 immunostaining, 2 days after seeding. *LEFT*, Scale bar: 100 µm, Magnification: 200x; *RIGHT*, Scale bar: 100 µm, Magnification: 400x.

We confirmed the increased Oct4 expression of the iOX1 cell line in the presence of Dox (1µg/mL) by immunostaining and western blotting (Figure 17F, 18C). The identities of the iOX1 line were validated using colony formation assay on the feeder (Figure 18A) and a panel of pXEN-specific primer pairs. The iOX1 cells still maintained the pXEN-specific differentiation and gene expression pattern (Figure 18B). The primers for the pXEN-specific genes are listed in Table 4. Also, cell doubling time (CDT) of both wild type and iOX1 cells cultured with Dox (1.0 µg/mL) was not affected (WT, 15.0 ± 0.19; WT+Dox, 14.8 ± 0.17, iOX1, 15.06 ± 0.29; iOX1+Dox, 14.78 ± 0.17).

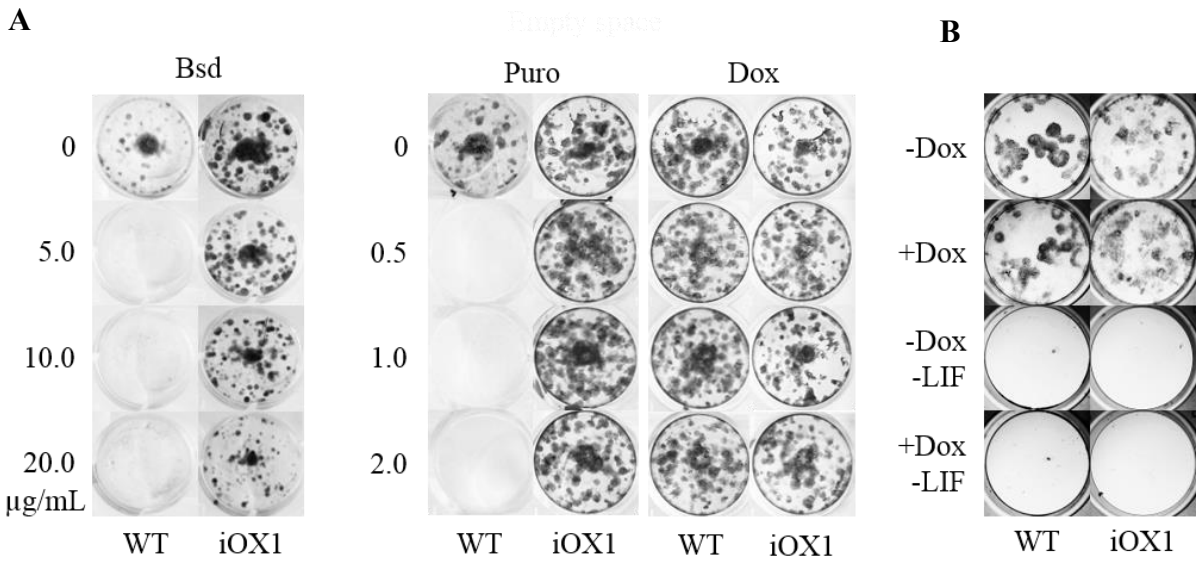

Figure 19: Validation of iOX1 cell line. (A) Selection drug sensitivity test on the wild type and iOX1 cells. (B) Cytokine LIF dependency test of wild type and iOX1 cells in the absence and presence of Dox (1.0 µg/mL).

As previously reported (Ahler et al., 2013), the high concentration of Dox (> 3.0 µg/mL) exhibited cytotoxic activity against the iOX1 line about 48 hours after treatment (Figure 17B). While in the moderate concentration of Dox (1.0 µg/mL), iOX1 cells maintained the regular proliferation rate (Figure 17C). Besides, the plating assay experiment demonstrated that LIF dependence was not overcome by Dox-induced human Oct4 (Figure 19B).

In summary, a transgenic pXEN cell line was successfully established and still maintained its original characteristics as a pXEN cell, including morphology, proliferation rate, and gene expression profile.

4.3.2 Forced Oct4 expression promotes elongation and cell motility in the early phase

Then we investigated the morphological change of iOX1 cells in the first 48 hours after doxycycline administration. In the iOX1 cells cultured with Dox (1.0 µg/mL), most cells exhibited mesenchymal-/elongated cell shape and increased cell motility. Hence, we first measured individual cells' length (~500 cells) from with and without Dox condition.

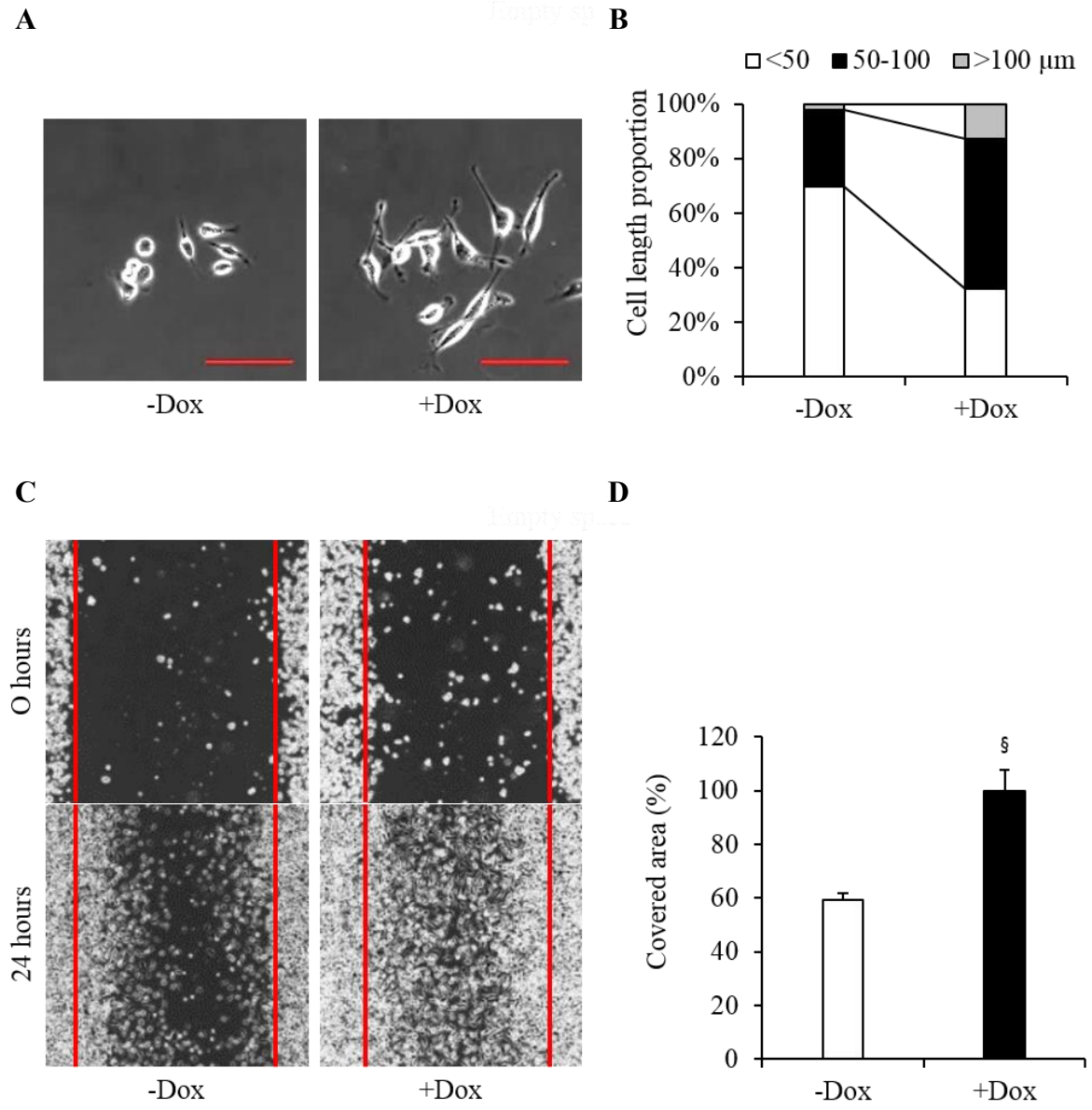

Figure 20: Effect of Dox-induced Oct4 in the early phase (<Day 2). (A) Representative phase-contrast image of Dox treated iOX1 cells at day 2. Scale bar: 100 µm, Magnification: 400x. (B) Dox-induced human Oct4 increases the proportion of elongated cells. (C) Cell migration assay in the absence or presence of Dox. Magnification: 40x (D) Quantitative analysis of the migration assay results. §, P<0.001.

From the cell length measurement, we observed that the population of cells exhibiting intermediate cell length range (50-100 µm) was significantly increased from 28.1 % to 55.0 % in +Dox condition. Furthermore, the population of cells that exhibit longer than 100 µm length was increased dramatically from 2.1 % to 12.5 % (Figure 20A).

Interestingly, the induced Oct4 expression in the LD condition appeared to stimulate migratory behavior parallel with a more elongated cell shape (Figure 20B).

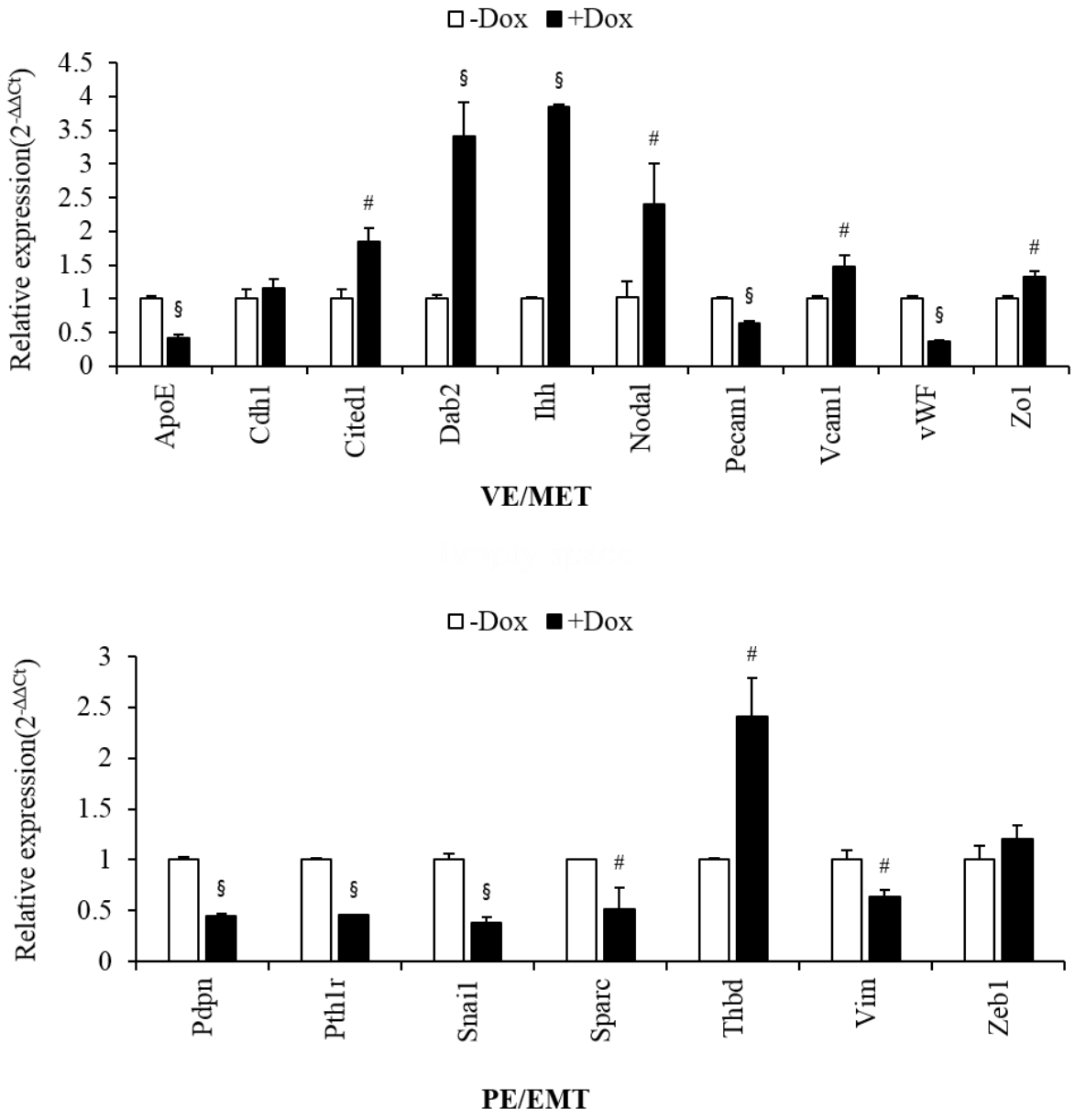

Figure 21: qRT-PCR analysis of selected marker gene expression 2 days after seeding. Gene expression was normalized to Gapdh levels, and average $2^{-\Delta\Delta Ct}$ values of the –Dox condition were set as 1. #, P<0.05; §, P<0.001.

To gain further insight into the morphological change by Oct4 overexpression, we performed qRT-PCR analysis. In contrast to the siRNA-mediated Oct4 knockdown result, forced Oct4 expression upregulated VE-associated gene expression, including Cited1, Dab2, Ihh, and Nodal. In parallel, the tight junction component, Zo1, expression was significantly increased (Figure 21 *UPPER*). While, PE or PE inducer genes such as Pth1r, Snai1, Sparc, and Vim were significantly downregulated. Besides, lymphatic endothelium or EMT marker Pdpn expression was downregulated in the presence of Dox. However, one of the PE marker genes involved in extracellular matrix remodeling, Thbd, was highly induced by Dox treatment (Figure 21 *LOWER*).

4.3.3 Oct4 overexpression induces MET and enhances VE gene expression in the advanced phase.

When allowing the Dox-stimulated pXEN cells to grow in HD condition, a greater tendency of the Dox-treated cells to undergo MET became readily apparent (Figure 22 *LEFT*); note that this also led to a moderate increase of endogenous Oct4 (Figure 22 *RIGHT*).

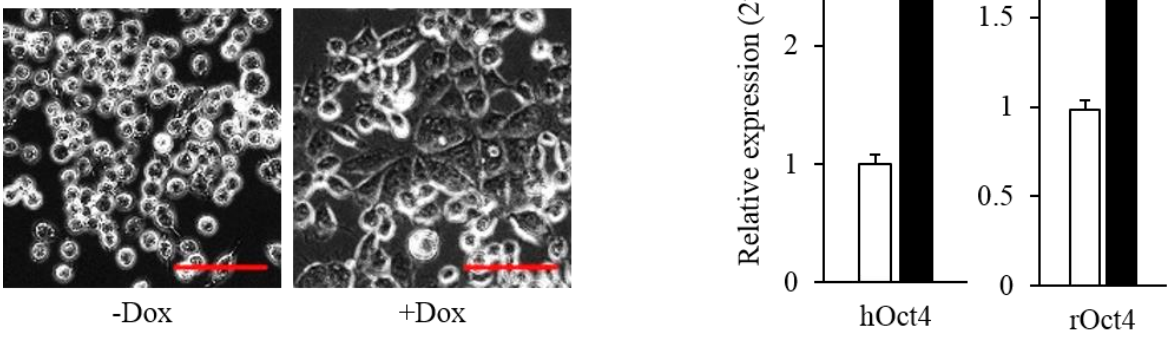

Figure 22: Sustained ectopic human Oct4 overexpression induced epithelial-like morphological change and endogenous Oct4 expression. *LEFT*, Representative phase-contrast images, 4 days after seeding. Scale bar: 100 µm, Magnification: 400x; *RIGHT*, Transgenic (hOct4) and endogenous (rOct4) Oct4 mRNA levels (determined by qRT-PCR) 2 and 4 days after seeding. Gene expression was normalized to Gapdh levels, and average $2^{-\Delta\Delta Ct}$ values of the Day 2 condition were set as 1.

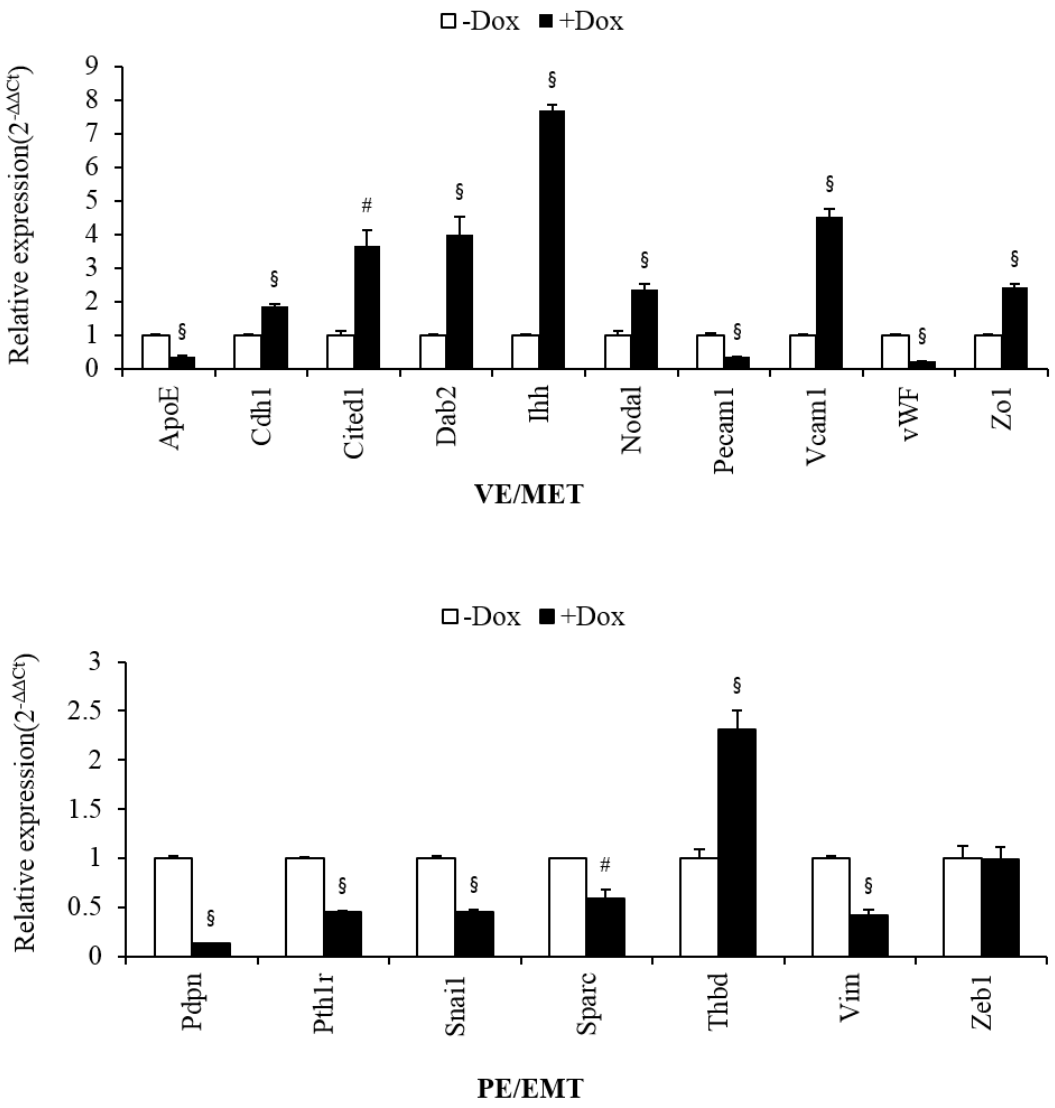

Figure 23: qRT-PCR analysis of selected marker gene expression 4 days after seeding. Gene expression was normalized to Gapdh levels, and average $2^{-\Delta\Delta Ct}$ values of the -Dox condition were set as 1. #, P<0.05; §, P<0.001.

This phenotypical change was accompanied by the increased expression of the epithelial markers, Zo1 and Cdh1. Simultaneously, we observed a significant upregulation of VE markers Dab2, Ihh, and Nodal (Figure 23 *UPPER*) and a substantial decrease of the PE markers Pth1r, Snai1, Sparc, and Vim. Potentially of interest, we also observed a reduction of endothelial marker expressions, Pecam1 and vWF (Figure 23 *LOWER*).

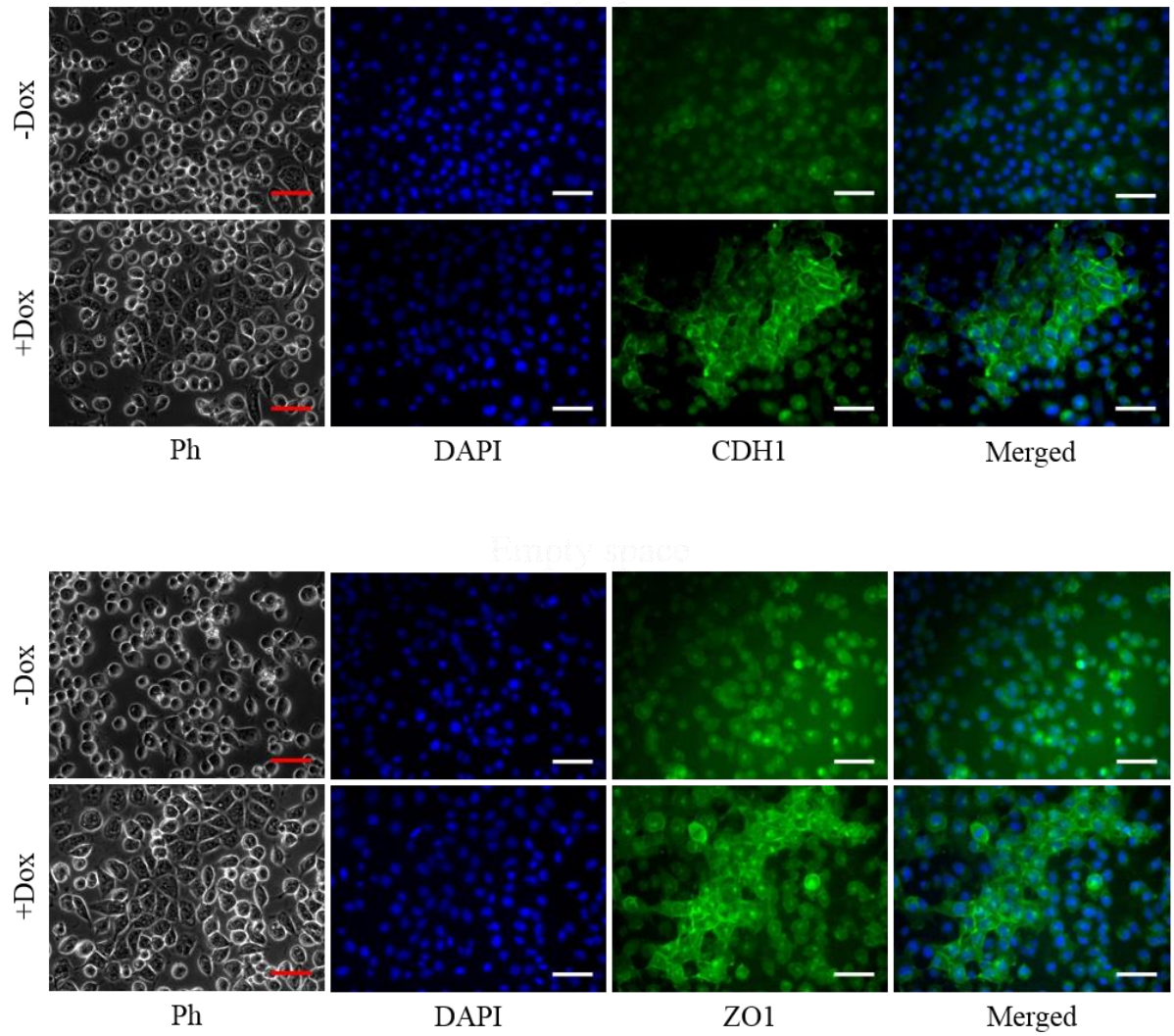

Figure 24: Immunostaining for the epithelial markers. Cdh1 (*UPPER*) and Zo1 (*LOWER*), 4 days after seeding. Scale bar: 100 µm, Magnification: 200x

We further detailed the epithelial sheet and cell-cell contacts in iOX1 cells treated with Dox (1.0 µg/mL) by immunostaining. The epithelial and tight junction marker CDH1 and ZO1 were localized at the border of cell-cell contact regions (Figure 24).

Thus, the transgenic experiments confirm the notion that an increased Oct4 level has the capacity to promote MET/VE differentiation of pXEN cells, which appears to occur after an initial stimulation of motility. Of note, the effect of upregulated Oct4 in transgenic cell line showed more pronounced gene expression contrast compare to the wild type LD VS HD condition (comp. Figure 10B *LOWER* with Figure 23 *LOWER*).

4.3.4 Forced human Oct4 expression prevents duct formation on the feeder

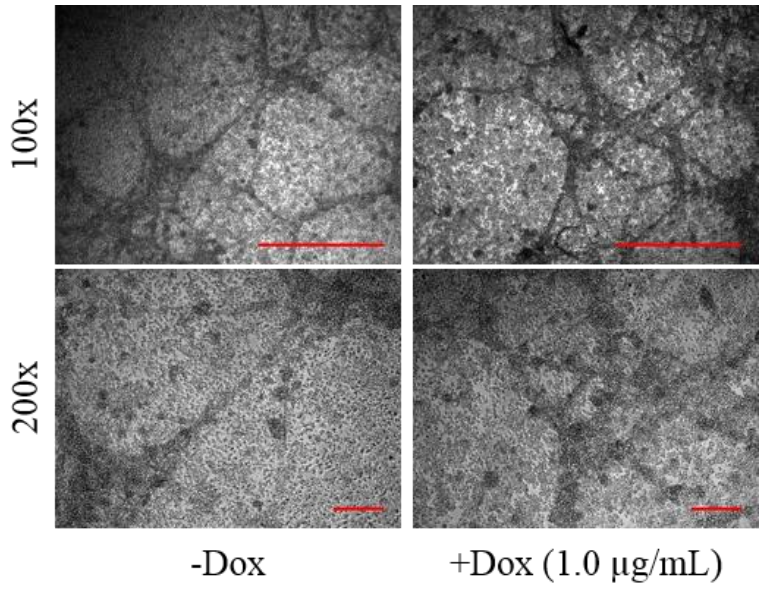

Figure 25: Doxycycline administration did not affect the pXEN-specific ductal structure formation in the wild-type cells. The cells were cultured on feeder cells for a week with high serum medium. Scale bar, 100x: 500 µm; 200x: 100 µm

In addition to the promoting MET process, the Dox-stimulated Oct4 expression in iOX1 also had a second morphological effect. As mentioned above, at HD condition, pXEN cells start to aggregate then undergo a duct-like structure formation spontaneously.

To investigate the effect of forced Oct4 during ductal structure formation, first, we need to clarify whether the Dox treatment can affect this phenotype or not. In the wild-type pXEN cells, Dox (1.0 µg/mL) administration did not alter the duct-like structure formation in HD condition (Figure 25).

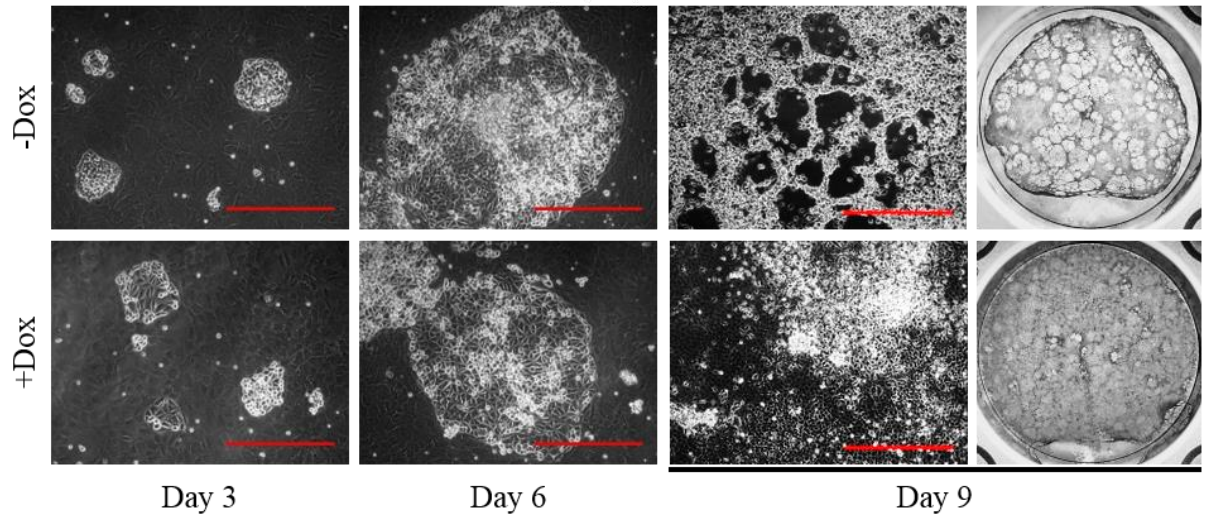

Figure 26: Dox-induced overexpression of hOct4 suppresses the formation of duct-like structures in iOX1 cells grown on the feeder. Representative phase-contrast photos (first three columns counting from the left; Scale bar: 500 µm, Magnification: 100x). *Far-right column.* Crystal violet-stained images of the whole wells on day 9.

Strikingly, in the transgenic iOX1 cells, this duct-like structure formation was abolished entirely in the presence of Dox (Figure 26). This phenomenon mirrors the foregoing observation that Oct4 RNAi accelerates the aggregation of the piled-up cells (see Figure 11 *LEFT*). The iOX1 cells with Dox became completely flattened as epithelial cells, this phenotype again confirming that increased Oct4 level promoted MET process in pXEN cells.

4.4 Endogenous Oct4 targeting causes defects in pXEN cell maintenance

In order to gain insight into the role of Oct4, we tried to abolish Oct4 expression in iOX1 cells by using TALEN and surrogate reporter system (Figure 27, 28A).

A

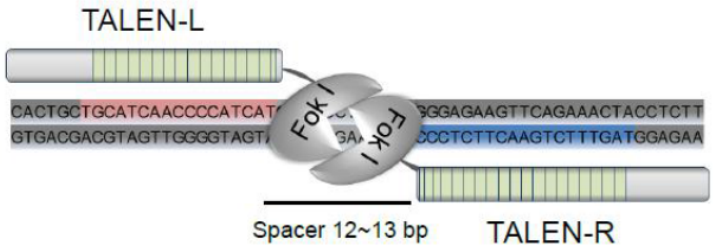

TALEN-L1-DAS sequence
5' TTCAGAGGTGCTGGGGATCT

TALEN-R1-RR sequence
5' TCCACAGAACTCGTATGCTG

B

Oct4 Target sequence (Exon1)
TCAGCAGGGCTGGAGCCGGGCTGGGTGGACCCTCGAACCTGGCTAAGCTTCCA
GGGGCCTCCAAGTGGGCCTGGAATCGGACCAGGTTCAGAGGTGCTGGGGATCT
CCCCGTGTCCCCCAGCATACGAGTTCTGTGGAGGG**ATG**GCATACTGTGGACCTC
AGGTTGGACTGGGCCTAGTCCCCCAAGTTGGCGTGGAGACTCTGCAGCCCGAG
GGCCAGGCAGGAGCACGAGTGGAGAGCAACTCGGAGGGAGCCTCCTCTGGGC
CCTGTACTGCCCGCCCCAGCGCCGTGAAGTTGGAGAAGGTGGAACCTAGTCCC
GAGGA

C

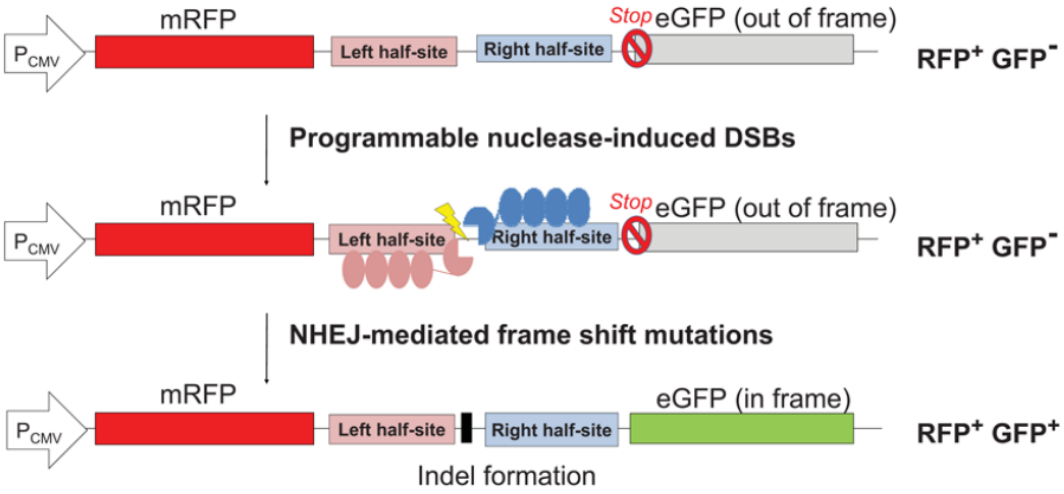

Figure 27: Oct4 knockout by TALEN. (A) Schematic illustration of Oct4 targeted TALEN and its sequence. (B) Rat Oct4 target sequence. (C) Schematic illustration of surrogate reporter system. Reporter gene (eGFP) expression is recovered by frameshift mutation induced by engineered nucleases (Modified from ToolGen TALEN datasheet).

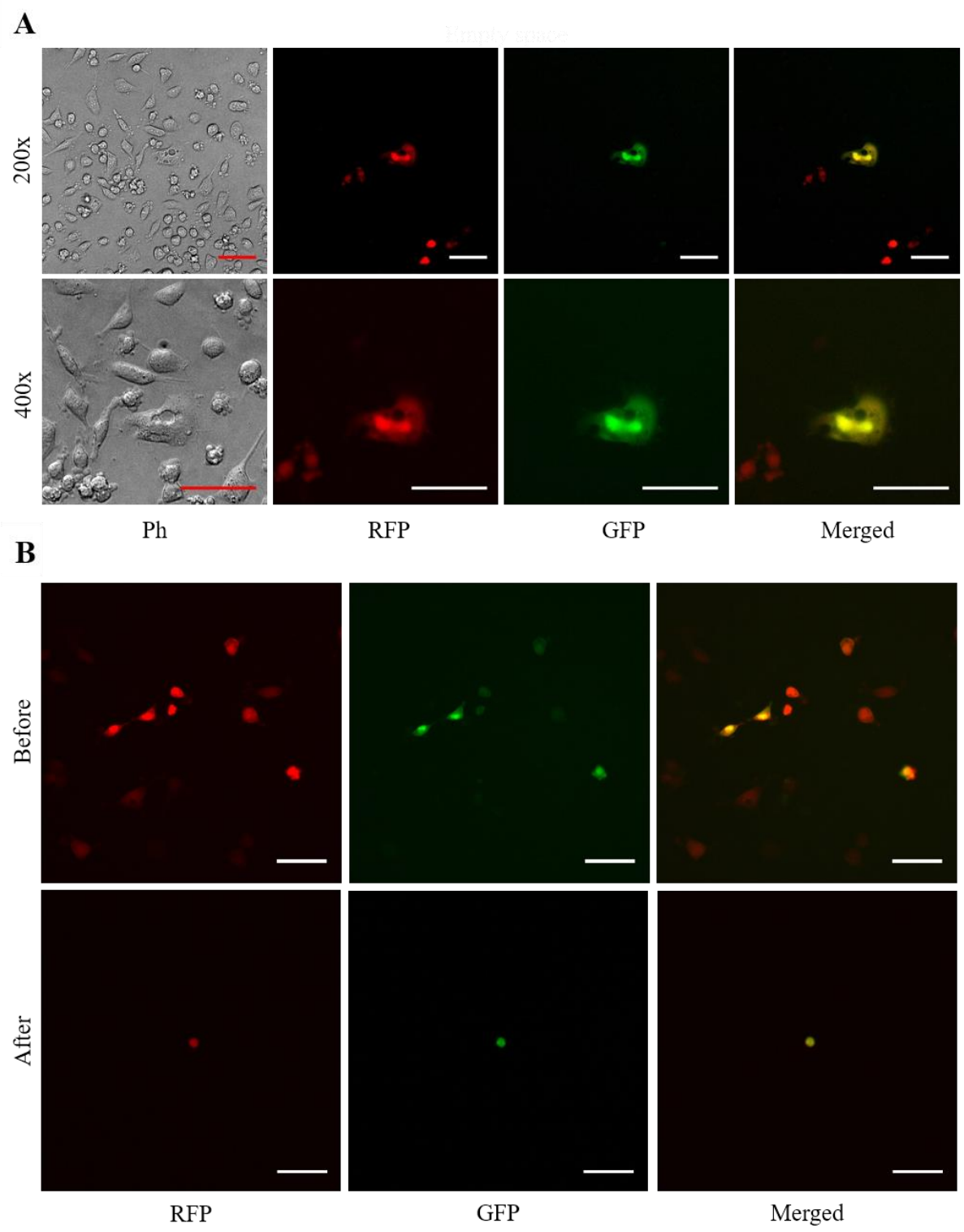

Figure 28: TALEN mediated Oct4 knockout. (A) Frameshift mutation induced by TALENs recovered surrogate reporter expression (GFP). Scale bar: 100 µm, (B) Isolation of GFP/RFP double-positive single cell by using manipulator after TALEN/surrogate reporter vector co-transfection. Scale bar: 500 µm, Magnification: 100x.

Due to the poor knockout efficiency, we could not use the limiting dilution step for single-cell cloning. Hence, a total of 28 GFP/RFP double-positive single cells were manually picked up using a micromanipulator from three independent TALEN/reporter co-transfection experiments. However, any single cell-derived colonies could not be recovered even in the presence of Dox (1.0 μg/mL) from the repeated experiments (Figure 28B). Perhaps this indicating a requirement of a sophisticated adjustment/fine-tuning of endogenous Oct4 expression or frameshifting of the Oct4 locus is critical for pXEN cell survival and proliferation.

4.5 cAMP analog forskolin, but not various Wnt pathway inhibitors, counteracts doxycycline induced Oct4 effect

Wnt signaling has been shown that as a critical factor for promoting MET/VE, while cAMP/Pthrp signaling induces PE differentiation in rat XEN cells (Chuykin et al., 2013). Based on this study, we further investigated whether the activation of Wnt or cAMP signaling pathways also can induce VE or PE differentiation in pXEN cells, respectively. For this, we tested GSK3 inhibitor, CHIR99021 (CHIR), an analog of cAMP, forskolin (FSK). After four days of CHIR and FSK administration, we can observe significant morphological changes in both conditions. As previously demonstrated in rat XEN cells, FSK treatment on pXEN cells results in mesenchymal transition together with filopodia formation.

In contrast, CHIR-treated cells displayed epithelialization (Figure 29A). These results also support that, like rat XEN cells, GSK3-mediated activation of canonical Wnt signaling pathway induces VE differentiation. Whereas, cAMP/Pthrp signaling pathway promotes PE differentiation in rat pXEN cells.

To see whether the morphological changes are associated with MET gene regulation, we performed the qRT-PCR analysis. Figure 29B shows alteration of gene expression in FSK- and CHIR-treated pXEN cells. The overall gene expression pattern was similar to the previous result from the rat XEN cells. However, in the FSK-treated group, Lamb1 (PE-associated extracellular matrix molecule) and Nodal (VE marker) expressions were significantly increased in pXEN cells, which is the opposite pattern to the previous study in rat XEN cells (Chuykin et al., 2013). Our results may suggest that the fundamental difference between rat XEN and pXEN cells.

Interestingly but as expected, Dox-treated iOX1 cells showed a comparable gene expression pattern to CHIR-treated cells. Namely, epithelial and VE-associated genes Cdh1, Cited1, and Nodal were increased. Also, PE-associated genes Pth1r, Snai1, and Vim were decreased in both +Dox and CHIR-treated groups (Figure 29B).

Furthermore, we found that endogenous Oct4 level was significantly downregulated in both FSK and CHIR-treated cells (Figure 29B *UPPER*). In fact, Oct4 has been noted that collaborate with Wnt signaling to facilitate endodermal differentiation (Ying et al., 2015).

A

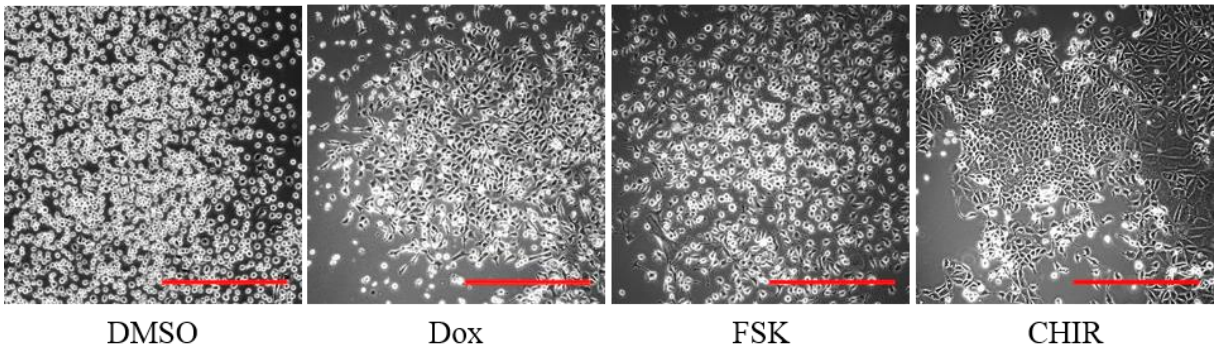

B

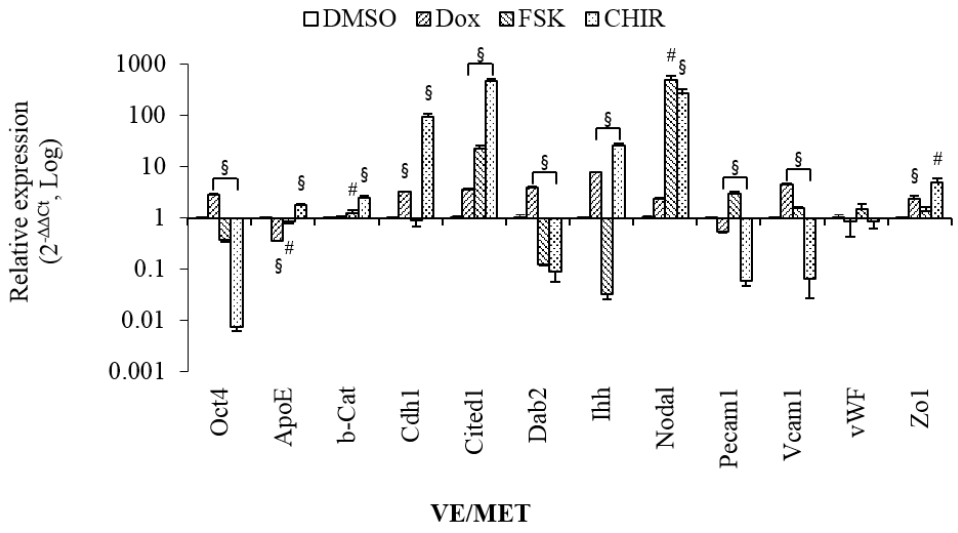

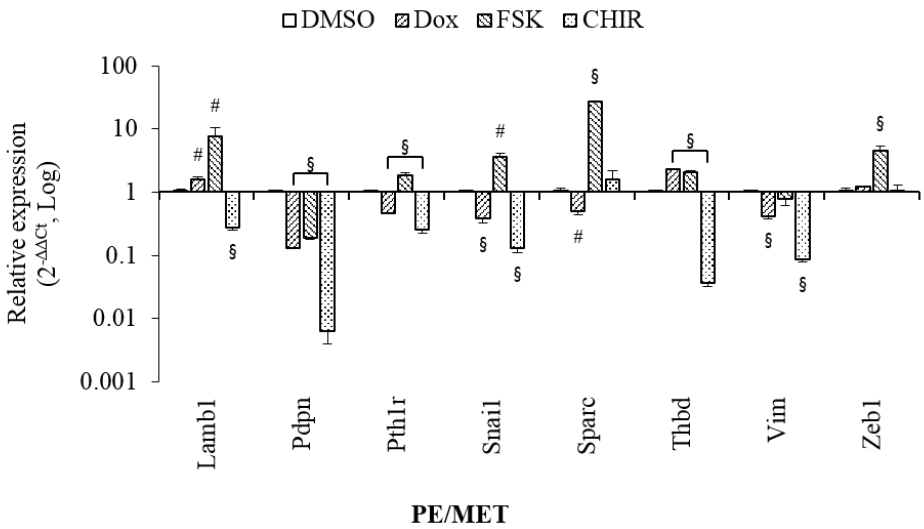

Figure 29: Effect of FSK and CHIR on iOX1 cells. (A) Phase-contrast photos of iOX1 cells treated with Dox (1.0 µg/mL), FSK (10 µM), and CHIR (3.0 µM) for 4 days. Scale bar: 500 µm, Magnification: 100x. (B) Validation of FSK and CHIR effect on iOX1 cells by qRT-PCR. Relative expression was normalized to Gapdh levels, and average $2^{-\Delta\Delta Ct}$ values of the DMSO condition were set as 1. #, P<0.05; §, P<0.001.

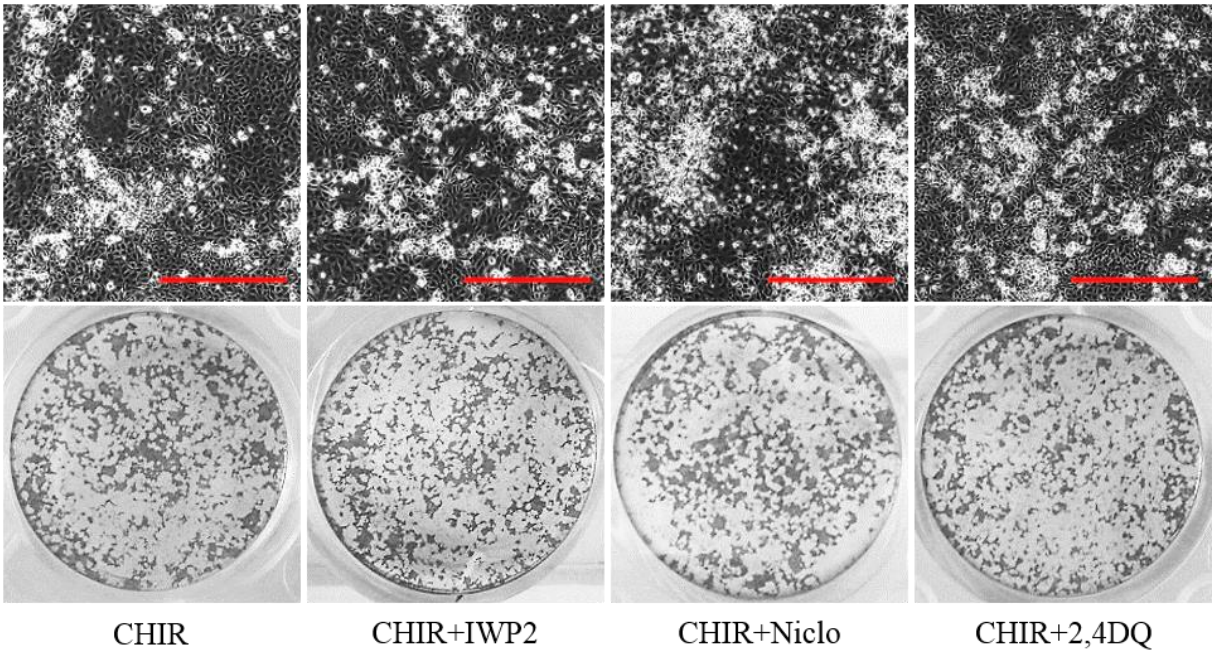

Figure 30: Effect of three different Wnt inhibitors in CHIR-treated wild-type cells. Cells were cultured for 4 days in the presence of CHIR (3.0 µM). *UPPER*, Shown are phase-contrast photos on day 4. Scale bar: 500µm, Magnification: 100x; *BOTTOM*, Stereomicroscopic images after Crystal violet staining. IWP2: 1µM, Niclosamide (Niclo) and 2,4 Diaminoquinazoline (2,4DQ): 0.1 µM,

Since Wnt signaling appears to promote MET/VE differentiation in pXEN cells, we then tested three inhibitors with different targets in Wnt signaling cascade stage (IWP2, Porcupine-; Niclosamide, Frizzled-, 2,4-DAQ, TCF/β-catenin-inhibitor, Ref. Figure 6). However, none of them can block/blunt the morphological change or MET induced by CHIR-treatment in pXEN cells (Figure 31A). Likewise, none of the inhibitors altered MET/VE marker expression in the Dox-treated iOX1 cells; instead, the inhibitors suppressed the mesenchymal marker Snai1 (Figure 31B).

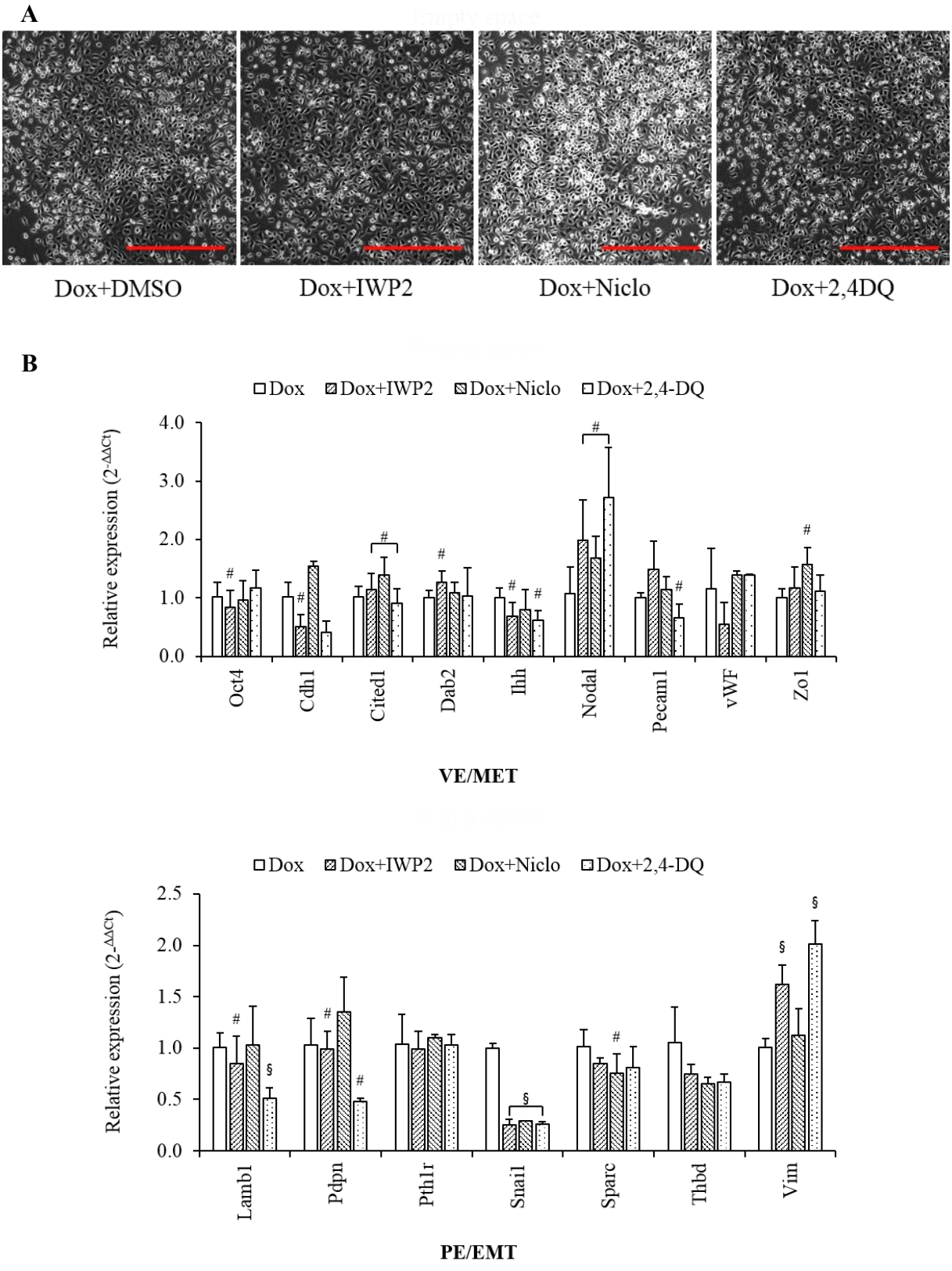

Figure 31: Assessment of Wnt inhibitors in the presence of Dox for 4 days. (A) iOX1 cells were culture for 4 days in the presence of Dox (1.0 µg/mL); IWP2: 1µM; Niclo and 2,4DQ: 0.1 µM. Scale bar: 500µm, Magnification: 100x. (B) Validation of Wnt inhibitors effect on iOX1 cells by qRT-PCR. Gene expression was normalized to Gapdh levels, and average $2^{-\Delta\Delta Ct}$ values of the Dox condition were set as 1. #, P<0.05; §, P<0.001.

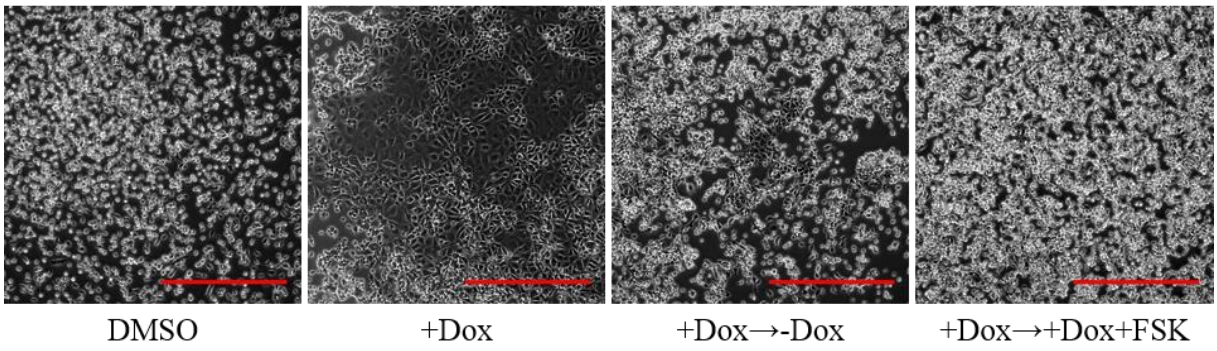

Figure 32: Sustained Oct4 overexpression is required to achieve MET, which is counteracted by forskolin treatment. The cells were cultured for 4 days as follows. DMSO, 1 µl/mL of DMSO; +Dox, 1.0 µg/mL of Dox (1.0 µg/µL); +Dox→-Dox, 1.0 µg/mL of Dox for the first two days then withdrawn; +Dox→+Dox+FSK, 1.0 µg/mL of Dox throughout for 4 days, but with forskolin (10 µM) in the final two days. Shown are phase-contrast photos on Day 4. Magnification: 100x, Scale bar: 500 µm,

Since the forskolin is known to promote the PE and inhibit the VE differentiation, we asked whether forskolin can counteract the forced Oct4-induced phenotype (*i.e.,* VE differentiation and prevention of the duct-like structure formation). And this was indeed the case (Figure 32). 24 hours administration, then the withdrawal of Dox stagnated MET/VE differentiation. Moreover, Dox. and FSK co-treated cells completely block the upregulated Oct4-mediated epithelialization. This result suggests that Oct4 induced MET was entirely counteracted by the adenylate cyclase activator, forskolin.

4.6 TGFβ ligand Activin A, but not BMP4, effectively induces MET

According to previous studies, TGFβ signaling (via Nodal/ Activin and BMP) can promote the MET process in XEN cells (Kruithof-de Julio et al., 2011, Paca et al., 2012). Since XEN and pXEN cells are closely related, we investigated the effect of BMP4 and Activin A on pXEN cells.

A

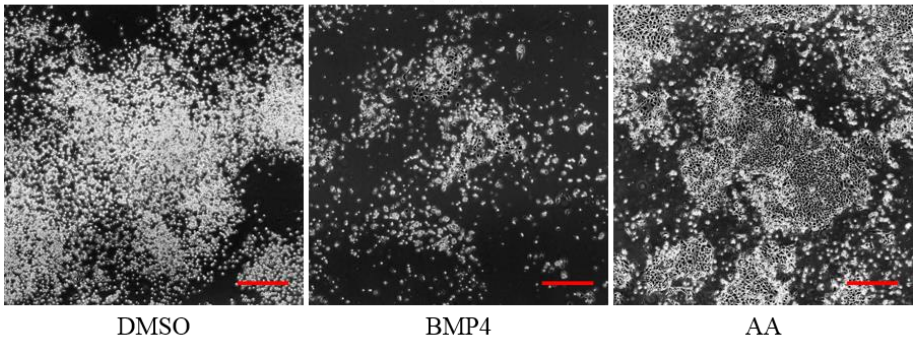

B

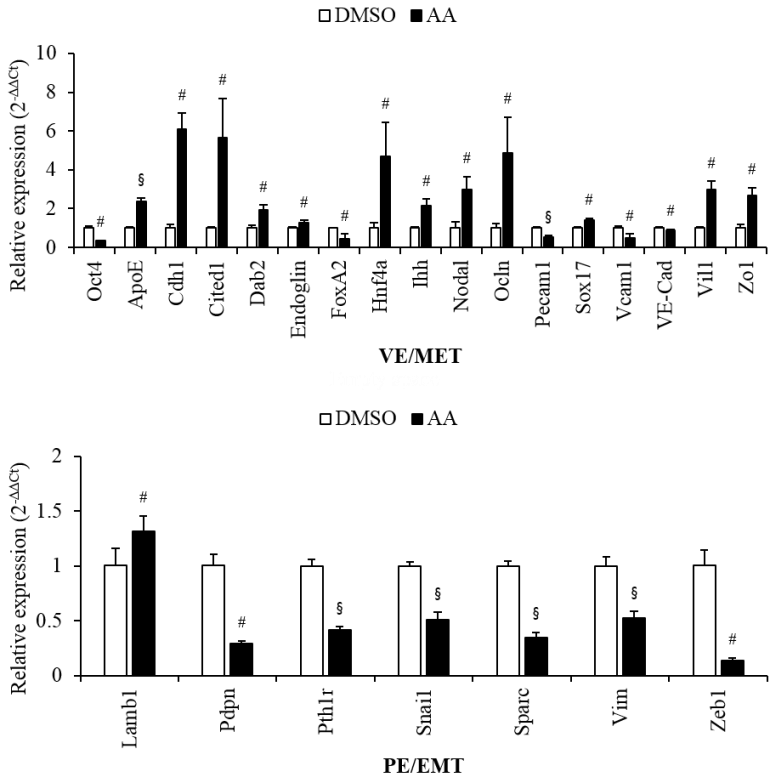

Figure 33: Activin A-induced VE/MET in pXEN cells. (A) Representative phase-contrast images of BMP4 (50 ng/mL) and Activin A- (AA, 10 ng/mL) treated pXEN cells on day 4. Scale bar: 500 µm, Magnification: 100x. (B) qRT-PCR analysis of selected VE/MET or PE/EMT marker genes expression in Activin A-treated pXEN cells. Gene expression was normalized to Gapdh levels, and the average $2^{-\Delta\Delta Ct}$ value of DMSO condition was set as 1. #, P<0.05; §, P<0.001.

Unlike the rat XEN cells, BMP4 treatment (50 ng/mL) exhibited cytotoxicity instead of promoting the MET process. While Activin A treatment efficiently generated a homogenous epithelial-like cell population without cytotoxicity (Figure 33A). This result also supported that pXEN cells possess unique characteristics distinct from XEN cells.

The qRT-PCR analysis revealed that Activin A (10 ng/mL) treatment upregulates VE-associated gene expression. Generic VE marker ApoE and extraembryonic VE genes such as Cited1, Ihh, and Hnf4a were significantly induced altogether after 4 days of Activin A treatment. As expected, MET-associated and tight junction marker genes (Cdh1, Ocln, and Zo1) were significantly induced. Also, concomitant reduction of mesenchymal genes (Snai1, Vim, and Zeb1) was observed. However, the PE-associated ECM gene, Lamb1, was highly upregulated in Activin-treated cells (Figure 33B).

4.7 TGFβ (ALK5) inhibitor Repsox blunts Dox- and high density-induced MET

We next investigated different TGFβ inhibitors to identify which target or downstream effector is directly involved in the MET process. SB431542 (an inhibitor of the Activin type I receptor ALK4 and the Nodal type I receptor ALK7) treatment did not block the CHIR-induced MET, but Repsox (a TGFβ R1/Alk5 inhibitor) treated cells were effective (Figure 34).

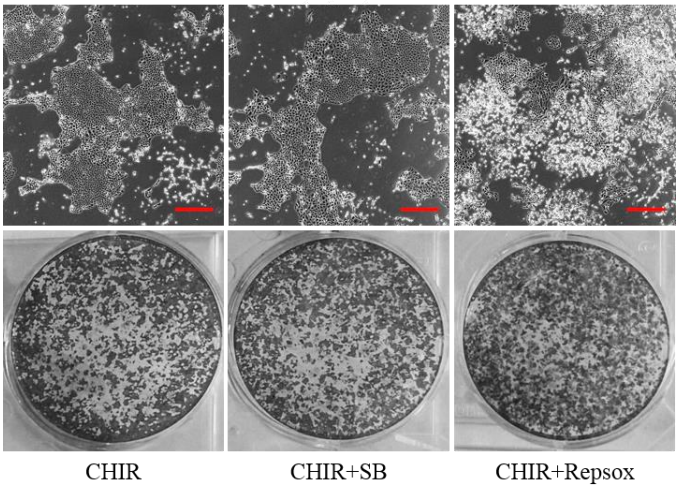

Figure 34: TGFβ inhibitor Repsox blunted CHIR-induced MET. Wild-type cells were cultured in a CHIR-containing medium for 4 days in the presence of SB431542 (SB; 10 µM) and Repsox (10 µM). *UPPER*, Phase contrast images of TGFβ inhibitor-treated wild-type cells in day 4. Magnification: 40x, Scale bar: 500 µm, *LOWER*, Stereomicroscopic images after Crystal violet staining.

In parallel, we tested these TGFβ inhibitors to see whether these also can block the Dox-induced Oct4 effect. Again, SB431542, the inhibitor of Alk2/4/7, did not show significant results. In contrast, Repsox-treated cells showed a strong tendency to maintain the mesenchymal phenotypes, although minor epithelial islands were still present (Figure 35A). It seems like a controversial result from the other previous studies that the β-catenin-mediated MET process mentioned before. It might suggest that different β-catenin-mediated MET regulatory mechanism presents in pXEN cells. To gain insight into this unexpected Repsox effect, we conducted gene expression analysis. The qRT-PCR result reveals that Repsox and Dox co-treatment significantly downregulates epithelial markers (Cdh1 and Zo1) as well as VE markers (Dab2, Ihh, and Nodal) (Figure 35B *UPPER*). In contrast, PE-specific markers Lamb1, Pth1r, and Sparc were induced in Repsox treated cells. Also, the mesenchymal markers were increased (Snai1) or not significantly changed (Vim, Zeb1) (Figure 35B *LOWER*). In correspondence with the gene expression results, the addition of Repsox made the mesenchymal morphology more prominent in the culture.

A

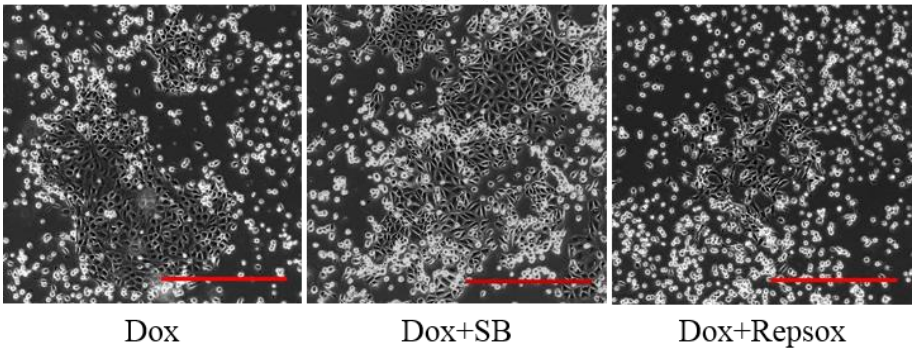

B

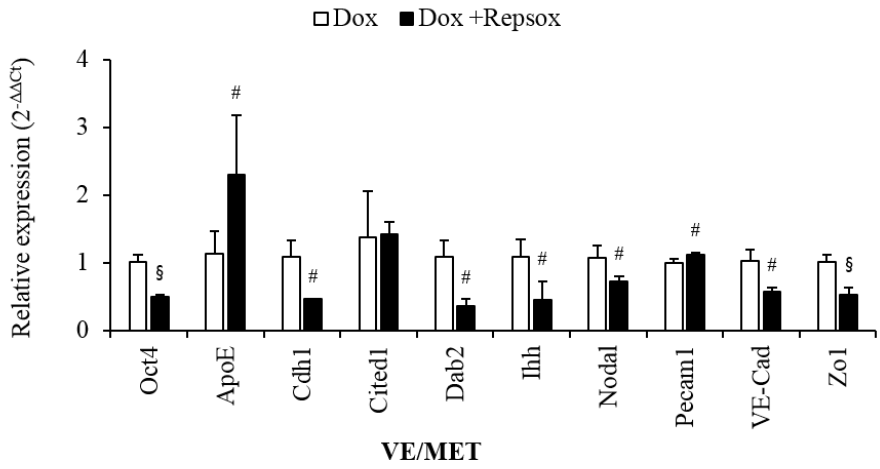

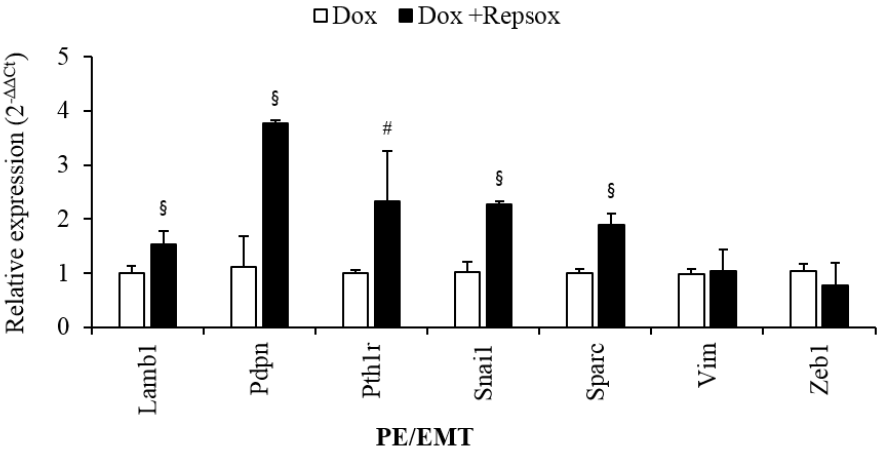

Figure 35: ALK5 inhibitor Repsox blunts Dox-induced MET. (A) iOX1 cells were culture in Dox-containing (1.0 µg/mL) medium for 4 days in the presence of SB (SB431542, 10µM) and Repsox (10µM). (B) Effect of Repsox treatment on selected marker genes in the presence of Dox. Gene expression was normalized to Gapdh levels, and the average $2^{-\Delta\Delta Ct}$ value of the Dox condition was set as 1. #, P<0.05; §, P<0.001.

A

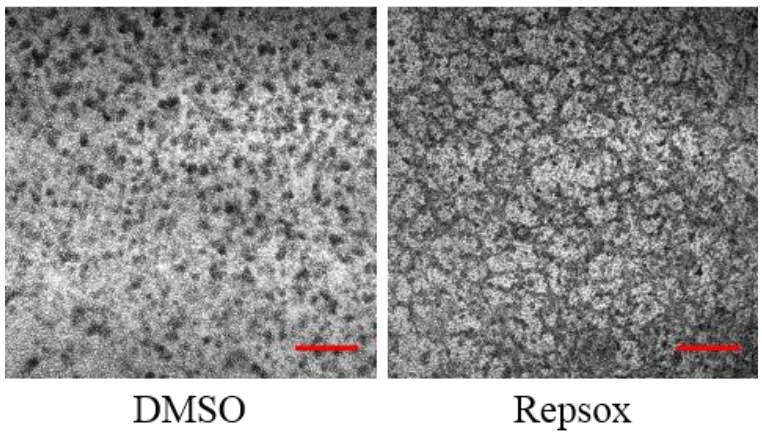

B

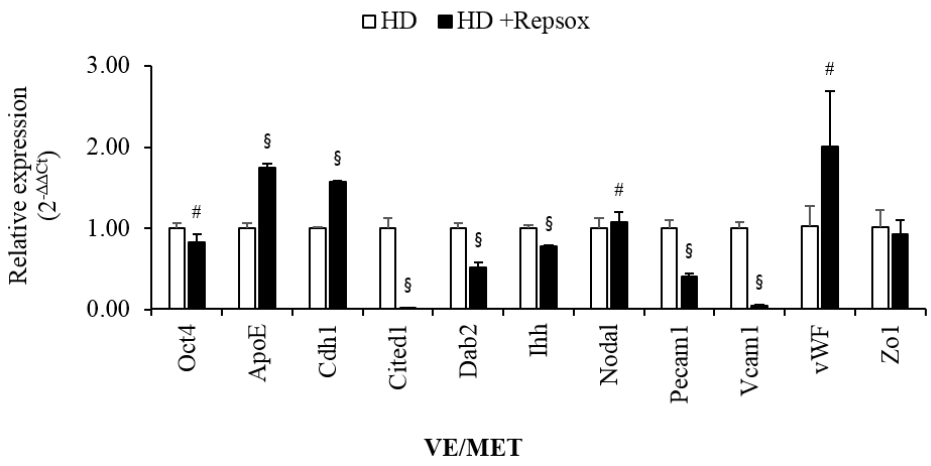

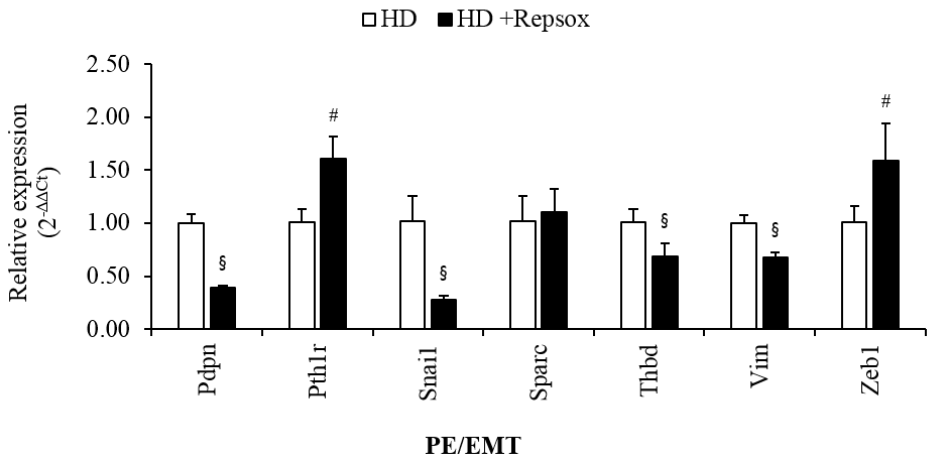

Figure 36: Repsox facilitates aggregation/duct formation in HD culture condition. (A) Wild-type cells were cultured for 3 days in the presence or absence of Repsox (10 µM). Scale bar: 500 µm, (B) Effect of Repsox treatment on selected marker gene expression at HD. Gene expression was normalized to Gapdh levels, and the average $2^{-\Delta\Delta Ct}$ value of HD condition was set as 1. #, P<0.05; §, P<0.001.

We then further test the Repsox on the wild-type cells at HD condition, which initially observed the increase of endogenous Oct4. In the HD culture condition, similar to the effect of the Oct4 knockdown, Repsox facilitated aggregation and accelerated duct-like structure formation (See Figure 11, Figure 36A).

On the level of gene expression, we observed suppression of VE markers (Dab2, Ihh, and Cited1) and a moderate upregulation of PE and mesenchymal cell markers (Pthr1 and Zeb1) but no change of Sparc expression. With respect to the mesenchymal versus epithelial phenotype, we did not observe any significant changes that would replicate the results of the Oct4 RNAi. The epithelial marker Cdh1 increased, and Snai1 decreased (in accord with MET that tends to go along with VE differentiation), Zeb1 (mesenchymal), and Pthr1 and Sparc (PE) were not decreased or even slightly increased (Figure 36B) in Repsox treated HD condition.

Overall, The effects of Repsox on Oct4 inducing conditions (Dox. and HD-induced Oct4) exhibit similar gene expression profiles. Additionally, the experimental group using transgenic cell line revealed more reproducible and predictable results than the HD condition group due to the heterogeneous cell population in the HD condition.

4.8 Inhibition of Rho/Rock signaling pathway induced PE differentiation and disrupted Dox-induced MET transition

The Rho/Rho-associated coiled-coil-forming protein kinase (Rock) signaling pathway has been demonstrated as a regulator of lineage commitment (McBeath et al., 2004), cytoskeleton rearrangement, and cell polarity (Amano et al., 2010). Also, it may participate in the fibroblast differentiation and expression of smooth muscle actin protein (Ji et al., 2014). Besides, it has been reported that inhibition of the Rho/Rock signaling pathway is required for TGFβ-induced EMT of epithelial cells (Korol et al., 2016).

Meanwhile, according to Chuykin et al., CHIR-induced epithelial transition in rat XEN cells exhibited cortical actin expression together with Cdh1 and Zo1 (Chuykin et al., 2013). More importantly, Pdpn activates RhoA and promotes the EMT process in epithelial Madin-Darby canine kidney (MDCK) type II cells (Martin-Villar et al., 2006). In this context, we investigated the Pdpn level from the different conditions to see the correlation between EMT and Pdpn expression. Interestingly, the qRT-PCR results consistently exhibited opposite Pdpn patterns against endogenous Oct4 (HD, siRNA, and Dox-induced Oct4 condition).

Based on the previous studies, we headed toward the Rock inhibitor (Ri, Y-27632) to investigate the correlation between the RhoA/Rock signaling pathway and Oct4-induced phenomena.

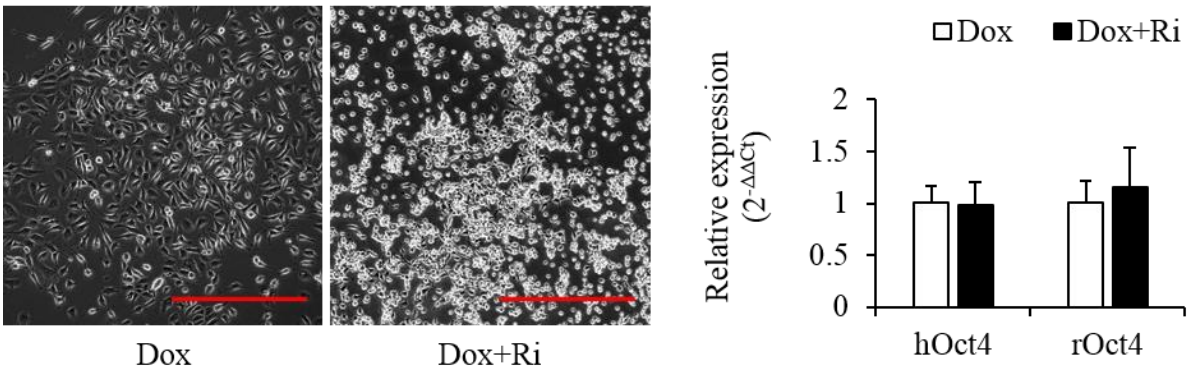

Figure 37: Rock inhibitor Y-29632 counteracts Oct4 induced MET transition. *LEFT*, Representative phase-contrast images of Ri (Rock inhibitor; Y-27632, 10 µM) treated iOX1 cells in the presence of Dox (1.0 µg/mL, Day 4). Scale bar: 500 µm: Magnification: 100x. *RIGHT*, Human and rat Oct4 expression level of the Rock inhibitor-treated-iOX1 cells in the presence of Dox (1.0 µg/mL). Oct4 expression was normalized to Gapdh levels, and the average $2^{-\Delta\Delta Ct}$ value of the Dox condition was set as 1.

As we hypothesized, Rock inhibitor (Ri), Y-27632 increased cell motility and completely disrupted Dox-induced epithelialization within 4 days (Figure 37) and revealed a similar effect on gene expression pattern as the Repsox (Figure 38). However, unlike the Repsox treatment, Ri did not change the endogenous Oct4 level. Instead, it significantly suppressed VE markers such as Vil1 and β-catenin (Figure 38). As we depicted before, Ri selectively mimics the effect of Repsox in gene expression patterns. Although the Pth1r expression level was not affected, the VE/MET markers Cdh1, Dab2, VE-cad, and Zo1 were also significantly downregulated. While PE/EMT genes Lamb1, Snai1, and most importantly, Pdpn were significantly increased (Figure 38). In conclusion, inhibition of the Rho/Rock signaling pathway induces Pdpn expression and disrupts MET without altering the endogenous Oct4 expression in pXEN cells.

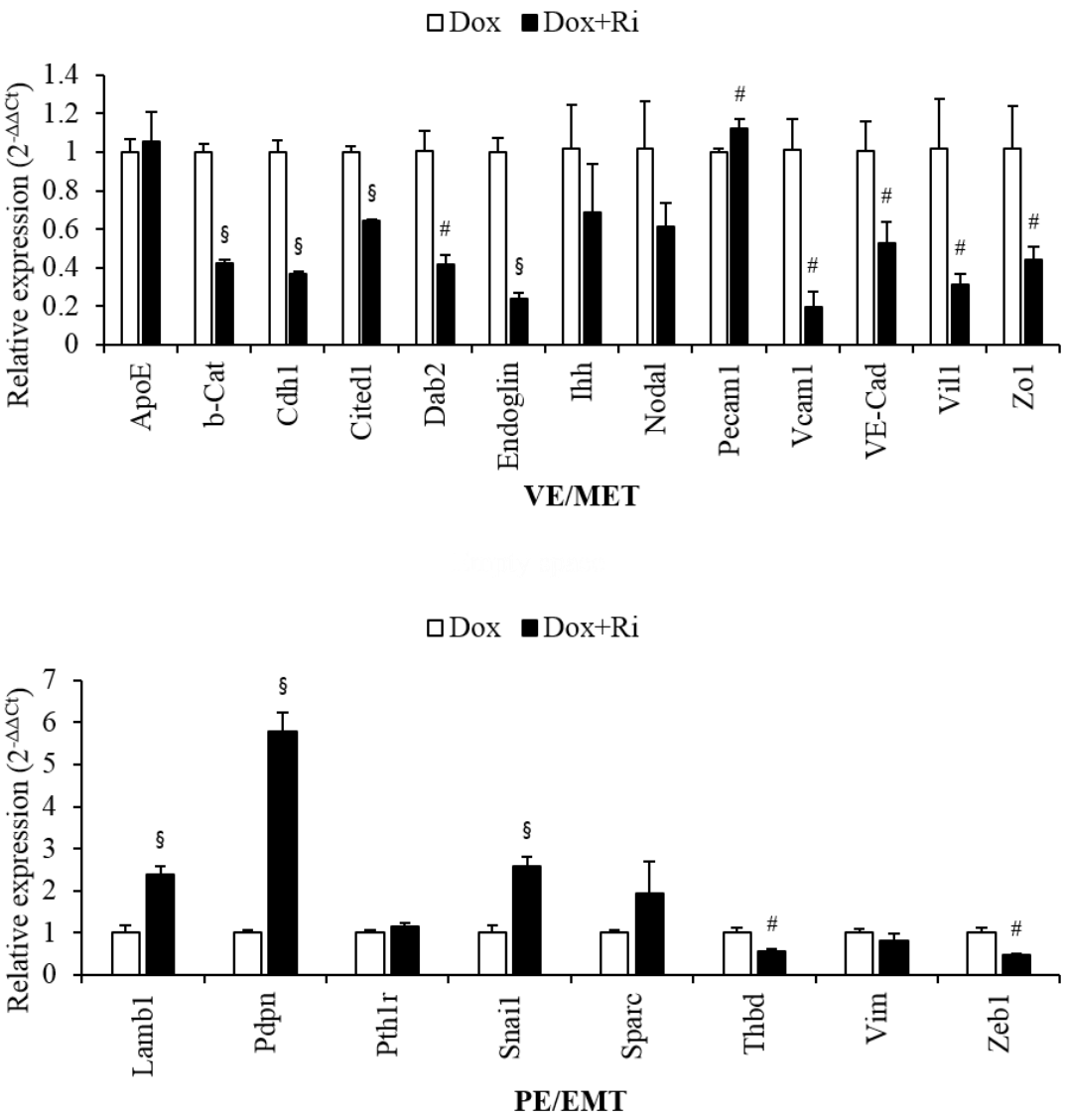

Figure 38: Effect of Rock inhibitor on selected marker gene expression in Dox-treated iOX1 cells. Gene expression was normalized to Gapdh levels, and the average $2^{-\Delta\Delta Ct}$ value of the Dox condition was set as 1. #, P<0.05; §, P<0.001.

4.9 Modified rat ES cell culture condition facilitates epithelial duct-like structure formation

Many researchers have demonstrated that somatic cells could be reverted into an ES cell-like state by introducing a set of transcription factors. It has been shown that the Oct4 overexpression together with a specific combination of small molecules was sufficient to generate iPSCs from mouse fibroblasts (Li et al., 2011). Also, fine-tuning of β-catenin activity is crucial for rat ES cell self-renewal and stemness stabilization (Meek et al., 2013). Based on these previous studies, we tried to generate rat ES-like cells from iOX1 cells using conditional Oct4 overexpression together with classical or modified rat ES cell culture conditions.

First, we investigated pXEN cells' response to classical 2i ES cell culture medium (2i). The 2i medium contains two inhibitors, MEK (or MAPK/ERK kinase) pathway inhibitor (PD0325901 or PD) and GSK3 inhibitor (CHIR99021 or CHIR). As mentioned above, sophisticated regulation of β-catenin expression is critical for rat ES cell maintenance, so we tested 2i medium and modified media in parallel.

Interestingly, the complete 2i medium induced a highly homogenous cell population: flattened endoderm or epithelial sheet-like cells compared to the other media (see Figure 29A, Figure 39). Interestingly, the pXEN cells cultured in the 2i medium without GSK inhibitor (2i-CHIR) exhibited a round-shaped and highly motile phenotype (Figure 39).

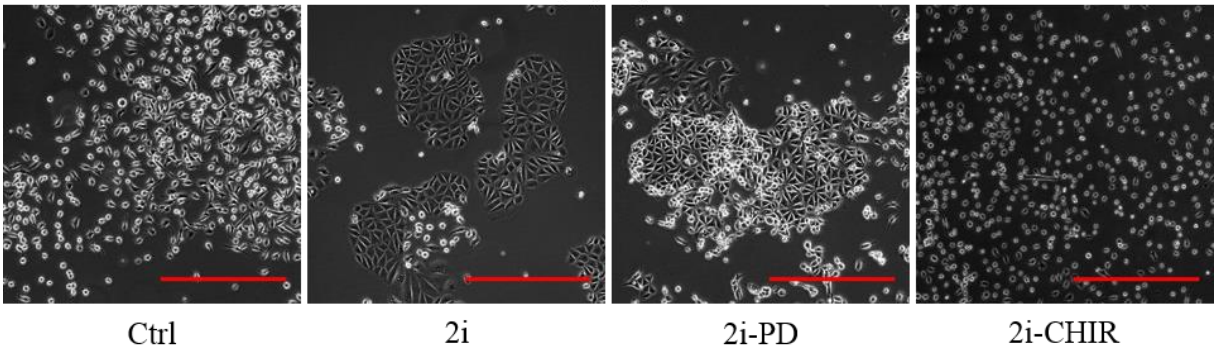

Figure 39: Effect of complete 2i rat ES cell- and modified-medium on wild-type pXEN cells. Representative phase-contrast images on day 2. Scale bar: 500 µm, Magnification: 100x.

Strikingly, from day 5, pXEN cells were cultured with 2i-CHIR medium started to differentiate into the homogenous duct-like structures (Figure 40A). So far, the duct-like structure formation

has been achieved in “on feeder” and “HD” conditions (see Figure 8D, 8G). Here, we found a novel culture condition for duct-like structure formation and named 1i condition. To identify characteristics of the duct-like structure, we performed qPCR analysis and immunostaining including endothelial vessel-specific markers (Lyve1, Pdpn, Prox1, and Vegfr3) (Figure 40B, 41B, and 43). The expression of the lymphatic endothelial cell (LEC) markers was slightly increased in the 1i culture condition. However, the overall ΔCt values of epithelial-related genes were greater than 15.

In the duct-like lattice structure, endogenous Oct4 expression was significantly downregulated. While mesendoderm markers (aSM, Eomes, T, and vWF) were highly induced more than 50 folds compare to maintain condition. Besides, epithelial/tight junction genes (Cdh1, Cited1, Pecam1, and Zo1) were highly induced in the culture 1i condition.

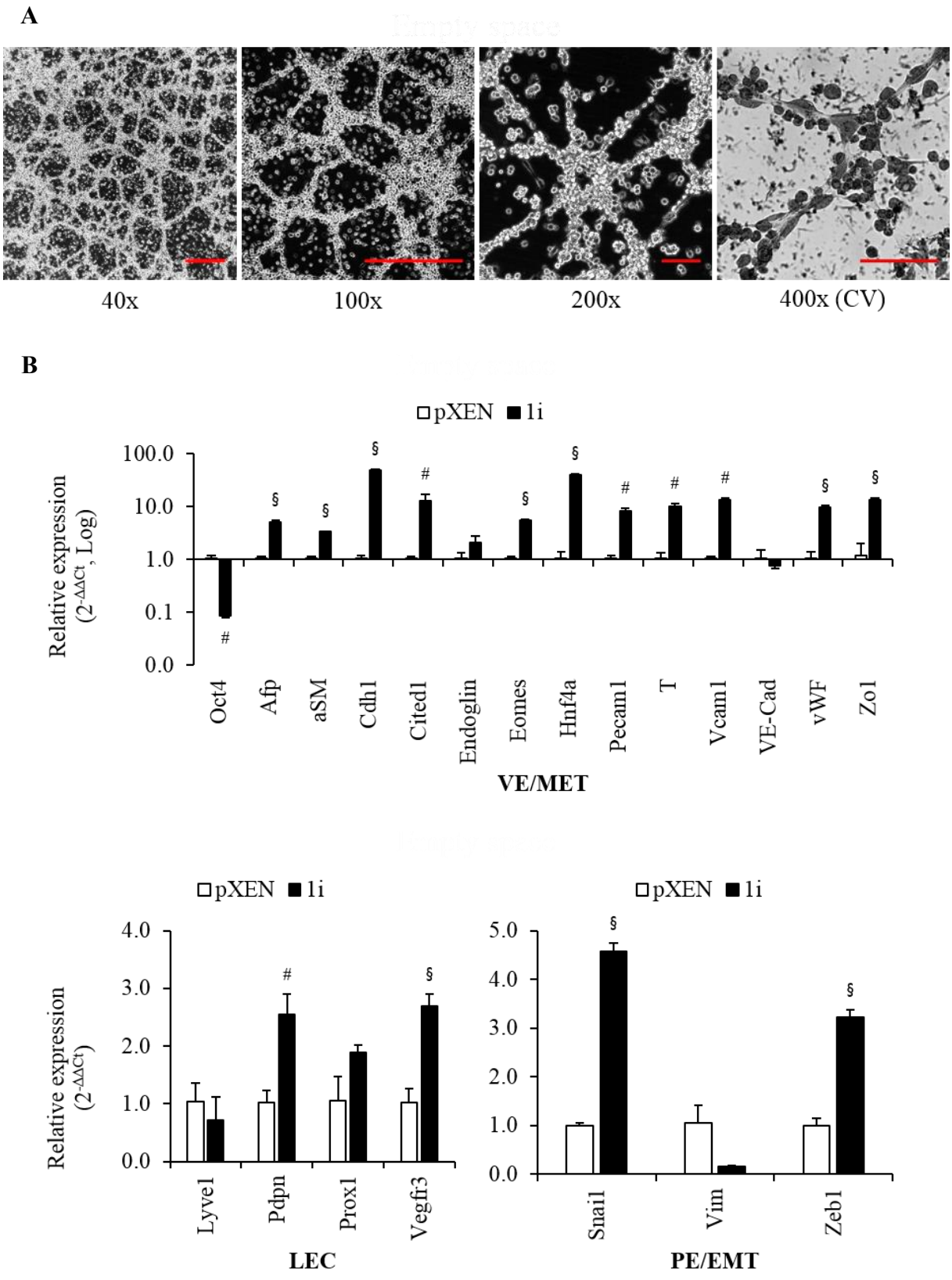

Figure 40: 1i culture condition facilitates duct-like structure formation of pXEN cells. (A) Representative phase-contrast images of pXEN cells cultured in 1i medium for 5 days. Scale bar: 500 µm (40x, 100x) and 100 µm (200x, 400x). (B) 1i condition increased mesendoderm and epithelial associated gene expression. #, P<0.05; §, P<0.001.

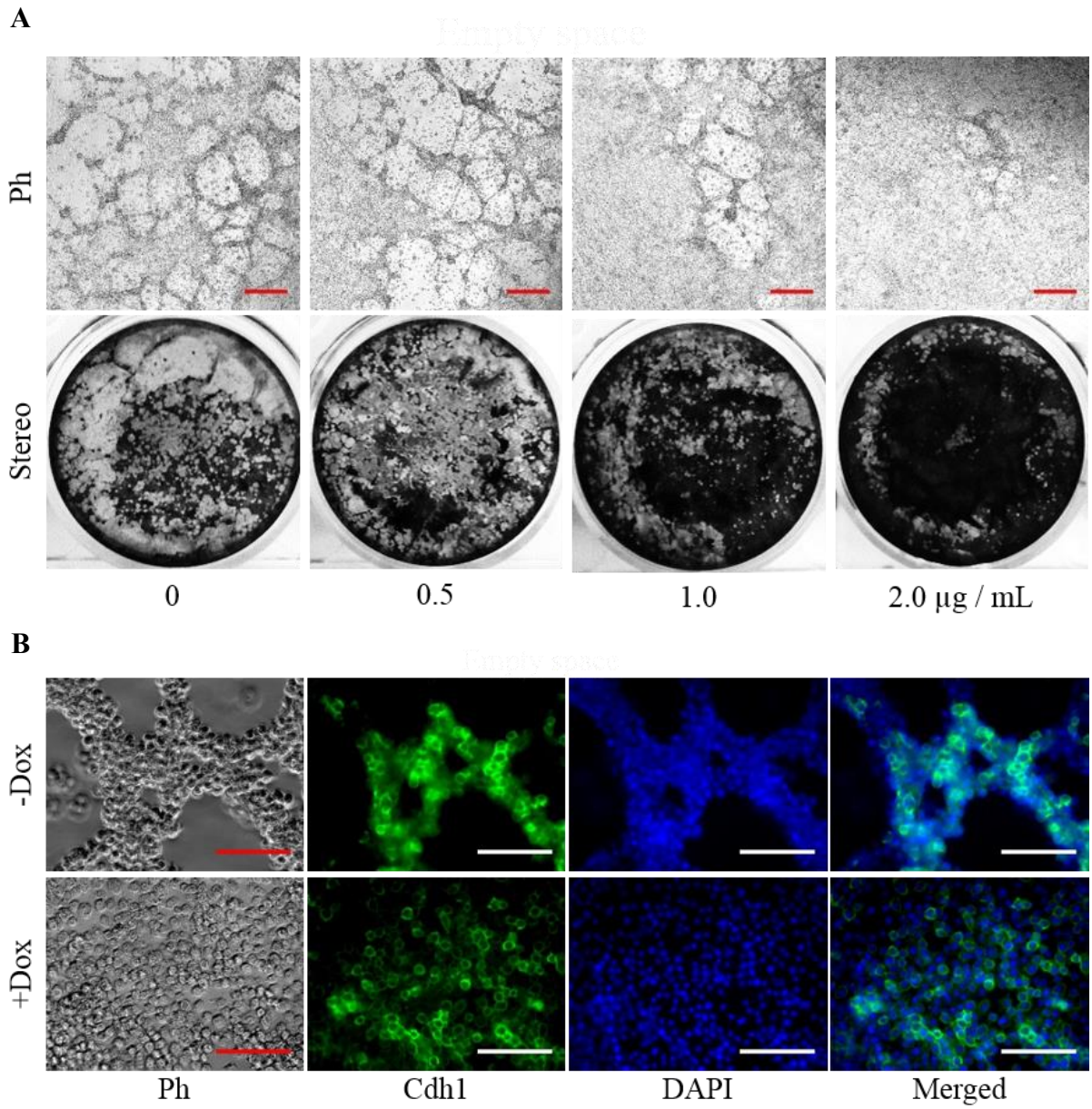

Figure 41: Forced hOct4 expression prevents duct formation and enforces epithelialization. (A) *UPPER*, representative phase-contrast images of iOX1 cells (Day 5). Cells were cultured with the indicated concentration of Dox. Scale bar: 500 µm, Magnification: 40x; *LOWER*, stereo microscopic images of whole wells (12-well) after Crystal violet staining. (B) Immunostaining for epithelial marker Cdh1. Scale bar: 100 µm, Magnification: 400x

In order to gain more confidence in Oct4-mediated MET, we employed the 1i condition to the iOX1 transgenic cell line. As expected, in the presence of Dox, homogenous epithelial-like flattened cell differentiation was observed in the Dox dose-response manner (Figure 41A).

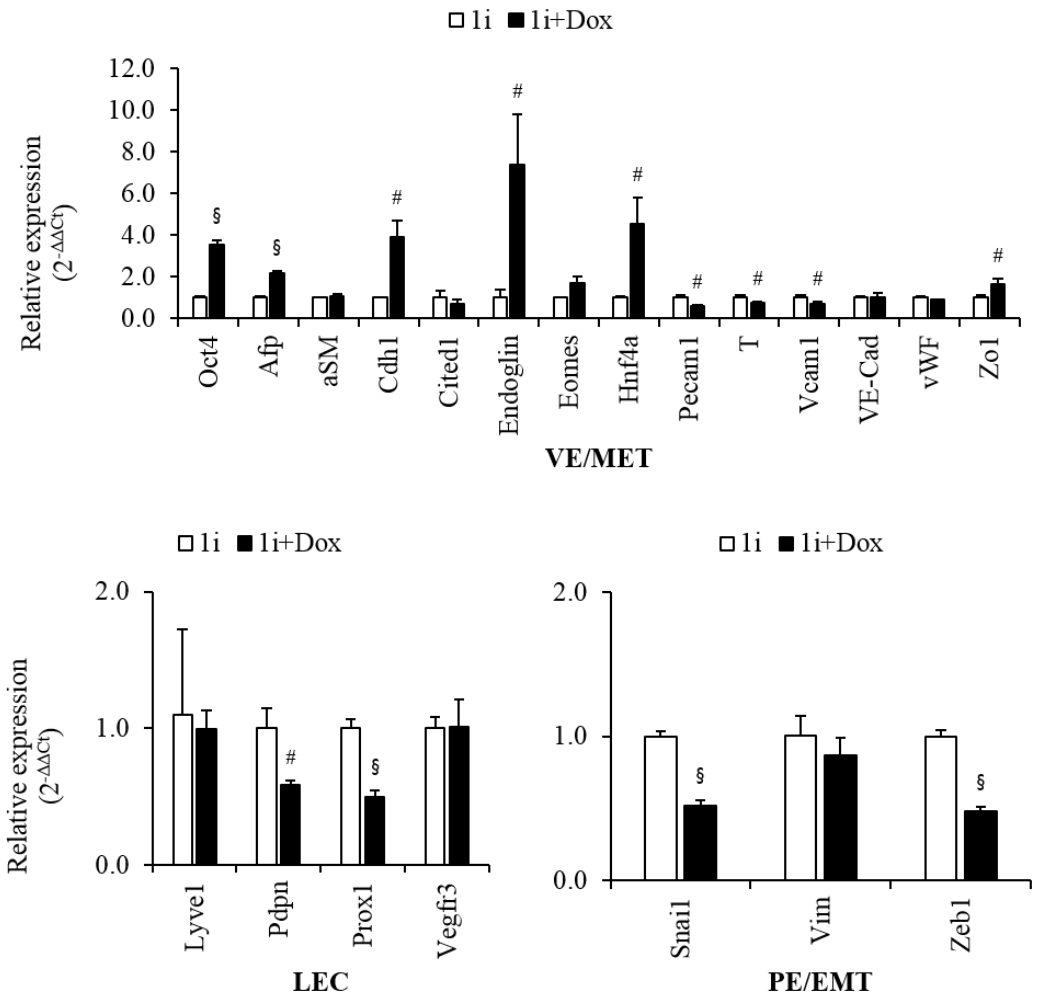

Figure 42: Assessment of 1i condition in the presence of Dox for 5 days. Gene expression was normalized to Gapdh levels, and average $2^{-\Delta\Delta Ct}$ values of the 1i condition were set as 1. The data represent three independent experiments, each performed in duplicate. The values are the means ± S.D. of triplicate samples. #, P<0.05; §, P<0.001.

The iOX1 cells cultured in the 1i medium and Dox (1.0 µg/mL) showed increased expression of endogenous Oct4. Taken together, we observed the induction of other VE genes (Afp, Cdh1, Hnf4a, and Zo1) as previously depicted. In contrast, mesenchymal markers Snai1 and Zeb1 were significantly downregulated. In parallel, LEC markers, Pdpn and Prox1 were decreased in the presence of Dox. As the phase-contrast images showed, vascular endothelial/mesoderm genes (Pecam1, T, and Vcam1) were suppressed in Dox-treated iOX1 cells. (Figure 42). In summary, Oct4 induced MET/VE differentiation is a common feature in different culture conditions. This result suggests the role of Oct4 as a core regulatory unit for epithelial transition and lineage specification in the various external environment.

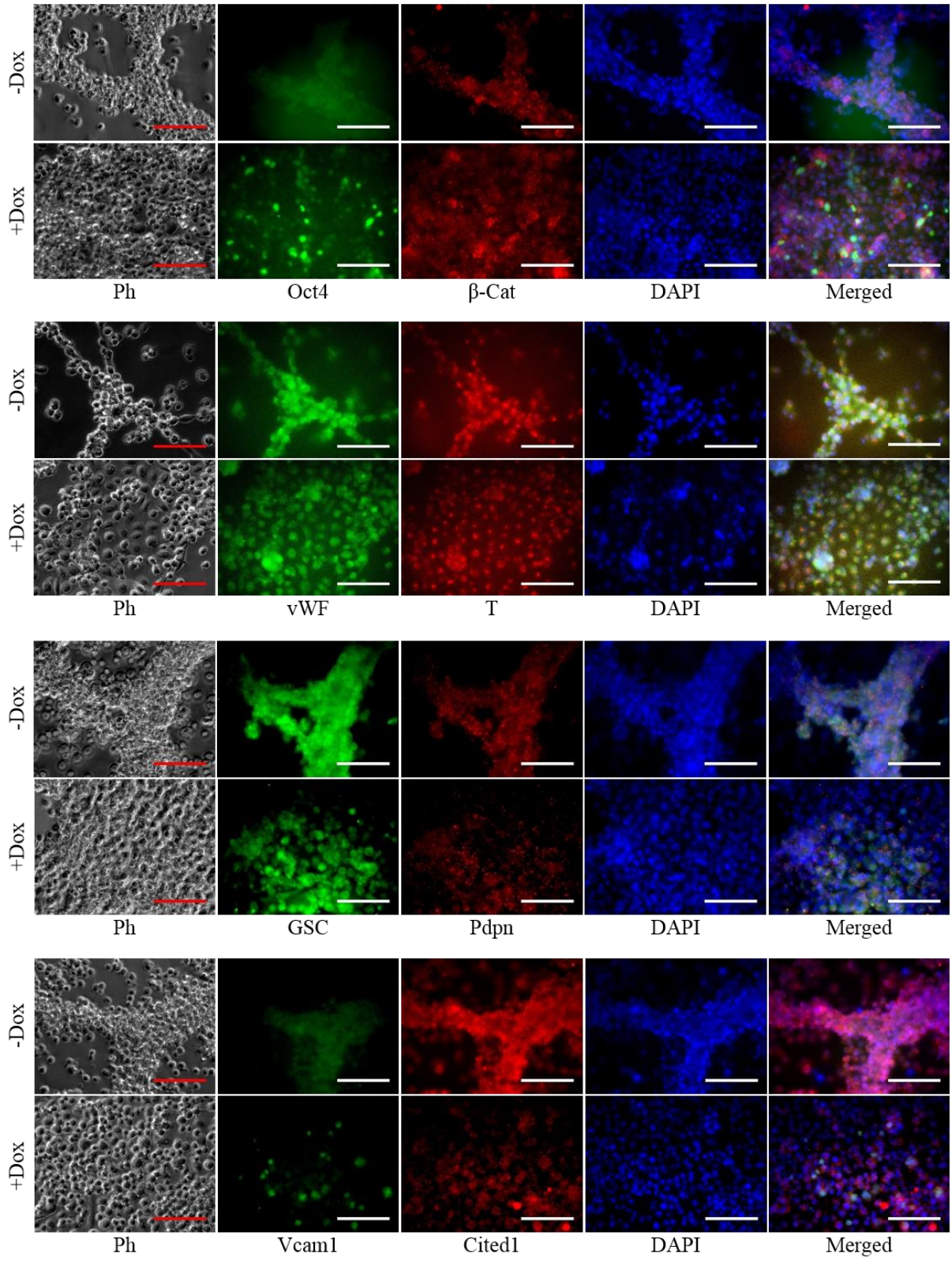

Figure 43: Immunostaining for Oct4, mesendoderm, and epithelial markers. iOX1 cells were cultured for 5 days. Duct formation assay using 1i condition in the presence of Dox (1.0 µg/mL). Scale bar: 100 µm, Magnification: 400x.

4.10 Oct4 induced VE/MET acts non-autonomous manner

To understand more about the mechanisms, we investigated the autonomous/paracrine effect of Oct4. For that, we labeled the transgenic iOX1 and the wild-type cell line with different fluorescence, GFP and tdTomato, respectively. Then we conducted co-culture experiments to see the autonomous/paracrine effect of Oct4 in pXEN cells.

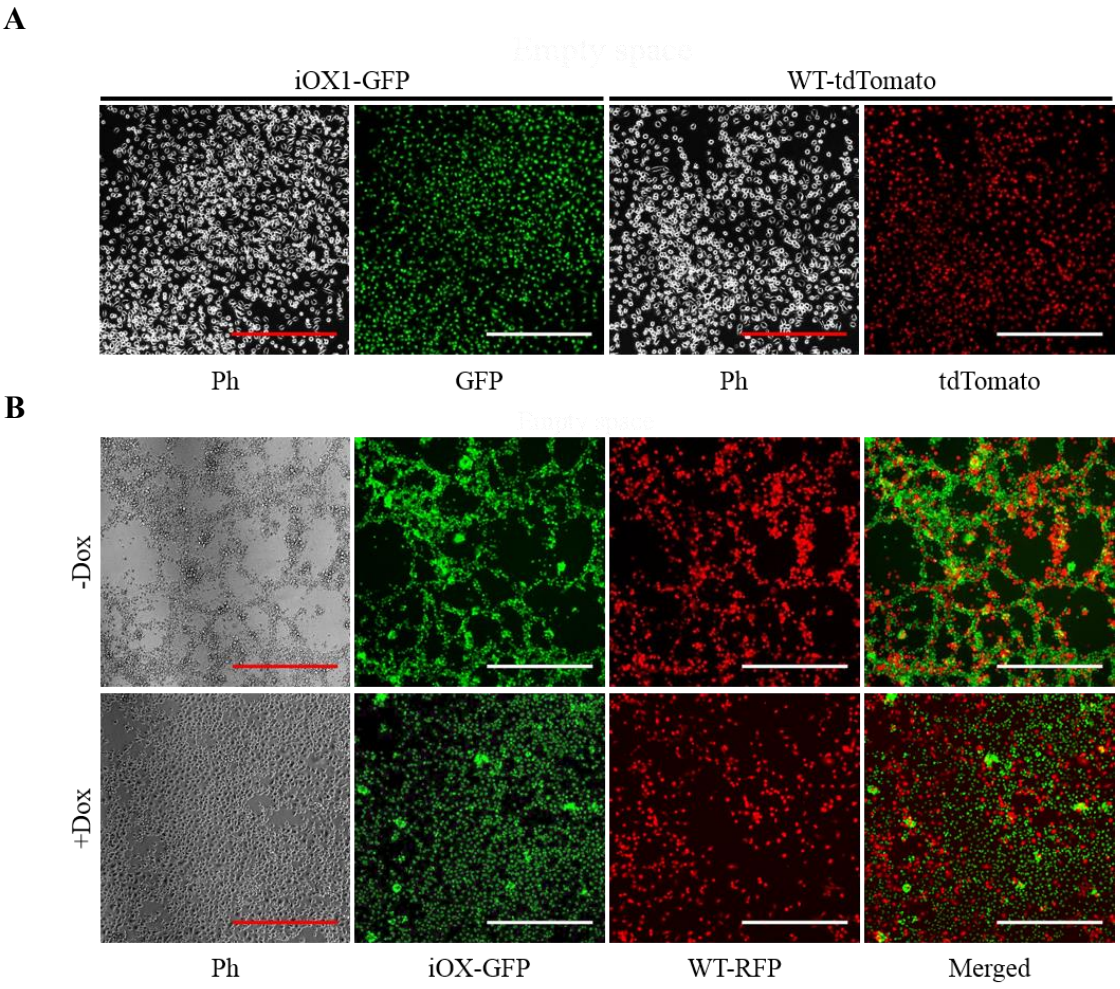

Figure 44: Paracrine effect of Oct4. (A) Representative phase-contrast and fluorescent images of iOX-GFP and WT-RFP cell under maintain condition. (B) Dox-induced transgenic Oct4 expression causes MET in both transgenic and co-cultured non-Oct4-transgenic cells. Scale bars: 500 µm.

In the absence of Dox, the cells in both conditions formed duct-like structures in HD condition as expected; note that those "ducts" were composed of both cell types-iOX and wild type (Figure 44B *UPPER*). However, in the presence of Dox, not only the transgenic iOX cells but also the wild-type cells no longer efficiently formed "ducts" (Figure *LOWER*). Therefore, the stimulatory effect of the increased Oct4 level on the MET/VE differentiation appears to be non-cell-autonomous.

5. DISCUSSION

The transcription factor Oct4 is a central pluripotency determinant and reprogramming factor, but additionally, dosage-dependent functions in lineage commitment and plasticity are emerging. Understanding and controlling endogenous and exogenous Oct4 is therefore crucial for developing rational approaches for the isolation, creation, maintenance, and differentiation of therapeutic stem cells.

pXEN cells are Oct4 positive, committed to the extraembryonic endoderm lineage, and contribute after microinjection exclusively to PE and VE (Debeb et al., 2009). However, they also show multilineage somatic differentiation capacity in vitro (Kumar et al., 2013). It may reflect the plasticity of their in vivo counterpart, the pre-implantation-stage extraembryonic endoderm precursor cells (Nichols et al., 2009, Yamanaka et al., 2010, Binas and Verfaillie, 2013). This broad somatic differentiation capacity of pXEN cells is revealed under conditions of directed (Lo Nigro et al., 2012, Kumar et al., 2013) or chaotic differentiation (Zhong et al., 2018). More than for ES cells, density is a critical parameter in pXEN cell differentiation, and high density appears to reduce external control and favor the chaotic multilineage differentiation (Zhong et al., 2018). It has previously been noticed that XEN cells tend to become epithelial at the HD culture condition (Paca et al., 2012).

We found that the newly discovered blastocyst-derived pXEN cells exhibit lineage plasticity and latent pluripotency, express basal Oct4, and surprisingly show a further differentiation-associated increase in a certain culture condition (HD condition). In the present study, we paved a way to understand the role and regulation of Oct4 in the pXEN cells and then extended the study to the related TGFβ (or Wnt) signaling pathway. Specifically, we investigated the role of basal and increased Oct4 in pXEN cells; we hypothesized that basal Oct4 confers plasticity and increased Oct4 directs differentiation. To test this, we established a doxycycline-inducible Oct4 expression system in these cells as well as targeted mutants lacking Oct4 and studied the resulting phenotypes.

5.1 Cell density is a crucial parameter in pXEN cell differentiation

Here, we have shown that in rat pXEN cells, the HD condition not only promotes their epithelial/VE-like differentiation but also increases the endogenous Oct4. In line with the multipotentiality and lineage plasticity, markers of various lineages became upregulated in the

present study when pXEN cells were cultured under the HD conditions. The novel finding here is that when the cell density increased, the pXEN cell (trans-) differentiation was associated with a further dramatic increase of Oct4 gene expression. The increased Oct4 expression is not just a by-phenomenon but promotes the expression of epithelial and VE markers and slows (but does not block) a competing HD-stimulated process, namely cell aggregation and the subsequent formation of duct-like structures of unknown nature. Thus, both morphologically and by gene expression, HD culture rapidly resulted in a heterogeneous picture but undeniably included signs of a MET with VE differentiation.

The endothelial/ductal differentiation appears to be mechanistically linked with the increased expression of Oct4 since that differentiation was significantly affected by a knockdown of Oct4. Contrary to what we expected based on the positive correlation between the endothelial/ductal differentiation and the Oct4 gene expression under undisturbed conditions, the Oct4 knockdown accelerated the differentiation. The RNAi experiment in HD condition indicates that the density-induced Oct4 affects the balance by facilitating the epithelial pathway. In the HD condition, the decrement caused by the knockdown was much more significant than basal Oct4 expression in the maintain condition (*i.e.*, in the undifferentiated cells); hence the knockdown clearly had a significant effect on the HD-induced Oct4 (*i.e.*, in the differentiating cells). We favor the first possibility because the total cell numbers were not changed by the knockdown at the high density, implying that the undifferentiated pXEN cells, which are known to rapidly proliferate in that medium (Lo Nigro et al., 2012), were not phenotypically affected or simply no longer present.

We were able to expose this Oct4 effect more clearly by artificially overexpressing Oct4 at moderate cell density; under this condition, the duct-like morphogenesis became strikingly suppressed in favor of the MET/VE differentiation. In addition, this occurs through a non-cell-autonomous mechanism that appears to involve TGFβ signaling. Prima facie, this outcome contradicts the typical roles of Oct4 and TGFβ in facilitating EMT. It is, however, difficult to formally distinguish whether the observed phenotype is due to the prevention of the increased Oct4 or due to the reduction of the basal Oct4 level.

Even though, clearly, the availability of pXEN cells provides a major new tool for studying novel aspects of Oct4 function, especially the links between pluripotency and lineage plasticity

5.2 Oct4 supports Wnt/β-catenin-independent MET process in pXEN cells

On study, there are various possibilities for constructing links between Oct4 and MET/VE differentiation. For once, since Oct4 can form a complex with β-catenin at the membrane level (Faunes et al., 2013), a higher level of Oct4 might affect the epithelialization of pXEN cells directly. Furthermore, given that CHIR99021 (CHIR), a stabilizer of β-catenin, promotes MET/VE-like differentiation of pXEN and XEN cells (Bangs et al., 2015), Oct4 might facilitate the epithelialization or differentiation of pXEN cells through promoting Wnt signaling. In fact, Oct4 can bind β-catenin and can co-occupy regulatory DNA sequences together with transcriptional effectors of canonical Wnt signaling such as LEF/TCF (Li et al., 2013). We, therefore, expected that inhibition of Wnt signaling would interfere with the effects of overexpressed Oct4.

However, we did not see an inhibitory effect of various Wnt pathway inhibitors on the Oct4-induced MET/VE transition of pXEN cells. Also, we noticed that the above-described CHIR-induced MET was not blocked by the tested Wnt pathway inhibitors, possibly indicating an effect outside of the Wnt or β-catenin pathway.

Yet another possibility of how Oct4 might promote MET/VE differentiation could be through modulating TGFβ/Smad signaling. Oct4 and Smads co-occupy enhancer elements (Funa et al., 2015), and XEN cells undergo a similar MET/VE upon treatment with BMP (Paca et al., 2012) and Nodal (Kruithof-de Julio et al., 2011). In agreement with an Oct4-TGFβ connection, in our study, Oct4 increased the expression of Nodal, and inhibition of Oct4 decreased it; we saw that Activin A, a TGFβ family protein with similar effects as Nodal, induced a MET/VE-like transition of pXEN cells. However, we did not find an inhibitory effect of SB431542, which blocks Nodal-induced VE-like differentiation of mouse XEN cells (Kruithof-de Julio et al., 2011) on the Oct4-induced MET/VE transition. Instead, Repsox, an inhibitor primarily of TGFβ signaling, partially neutralized the effect of Oct4. This seems paradoxical since TGFβ is a well-established EMT inducer (Moustakas and Heldin, 2016), and therefore Repsox would have been expected to at least not counteract Oct4.

The effect of the increased Oct4 level to facilitate MET/VE differentiation seems paradoxical also from another perspective: Literature tends to associate increased Oct4 expression with EMT rather than MET (Morata-Tarifa et al., 2016, Pan et al., 2016, Sun et al., 2017). Notably, the previously demonstrated conversions of ES and epiblast cells into mesodermal and

extraembryonic endoderm cells by increased Oct4 levels involved EMT (Niwa et al., 2000, Zeineddine et al., 2006), and loss of Oct4 expression was found to upregulate Cdh1 and impede the EMT during gastrulation in vivo (Mulas et al., 2018). There are, however, also examples of the reverse: In the reprogramming of fibroblasts into iPSCs, Oct4 could be replaced by Cdh1 (Redmer et al., 2011), and in spermatogonial stem cells, increased Oct4 promoted MET, although this was opposed by TGFβ signaling, in line with the traditional role of TGFβ (An et al., 2017).

5.3 Oct4 overexpression drives a subsequential EMT-MET in pXEN cells in a paracrine way.

More detailed analysis will be needed to resolve the paradox. In this respect, we noticed that in the initial phase of Dox-induced Oct4 upregulation, the rat pXEN cells became more elongated and showed increased motility, which rather fits with more mesenchymal behavior. The transitions between EMT and its reversed action, MET, have been demonstrated in many processes, including metastasis and reprogramming. Our observation is reminiscent of the finding that the reprogramming of fibroblasts to iPS cells entails two stages: the first one makes the fibroblasts even more mesenchymal (EMT) and requires Oct4 (along with Klf4), the second is a MET (Liu et al., 2013). Therefore, it is possible that in our system, the primary role of Oct4 and TGFβ is a mesenchymal stimulation that might trigger the MET/VE. Note in this respect that in reprogramming, Oct4 has previously been replaced by the cAMP-raising drug forskolin (Fritz et al., 2015), which also promotes the mesenchymal phenotype of rat pXEN cells (Chuykin et al., 2013). Alternatively, it is conceivable that because of the lineage plasticity and near-pluripotent nature of pXEN cells (Lo Nigro et al., 2013), the increased Oct4 expression promotes some (mesendodermal?) differentiation, similar to what was seen with the closely related ES cells (Niwa et al., 2000, Zeineddine et al., 2006); those cells may promote MET/VE in the rest of the culture.

We note in this respect that in our experiments, the Dox-induced Oct4 led to the MET in a non-cell-autonomous way. A non-cell-autonomous role for Oct4 has previously been seen in the cardiac differentiation of mouse ES cells (Stefanovic et al., 2009). Both of these more complex mechanisms are in line with the fact that VE-like epithelial cells derived from pXEN cells do not actually express Oct4 (Debeb et al., 2009).

Thus, either Oct4 only plays a transient role (potentially in a first-step EMT), or there is mixed differentiation, with one cell type promoting MET/VE differentiation in another subset. It will be difficult to dissect these mechanisms in pXEN cell culture exhibiting increased expression if endogenous Oct4; in this HD system, the MET/VE differentiation was less pronounced, and multiple differentiation pathways (including somatic trans-differentiation) appear to occur. However, our Dox-dependent Oct4 overexpression system shows the MET/VE differentiation more clearly and may be used in the future to test the hypothesis that the increased Oct4 level is only required in a restricted time interval or by a certain cell type.

Generally, Oct4 has been shown to exhibit effects that both counteract and promote differentiation in a context- and dose-dependent manner (Zeineddine et al., 2006). The present study adds another example to the latter, now within the extraembryonic endoderm lineage. It remains to be seen whether our observations apply to mouse pXEN cells (Zhong et al., 2018), which also express Oct4, or have relevance for mouse XEN cells, which do not express Oct4 (Niakan et al., 2013) but can-like pXEN cells-efficiently be converted towards MET/VE by CHIR99021 or TGFβ family signaling (Chuykin et al., 2013, Paca et al., 2012). This parallel indicates fundamentally similar mechanisms possibly pointing towards a hidden role of Oct4 in the mouse extraembryonic endoderm lineage as well.

5.4 A novel culture condition for mesendodermal differentiation of pXEN cells.

Here, we developed a novel chemically-defined 1i medium for efficient mesendodermal lattice structure formation of pXEN cells. The results from this study demonstrated that mesodermal or endothelial differentiation of pXEN cells under 1i culture condition was more rapid (<5 days), effective, and homogenous compare to classical “HD” or “on feeder” condition. Notably, many endothelial genes were highly upregulated except VE-cad, unlike HD/feeder-culture condition mediated duct formation. This might indicate that fundamental difference between HD/feeder- and 1i-induced endothelial differentiation in pXEN cells. In fact, the HD-mediated endothelial duct exhibited chaotic/heterogeneous, covered with aggregated cells on the surface and clear luminal structure, depicted by fluid filtration experiment (FITC-conjugated dextran absorbance assay) (data not shown), while 1i condition induced very thin, monolayer, and homogenous lattice structure. Moreover, under this novel culture condition, differentiated pXEN cells represented low expression of Oct4 as compared with HD/feeder condition.

This mesendodermal differentiation of pXEN cells under 1i condition might involve Rho/Rock and MAPK pathway and biased differentiation toward PE lineage. According to Huang et al., MAPKs play pivotal roles in cell movement and migration by myosin phosphorylation (Huang et al., 2004). In addition, Zohrabian et al. also reported that Rho/Rock and MAPK signaling pathways regulate cell migration in glioblastoma cell (Zohrabian et al., 2009). In this context, it has been discussed that interaction with migration-promoting factors (in our case, 1i condition and Ri), such as extracellular matrix, were sufficient to induce PE lineage differentiation from cell aggregates that contained VE (retinoic acid-treated F9 aggregates). *In vivo*, PE cells contribute to parietal yolk sac, which contained basement membrane and blood islands to facilitate nutrients, gas, and waste exchange between the mother and the embryo. The blood island formation indicates the first events of hematopoiesis and vasculogenesis (Grabel and Watts, 1987). This nature of PE might reflect the mesendodermal differentiation capacity of pXEN cells *in vitro*.

Modulation of cell plasticity and fate (in our case, VE or PE) by timing (density or motility) and gene dosage (Oct4) are emerging. Although the mechanisms and molecular differences between HD/Feeder- and 1i-induced endothelial cells have not been fully elucidated yet, pXEN cells offer a promising *in vitro* model for studying certain angiogenesis events and MET process.

In conclusion, the data presented in this study suggest that differentiation-associated Oct4 expression can act as a feedback inhibitor and pXEN cells are a promising cell culture model with which to study new aspects of Oct4 and endothelial/epithelial cell biology-related not only to pluripotency but also lineage plasticity and differentiation.

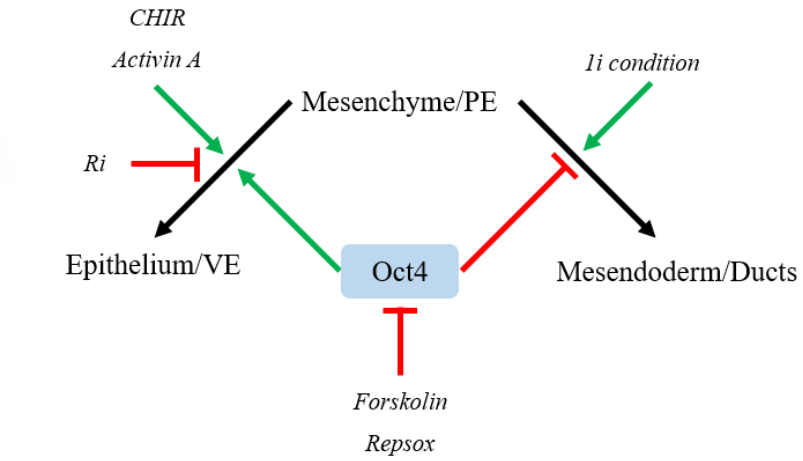

Figure 45: A suggested model for pXEN cell lineage specification and differentiation.

Table 12: Direct comparison of selected VE/MET and PE/EMT markers identified in previous studies. The fold changes greater than 1.5-fold are in color (Red, increase; Blue, decrease). *, (Paca et al., 2012); **, (Chuykin et al., 2013)

Gene	Fold change (Inducer VS control)												Region	Reference
	BMP*	CHIR**	HD	Dox	CHIR	AA	FSK**	siRNA	FSK	Dox +Rep	Dox +Ri	1i		
VE/MET														
ApoE	19.8	N/A	4.2	-2.8	1.8	2.0	N/A	-1.2	-1.2	2.3	1.1	N/A	VE	(Basheeruddin et al., 1987)
Cdh1	10.7	2.3	10.0	1.9	92.6	9.1	-2.3	-1.8	-1.1	-2.2	-2.7	49.0	VE/Epithelia	(Kimura-Yoshida et al., 2005)
Cited1	2.5	7	46.8	3.7	475.4	15.0	4.2	-3.1	22.4	1.4	-1.6	13.0	exVE	(Kunath et al., 2005)
Dab2	1.7	N/A	2.6	4.0	-11.2	2.7	N/A	-1.7	-4.5	-2.8	-2.4	N/A	VE	(Yang et al., 2002)
Hnf4a	N/A	2	2.0	N/A	N/A	4.6	-2.9	N/A	N/A	-1.1	N/A	39.8	VE	(Kunath et al., 2005)
Ihh	2.2	2.6	4.8	7.7	26.1	2.2	1	-1.5	-14.0	-2.3	-1.5	N/A	exVE	(Maye et al., 2000)
Nodal	1.0	~2	3.2	2.4	273.8	3.4	~ -3.8	-1.5	492.1	-1.4	-1.6	N/A	emVE	(Mesnard et al., 2006)
Ocln	N/A	1.3	5.2	N/A	N/A	8.7	-2.3	N/A	N/A	1.1	1.2	N/A	VE	(Verheijen and Defize, 1999)
Oct4	N/A	N/A	5.1	1.6	-133.0	1.6	N/A	-2.7	-2.7	-2.5	1.2	-11.6	Pluripotency	(Nichols et al., 1998)
Pecam1	N/A	N/A	5.1	-2.8	-17.0	1.8	N/A	2.2	3.0	1.1	1.1	8.3	Endothelial	(Yeh et al., 2008)
Vcam1	N/A	N/A	3.6	4.5	-15.8	N/A	N/A	-1.8	1.6	N/A	-5.0	13.2	Endothelial	(Cybulsky et al., 1991)
vWF	N/A	N/A	-2.8	-4.3	-1.2	-3.5	N/A	-1.2	1.5	N/A	5.9	9.6	Endothelial	(Jaffe et al., 1974)
Zo1	N/A	1.1	8.9	2.4	4.8	4.6	-1.3	-2.4	1.4	-1.9	-2.3	13.1	VE/Tight junction	(Balda and Matter, 2000)
PE/EMT														
Lamb1	-1.7	-1.4	14.3	N/A	-2.2	N/A	1	N/A	7.6	1.2	2.4	N/A	PE ECM	(Gardner, 1983)
Pdpn	N/A	N/A	-1.2	-7.8	-6.0	-1.5	N/A	2.8	-5.3	3.8	5.8	2.5	LEC/EMT	(Martin-Villar et al., 2006)
Pth1r	1.0	-1.6	1.5	-2.2	-3.9	-90.4	1	3.1	1.8	2.3	1.1	N/A	PE	(Verheijen and Defize, 1999)
Snai1	-1.4	-1.4	1.5	-2.2	-7.8	-1.8	1.8	2.0	3.6	2.3	2.6	4.6	PE/Mesenchyme	(Veltmaat et al., 2000)
Sparc	-1.1	-1.1	37.6	-1.7	1.6	1.0	1.9	1.3	44.0	1.9	1.9	N/A	PE	(Kunath et al., 2005)
Thbd	-2.5	-2.7	2.7	2.3	-27.2	N/A	1.3	1.1	2.0	N/A	-1.8	N/A	PE	(Kunath et al., 2005)
Vim	-1.6	-16.3	-4.1	-2.4	-11.4	-4.4	-1.3	1.0	-1.3	1.0	-1.2	-6.4	PE/Mesenchyme	(Kunath et al., 2005)
Zeb1	-2.4	N/A	-64.7	1.0	1.1	-3.0	N/A	1.4	4.6	-1.3	-2.1	3.2	Mesenchyme	(Funahashi et al., 1993)

6. LIST OF FIGURES

7. LIST OF TABLES

8. REFERENCES

AHLER, E., SULLIVAN, W. J., CASS, A., BRAAS, D., YORK, A. G., BENSINGER, S. J., GRAEBER, T. G. & CHRISTOFK, H. R. 2013. Doxycycline alters metabolism and proliferation of human cell lines. *PLoS One,* 8**,** e64561.

AMANO, M., NAKAYAMA, M. & KAIBUCHI, K. 2010. Rho-kinase/ROCK: A key regulator of the cytoskeleton and cell polarity. *Cytoskeleton (Hoboken),* 67**,** 545-54.

AN, J., ZHENG, Y. & DANN, C. T. 2017. Mesenchymal to Epithelial Transition Mediated by CDH1 Promotes Spontaneous Reprogramming of Male Germline Stem Cells to Pluripotency. *Stem Cell Reports,* 8**,** 446-459.

ARATA, Y., TAKAGI, H., SAKO, Y. & SAWA, H. 2014. Power law relationship between cell cycle duration and cell volume in the early embryonic development of Caenorhabditis elegans. *Front Physiol,* 5**,** 529.

ARTUS, J., DOUVARAS, P., PILISZEK, A., ISERN, J., BARON, M. H. & HADJANTONAKIS, A. K. 2012. BMP4 signaling directs primitive endoderm-derived XEN cells to an extraembryonic visceral endoderm identity. *Dev Biol,* 361**,** 245-62.

BAKER, J. C. & HARLAND, R. M. 1997. From receptor to nucleus: the Smad pathway. *Curr Opin Genet Dev,* 7**,** 467-73.

BALDA, M. S. & MATTER, K. 2000. The tight junction protein ZO-1 and an interacting transcription factor regulate ErbB-2 expression. *EMBO J,* 19**,** 2024-33.

BANGS, F. K., SCHRODE, N., HADJANTONAKIS, A. K. & ANDERSON, K. V. 2015. Lineage specificity of primary cilia in the mouse embryo. *Nat Cell Biol,* 17**,** 113-22.

BARCROFT, L. C., OFFENBERG, H., THOMSEN, P. & WATSON, A. J. 2003. Aquaporin proteins in murine trophectoderm mediate transepithelial water movements during cavitation. *Dev Biol,* 256**,** 342-54.

BASHEERUDDIN, K., STEIN, P., STRICKLAND, S. & WILLIAMS, D. L. 1987. Expression of the murine apolipoprotein E gene is coupled to the differentiated state of F9 embryonal carcinoma cells. *Proc Natl Acad Sci U S A,* 84**,** 709-13.

BASSALERT, C., VALVERDE-ESTRELLA, L. & CHAZAUD, C. 2018. Primitive Endoderm Differentiation: From Specification to Epithelialization. *Curr Top Dev Biol,* 128**,** 81-104.

BEATTIE, G. M., LOPEZ, A. D., BUCAY, N., HINTON, A., FIRPO, M. T., KING, C. C. & HAYEK, A. 2005. Activin A maintains pluripotency of human embryonic stem cells in the absence of feeder layers. *Stem Cells,* 23**,** 489-95.

BEDDINGTON, R. S. & ROBERTSON, E. J. 1999. Axis development and early asymmetry in mammals. *Cell,* 96**,** 195-209.

BEHRENS, J., VON KRIES, J. P., KUHL, M., BRUHN, L., WEDLICH, D., GROSSCHEDL, R. & BIRCHMEIER, W. 1996. Functional interaction of beta-catenin with the transcription factor LEF-1. *Nature,* 382**,** 638-42.

BESSONNARD, S., DE MOT, L., GONZE, D., BARRIOL, M., DENNIS, C., GOLDBETER, A., DUPONT, G. & CHAZAUD, C. 2014. Gata6, Nanog and Erk signaling control cell fate in the inner cell mass through a tristable regulatory network. *Development,* 141**,** 3637-48.

BHANOT, P., BRINK, M., SAMOS, C. H., HSIEH, J. C., WANG, Y., MACKE, J. P., ANDREW, D., NATHANS, J. & NUSSE, R. 1996. A new member of the frizzled family from Drosophila functions as a Wingless receptor. *Nature,* 382**,** 225-30.

BILIC, J., HUANG, Y. L., DAVIDSON, G., ZIMMERMANN, T., CRUCIAT, C. M., BIENZ, M. & NIEHRS, C. 2007. Wnt induces LRP6 signalosomes and promotes dishevelled-dependent LRP6 phosphorylation. *Science,* 316**,** 1619-22.

BINAS, B. & VERFAILLIE, C. M. 2013. Concise review: Bone marrow meets blastocyst: lessons from an unlikely encounter. *Stem Cells,* 31**,** 620-6.

BOUTROS, M., PARICIO, N., STRUTT, D. I. & MLODZIK, M. 1998. Dishevelled activates JNK and discriminates between JNK pathways in planar polarity and wingless signaling. *Cell,* 94**,** 109-18.

BOYER, L. A., LEE, T. I., COLE, M. F., JOHNSTONE, S. E., LEVINE, S. S., ZUCKER, J. P., GUENTHER, M. G., KUMAR, R. M., MURRAY, H. L., JENNER, R. G., GIFFORD, D. K., MELTON, D. A., JAENISCH, R. & YOUNG, R. A. 2005. Core transcriptional regulatory circuitry in human embryonic stem cells. *Cell,* 122**,** 947-56.

BRAUCHLE, M., BAUMER, K. & GONCZY, P. 2003. Differential activation of the DNA replication checkpoint contributes to asynchrony of cell division in C. elegans embryos. *Curr Biol,* 13**,** 819-27.

BRENNAN, J., LU, C. C., NORRIS, D. P., RODRIGUEZ, T. A., BEDDINGTON, R. S. & ROBERTSON, E. J. 2001. Nodal signalling in the epiblast patterns the early mouse embryo. *Nature,* 411**,** 965-9.

BUEHR, M., MEEK, S., BLAIR, K., YANG, J., URE, J., SILVA, J., MCLAY, R., HALL, J., YING, Q. L. & SMITH, A. 2008. Capture of authentic embryonic stem cells from rat blastocysts. *Cell,* 135**,** 1287-98.

BUEHR, M. & SMITH, A. 2003. Genesis of embryonic stem cells. *Philos Trans R Soc Lond B Biol Sci,* 358**,** 1397-402; discussion 1402.

BUZZARD, J. J., FARNWORTH, P. G., DE KRETSER, D. M., O'CONNOR, A. E., WREFORD, N. G. & MORRISON, J. R. 2003. Proliferative phase sertoli cells display a developmentally regulated response to activin in vitro. *Endocrinology,* 144**,** 474-83.

CADINANOS, J. & BRADLEY, A. 2007. Generation of an inducible and optimized piggyBac transposon system. *Nucleic Acids Res,* 35**,** e87.

CHANG, J. B. & FERRELL, J. E., JR. 2013. Mitotic trigger waves and the spatial coordination of the Xenopus cell cycle. *Nature,* 500**,** 603-7.

CHAZAUD, C., YAMANAKA, Y., PAWSON, T. & ROSSANT, J. 2006. Early lineage segregation between epiblast and primitive endoderm in mouse blastocysts through the Grb2-MAPK pathway. *Dev Cell,* 10**,** 615-24.

CHEW, J. L., LOH, Y. H., ZHANG, W., CHEN, X., TAM, W. L., YEAP, L. S., LI, P., ANG, Y. S., LIM, B., ROBSON, P. & NG, H. H. 2005. Reciprocal transcriptional regulation of Pou5f1 and Sox2 via the Oct4/Sox2 complex in embryonic stem cells. *Mol Cell Biol,* 25**,** 6031-46.

CHO, S. H., YAO, Z., WANG, S. W., ALBAN, R. F., BARBERS, R. G., FRENCH, S. W. & OH, C. K. 2003. Regulation of activin A expression in mast cells and asthma: its effect on the proliferation of human airway smooth muscle cells. *J Immunol,* 170**,** 4045-52.

CHOI, H. W., JOO, J. Y., HONG, Y. J., KIM, J. S., SONG, H., LEE, J. W., WU, G., SCHOLER, H. R. & DO, J. T. 2016. Distinct Enhancer Activity of Oct4 in Naive and Primed Mouse Pluripotency. *Stem Cell Reports,* 7**,** 911-926.

CHUYKIN, I., SCHULZ, H., GUAN, K. & BADER, M. 2013. Activation of the PTHRP/adenylate cyclase pathway promotes differentiation of rat XEN cells into parietal endoderm, whereas Wnt/beta-catenin signaling promotes differentiation into visceral endoderm. *J Cell Sci,* 126**,** 128-38.

COCKBURN, K. & ROSSANT, J. 2010. Making the blastocyst: lessons from the mouse. *J Clin Invest,* 120**,** 995-1003.

COLLART, C., ALLEN, G. E., BRADSHAW, C. R., SMITH, J. C. & ZEGERMAN, P. 2013. Titration of four replication factors is essential for the Xenopus laevis midblastula transition. *Science,* 341**,** 893-6.

CONLON, F. L., BARTH, K. S. & ROBERTSON, E. J. 1991. A novel retrovirally induced embryonic lethal mutation in the mouse: assessment of the developmental fate of embryonic stem cells homozygous for the 413.d proviral integration. *Development,* 111**,** 969-81.

CORMIER, N., YEO, A., FIORENTINO, E. & PAXSON, J. 2015. Optimization of the Wound Scratch Assay to Detect Changes in Murine Mesenchymal Stromal Cell Migration After Damage by Soluble Cigarette Smoke Extract. *J Vis Exp***,** e53414.

CYBULSKY, M. I., FRIES, J. W., WILLIAMS, A. J., SULTAN, P., DAVIS, V. M., GIMBRONE, M. A., JR. & COLLINS, T. 1991. Alternative splicing of human VCAM-1 in activated vascular endothelium. *Am J Pathol,* 138**,** 815-20.

D'AMOUR, K. A., AGULNICK, A. D., ELIAZER, S., KELLY, O. G., KROON, E. & BAETGE, E. E. 2005. Efficient differentiation of human embryonic stem cells to definitive endoderm. *Nat Biotechnol,* 23**,** 1534-41.

DEBEB, B. G., GALAT, V., EPPLE-FARMER, J., IANNACCONE, S., WOODWARD, W. A., BADER, M., IANNACCONE, P. & BINAS, B. 2009. Isolation of Oct4-expressing extraembryonic endoderm precursor cell lines. *PLoS One,* 4**,** e7216.

DENEKE, V. E., MELBINGER, A., VERGASSOLA, M. & DI TALIA, S. 2016. Waves of Cdk1 Activity in S Phase Synchronize the Cell Cycle in Drosophila Embryos. *Dev Cell,* 38**,** 399-412.

DUDLEY, A. T., LYONS, K. M. & ROBERTSON, E. J. 1995. A requirement for bone morphogenetic protein-7 during development of the mammalian kidney and eye. *Genes Dev,* 9**,** 2795-807.

EFE, J. A., HILCOVE, S., KIM, J., ZHOU, H., OUYANG, K., WANG, G., CHEN, J. & DING, S. 2011. Conversion of mouse fibroblasts into cardiomyocytes using a direct reprogramming strategy. *Nat Cell Biol,* 13**,** 215-22.

EVANS, M. J. & KAUFMAN, M. H. 1981. Establishment in culture of pluripotential cells from mouse embryos. *Nature,* 292**,** 154-6.

FALKNER, F. G. & ZACHAU, H. G. 1984. Correct transcription of an immunoglobulin kappa gene requires an upstream fragment containing conserved sequence elements. *Nature,* 310**,** 71-4.

FAUNES, F., HAYWARD, P., DESCALZO, S. M., CHATTERJEE, S. S., BALAYO, T., TROTT, J., CHRISTOFOROU, A., FERRER-VAQUER, A., HADJANTONAKIS, A. K., DASGUPTA, R. & ARIAS, A. M. 2013. A membrane-associated beta-catenin/Oct4 complex correlates with ground-state pluripotency in mouse embryonic stem cells. *Development,* 140**,** 1171-83.

FESKE, S., OKAMURA, H., HOGAN, P. G. & RAO, A. 2003. Ca2+/calcineurin signalling in cells of the immune system. *Biochem Biophys Res Commun,* 311**,** 1117-32.

FOGARTY, N. M. E., MCCARTHY, A., SNIJDERS, K. E., POWELL, B. E., KUBIKOVA, N., BLAKELEY, P., LEA, R., ELDER, K., WAMAITHA, S. E., KIM, D., MACIULYTE, V., KLEINJUNG, J., KIM, J. S., WELLS, D., VALLIER, L., BERTERO, A., TURNER, J. M. A. & NIAKAN, K. K. 2017. Erratum: Genome editing reveals a role for OCT4 in human embryogenesis. *Nature,* 551**,** 256.

FRANKENBERG, S., GERBE, F., BESSONNARD, S., BELVILLE, C., POUCHIN, P., BARDOT, O. & CHAZAUD, C. 2011. Primitive endoderm differentiates via a three-step mechanism involving Nanog and RTK signaling. *Dev Cell,* 21**,** 1005-13.

FRITZ, A. L., ADIL, M. M., MAO, S. R. & SCHAFFER, D. V. 2015. cAMP and EPAC Signaling Functionally Replace OCT4 During Induced Pluripotent Stem Cell Reprogramming. *Mol Ther,* 23**,** 952-963.

FRUM, T., HALBISEN, M. A., WANG, C., AMIRI, H., ROBSON, P. & RALSTON, A. 2013. Oct4 cell-autonomously promotes primitive endoderm development in the mouse blastocyst. *Dev Cell,* 25**,** 610-22.

FUNA, N. S., SCHACHTER, K. A., LERDRUP, M., EKBERG, J., HESS, K., DIETRICH, N., HONORE, C., HANSEN, K. & SEMB, H. 2015. beta-Catenin Regulates Primitive Streak Induction through Collaborative Interactions with SMAD2/SMAD3 and OCT4. *Cell Stem Cell,* 16**,** 639-52.

FUNAHASHI, J., SEKIDO, R., MURAI, K., KAMACHI, Y. & KONDOH, H. 1993. Delta-crystallin enhancer binding protein delta EF1 is a zinc finger-homeodomain protein implicated in postgastrulation embryogenesis. *Development,* 119**,** 433-46.

GAARENSTROOM, T. & HILL, C. S. 2014. TGF-beta signaling to chromatin: how Smads regulate transcription during self-renewal and differentiation. *Semin Cell Dev Biol,* 32**,** 107-18.

GARDNER, R. L. 1983. Origin and differentiation of extraembryonic tissues in the mouse. *Int Rev Exp Pathol,* 24**,** 63-133.

GORDON, M. D. & NUSSE, R. 2006. Wnt signaling: multiple pathways, multiple receptors, and multiple transcription factors. *J Biol Chem,* 281**,** 22429-33.

GOSSEN, M., FREUNDLIEB, S., BENDER, G., MULLER, G., HILLEN, W. & BUJARD, H. 1995. Transcriptional activation by tetracyclines in mammalian cells. *Science,* 268**,** 1766-9.

GRABEL, L. B. & WATTS, T. D. 1987. The role of extracellular matrix in the migration and differentiation of parietal endoderm from teratocarcinoma embryoid bodies. *J Cell Biol,* 105**,** 441-8.

HEMMATI-BRIVANLOU, A. & THOMSEN, G. H. 1995. Ventral mesodermal patterning in Xenopus embryos: expression patterns and activities of BMP-2 and BMP-4. *Dev Genet,* 17**,** 78-89.

HOCKEMEYER, D., SOLDNER, F., COOK, E. G., GAO, Q., MITALIPOVA, M. & JAENISCH, R. 2008. A drug-inducible system for direct reprogramming of human somatic cells to pluripotency. *Cell Stem Cell,* 3**,** 346-353.

HOGAN, P. G., CHEN, L., NARDONE, J. & RAO, A. 2003. Transcriptional regulation by calcium, calcineurin, and NFAT. *Genes Dev,* 17**,** 2205-32.

HOTTA, A., CHEUNG, A. Y., FARRA, N., VIJAYARAGAVAN, K., SEGUIN, C. A., DRAPER, J. S., PASCERI, P., MAKSAKOVA, I. A., MAGER, D. L., ROSSANT, J., BHATIA, M. & ELLIS, J. 2009. Isolation of human iPS cells using EOS lentiviral vectors to select for pluripotency. *Nat Methods,* 6**,** 370-6.

HUANG, C., JACOBSON, K. & SCHALLER, M. D. 2004. MAP kinases and cell migration. *J Cell Sci,* 117**,** 4619-28.

HUANGFU, D., MAEHR, R., GUO, W., EIJKELENBOOM, A., SNITOW, M., CHEN, A. E. & MELTON, D. A. 2008. Induction of pluripotent stem cells by defined factors is greatly improved by small-molecule compounds. *Nat Biotechnol,* 26**,** 795-7.

JAFFE, E. A., HOYER, L. W. & NACHMAN, R. L. 1974. Synthesis of von Willebrand factor by cultured human endothelial cells. *Proc Natl Acad Sci U S A,* 71**,** 1906-9.

JI, H., TANG, H., LIN, H., MAO, J., GAO, L., LIU, J. & WU, T. 2014. Rho/Rock cross-talks with transforming growth factor-beta/Smad pathway participates in lung fibroblast-myofibroblast differentiation. *Biomed Rep,* 2**,** 787-792.

JONES, K. T., CRUTTWELL, C., PARRINGTON, J. & SWANN, K. 1998. A mammalian sperm cytosolic phospholipase C activity generates inositol trisphosphate and causes Ca2+ release in sea urchin egg homogenates. *FEBS Lett,* 437**,** 297-300.

KIKUCHI, A., YAMAMOTO, H., SATO, A. & MATSUMOTO, S. 2011. New insights into the mechanism of Wnt signaling pathway activation. *Int Rev Cell Mol Biol,* 291**,** 21-71.

KIM, J. B., SEBASTIANO, V., WU, G., ARAUZO-BRAVO, M. J., SASSE, P., GENTILE, L., KO, K., RUAU, D., EHRICH, M., VAN DEN BOOM, D., MEYER, J., HUBNER, K., BERNEMANN, C., ORTMEIER, C., ZENKE, M., FLEISCHMANN, B. K., ZAEHRES, H. & SCHOLER, H. R. 2009a. Oct4-induced pluripotency in adult neural stem cells. *Cell,* 136**,** 411-9.

KIM, S. I., KWAK, J. H., NA, H. J., KIM, J. K., DING, Y. & CHOI, M. E. 2009b. Transforming growth factor-beta (TGF-beta1) activates TAK1 via TAB1-mediated autophosphorylation, independent of TGF-beta receptor kinase activity in mesangial cells. *J Biol Chem,* 284**,** 22285-96.

KIMURA-YOSHIDA, C., NAKANO, H., OKAMURA, D., NAKAO, K., YONEMURA, S., BELO, J. A., AIZAWA, S., MATSUI, Y. & MATSUO, I. 2005. Canonical Wnt signaling and its antagonist regulate anterior-posterior axis polarization by guiding cell migration in mouse visceral endoderm. *Dev Cell,* 9**,** 639-50.

KOROL, A., TAIYAB, A. & WEST-MAYS, J. A. 2016. RhoA/ROCK signaling regulates TGFbeta-induced epithelial-mesenchymal transition of lens epithelial cells through MRTF-A. *Mol Med,* 22**,** 713-723.

KRUITHOF-DE JULIO, M., ALVAREZ, M. J., GALLI, A., CHU, J., PRICE, S. M., CALIFANO, A. & SHEN, M. M. 2011. Regulation of extra-embryonic endoderm stem cell differentiation by Nodal and Cripto signaling. *Development,* 138**,** 3885-95.

KUHL, M., SHELDAHL, L. C., MALBON, C. C. & MOON, R. T. 2000. Ca(2+)/calmodulin-dependent protein kinase II is stimulated by Wnt and Frizzled homologs and promotes ventral cell fates in Xenopus. *J Biol Chem,* 275**,** 12701-11.

KUMAR, A., LO NIGRO, A., GYSEMANS, C., CAI, Q., ESGUERRA, C., NELSON-HOLTE, M., HEREMANS, Y., JIMENEZ-GONZALEZ, M., PORCIUNCULA, A., MATHIEU, C., BINAS, B., HEIMBERG, H., PROSPER, F., HERING, B., VERFAILLIE, C. M. & BARAJAS, M. 2013. Reversal of hyperglycemia by insulin-secreting rat bone marrow- and blastocyst-derived hypoblast stem cell-like cells. *PLoS One,* 8**,** e63491.

KUNATH, T., ARNAUD, D., UY, G. D., OKAMOTO, I., CHUREAU, C., YAMANAKA, Y., HEARD, E., GARDNER, R. L., AVNER, P. & ROSSANT, J. 2005. Imprinted X-

inactivation in extra-embryonic endoderm cell lines from mouse blastocysts. *Development,* 132**,** 1649-61.

KWON, G. S., VIOTTI, M. & HADJANTONAKIS, A. K. 2008. The endoderm of the mouse embryo arises by dynamic widespread intercalation of embryonic and extraembryonic lineages. *Dev Cell,* 15**,** 509-20.

LATOS, P. A. & HEMBERGER, M. 2016. From the stem of the placental tree: trophoblast stem cells and their progeny. *Development,* 143**,** 3650-3660.

LEVET, S., CIAIS, D., MERDZHANOVA, G., MALLET, C., ZIMMERS, T. A., LEE, S. J., NAVARRO, F. P., TEXIER, I., FEIGE, J. J., BAILLY, S. & VITTET, D. 2013. Bone morphogenetic protein 9 (BMP9) controls lymphatic vessel maturation and valve formation. *Blood,* 122**,** 598-607.

LI, F., HE, Z., SHEN, J., HUANG, Q., LI, W., LIU, X., HE, Y., WOLF, F. & LI, C. Y. 2010a. Apoptotic caspases regulate induction of iPSCs from human fibroblasts. *Cell Stem Cell,* 7**,** 508-20.

LI, J., LI, J. & CHEN, B. 2012. Oct4 was a novel target of Wnt signaling pathway. *Mol Cell Biochem,* 362**,** 233-40.

LI, R., LIANG, J., NI, S., ZHOU, T., QING, X., LI, H., HE, W., CHEN, J., LI, F., ZHUANG, Q., QIN, B., XU, J., LI, W., YANG, J., GAN, Y., QIN, D., FENG, S., SONG, H., YANG, D., ZHANG, B., ZENG, L., LAI, L., ESTEBAN, M. A. & PEI, D. 2010b. A mesenchymal-to-epithelial transition initiates and is required for the nuclear reprogramming of mouse fibroblasts. *Cell Stem Cell,* 7**,** 51-63.

LI, Y., YU, W., COONEY, A. J., SCHWARTZ, R. J. & LIU, Y. 2013. Brief report: Oct4 and canonical Wnt signaling regulate the cardiac lineage factor Mesp1 through a Tcf/Lef-Oct4 composite element. *Stem Cells,* 31**,** 1213-7.

LI, Y., ZHANG, Q., YIN, X., YANG, W., DU, Y., HOU, P., GE, J., LIU, C., ZHANG, W., ZHANG, X., WU, Y., LI, H., LIU, K., WU, C., SONG, Z., ZHAO, Y., SHI, Y. & DENG, H. 2011. Generation of iPSCs from mouse fibroblasts with a single gene, Oct4, and small molecules. *Cell Res,* 21**,** 196-204.

LIU, Y., MUKHOPADHYAY, P., PISANO, M. M., LU, X., HUANG, L., LU, Q. & DEAN, D. C. 2013. Repression of Zeb1 and hypoxia cause sequential mesenchymal-to-epithelial transition and induction of aid, Oct4, and Dnmt1, leading to immortalization and multipotential reprogramming of fibroblasts in spheres. *Stem Cells,* 31**,** 1350-62.

LO NIGRO, A., GERAERTS, M., NOTELAERS, T., ROOBROUCK, V. D., MUIJTJENS, M., EGGERMONT, K., SUBRAMANIAN, K., ULLOA-MONTOYA, F., PARK, Y., OWENS, J., BURNS, T. C., LOW, W., SHARMA, S., SOHNI, A., CRABBE, A., PAUWELYN, K., ROELANDT, P., AGIRRE, X., PROSPER, F., O'BRIEN, T. D., ZWIJSEN, A., HU, W. S., BINAS, B. & VERFAILLIE, C. M. 2012. MAPC culture conditions support the derivation of cells with nascent hypoblast features from bone marrow and blastocysts. *J Mol Cell Biol,* 4**,** 423-6.

LO NIGRO, L., MIRABILE, E., TUMINO, M., CASERTA, C., CAZZANIGA, G., RIZZARI, C., SILVESTRI, D., BULDINI, B., BARISONE, E., CASALE, F., LUCIANI, M., LOCATELLI, F., MESSINA, C., MICALIZZI, C., PESSION, A., PARASOLE, R., SANTORO, N., MASERA, G., BASSO, G., ARICO, M., VALSECCHI, M., BIONDI, A., CONTER, V. & ALL, A. I.-S. C. O. 2013. Detection of PICALM-MLLT10 (CALM-AF10) and outcome in children with T-lineage acute lymphoblastic leukemia. *Leukemia,* 27**,** 2419-21.

MACDONALD, B. T., TAMAI, K. & HE, X. 2009. Wnt/beta-catenin signaling: components, mechanisms, and diseases. *Dev Cell,* 17**,** 9-26.

MAO, J., WANG, J., LIU, B., PAN, W., FARR, G. H., 3RD, FLYNN, C., YUAN, H., TAKADA, S., KIMELMAN, D., LI, L. & WU, D. 2001. Low-density lipoprotein receptor-related protein-5 binds to Axin and regulates the canonical Wnt signaling pathway. *Mol Cell,* 7**,** 801-9.

MARIKAWA, Y. & ALARCON, V. B. 2012. Creation of trophectoderm, the first epithelium, in mouse preimplantation development. *Results Probl Cell Differ,* 55**,** 165-84.

MARTIN-VILLAR, E., MEGIAS, D., CASTEL, S., YURRITA, M. M., VILARO, S. & QUINTANILLA, M. 2006. Podoplanin binds ERM proteins to activate RhoA and promote epithelial-mesenchymal transition. *J Cell Sci,* 119**,** 4541-53.

MAYE, P., BECKER, S., KASAMEYER, E., BYRD, N. & GRABEL, L. 2000. Indian hedgehog signaling in extraembryonic endoderm and ectoderm differentiation in ES embryoid bodies. *Mech Dev,* 94**,** 117-32.

MCBEATH, R., PIRONE, D. M., NELSON, C. M., BHADRIRAJU, K. & CHEN, C. S. 2004. Cell shape, cytoskeletal tension, and RhoA regulate stem cell lineage commitment. *Dev Cell,* 6**,** 483-95.

MCCORMACK, N., MOLLOY, E. L. & O'DEA, S. 2013. Bone morphogenetic proteins enhance an epithelial-mesenchymal transition in normal airway epithelial cells during restitution of a disrupted epithelium. *Respir Res,* 14**,** 36.

MEEK, S., WEI, J., SUTHERLAND, L., NILGES, B., BUEHR, M., TOMLINSON, S. R., THOMSON, A. J. & BURDON, T. 2013. Tuning of beta-catenin activity is required to stabilize self-renewal of rat embryonic stem cells. *Stem Cells,* 31**,** 2104-15.

MESNARD, D., GUZMAN-AYALA, M. & CONSTAM, D. B. 2006. Nodal specifies embryonic visceral endoderm and sustains pluripotent cells in the epiblast before overt axial patterning. *Development,* 133**,** 2497-505.

MOLENAAR, M., VAN DE WETERING, M., OOSTERWEGEL, M., PETERSON-MADURO, J., GODSAVE, S., KORINEK, V., ROOSE, J., DESTREE, O. & CLEVERS, H. 1996. XTcf-3 transcription factor mediates beta-catenin-induced axis formation in Xenopus embryos. *Cell,* 86**,** 391-9.

MOMEN-ROKNABADI, A., DI TALIA, S. & WIESCHAUS, E. 2016. Transcriptional Timers Regulating Mitosis in Early Drosophila Embryos. *Cell Rep,* 16**,** 2793-2801.

MORATA-TARIFA, C., JIMENEZ, G., GARCIA, M. A., ENTRENA, J. M., GRINAN-LISON, C., AGUILERA, M., PICON-RUIZ, M. & MARCHAL, J. A. 2016. Low adherent cancer cell subpopulations are enriched in tumorigenic and metastatic epithelial-to-mesenchymal transition-induced cancer stem-like cells. *Sci Rep,* 6**,** 18772.

MOUSTAKAS, A. & HELDIN, C. H. 2016. Mechanisms of TGFbeta-Induced Epithelial-Mesenchymal Transition. *J Clin Med,* 5.

MUKHOPADHYAY, M., SHTROM, S., RODRIGUEZ-ESTEBAN, C., CHEN, L., TSUKUI, T., GOMER, L., DORWARD, D. W., GLINKA, A., GRINBERG, A., HUANG, S. P., NIEHRS, C., IZPISUA BELMONTE, J. C. & WESTPHAL, H. 2001. Dickkopf1 is required for embryonic head induction and limb morphogenesis in the mouse. *Dev Cell,* 1**,** 423-34.

MULAS, C., CHIA, G., JONES, K. A., HODGSON, A. C., STIRPARO, G. G. & NICHOLS, J. 2018. Oct4 regulates the embryonic axis and coordinates exit from pluripotency and germ layer specification in the mouse embryo. *Development,* 145.

NAKATANI, Y., MASUDO, K., MIYAGI, Y., INAYAMA, Y., KAWANO, N., TANAKA, Y., KATO, K., ITO, T., KITAMURA, H., NAGASHIMA, Y., YAMANAKA, S., NAKAMURA, N., SANO, J., OGAWA, N., ISHIWA, N., NOTOHARA, K., RESL, M. & MARK, E. J. 2002. Aberrant nuclear localization and gene mutation of beta-catenin in low-grade adenocarcinoma of fetal lung type: up-regulation of the Wnt signaling pathway may be a common denominator for the development of tumors that form morules. *Mod Pathol,* 15**,** 617-24.

NIAKAN, K. K., SCHRODE, N., CHO, L. T. & HADJANTONAKIS, A. K. 2013. Derivation of extraembryonic endoderm stem (XEN) cells from mouse embryos and embryonic stem cells. *Nat Protoc,* 8**,** 1028-41.

NICHOLS, J., SILVA, J., ROODE, M. & SMITH, A. 2009. Suppression of Erk signalling promotes ground state pluripotency in the mouse embryo. *Development,* 136**,** 3215-22.

NICHOLS, J. & SMITH, A. 2011. The origin and identity of embryonic stem cells. *Development,* 138**,** 3-8.

NICHOLS, J., ZEVNIK, B., ANASTASSIADIS, K., NIWA, H., KLEWE-NEBENIUS, D., CHAMBERS, I., SCHOLER, H. & SMITH, A. 1998. Formation of pluripotent stem cells in the mammalian embryo depends on the POU transcription factor Oct4. *Cell,* 95**,** 379-91.

NIWA, H., MIYAZAKI, J. & SMITH, A. G. 2000. Quantitative expression of Oct-3/4 defines differentiation, dedifferentiation or self-renewal of ES cells. *Nat Genet,* 24**,** 372-6.

NIWA, H., TOYOOKA, Y., SHIMOSATO, D., STRUMPF, D., TAKAHASHI, K., YAGI, R. & ROSSANT, J. 2005. Interaction between Oct3/4 and Cdx2 determines trophectoderm differentiation. *Cell,* 123**,** 917-29.

NORDHOFF, V., HUBNER, K., BAUER, A., ORLOVA, I., MALAPETSA, A. & SCHOLER, H. R. 2001. Comparative analysis of human, bovine, and murine Oct-4 upstream promoter sequences. *Mamm Genome,* 12**,** 309-17.

NUSSE, R. & VARMUS, H. E. 1982. Many tumors induced by the mouse mammary tumor virus contain a provirus integrated in the same region of the host genome. *Cell,* 31**,** 99-109.

OGURA, Y. & SASAKURA, Y. 2016. Developmental Control of Cell-Cycle Compensation Provides a Switch for Patterned Mitosis at the Onset of Chordate Neurulation. *Dev Cell,* 37**,** 148-61.

OGURA, Y. & SASAKURA, Y. 2017. Emerging mechanisms regulating mitotic synchrony during animal embryogenesis. *Dev Growth Differ,* 59**,** 565-579.

OKAE, H., TOH, H., SATO, T., HIURA, H., TAKAHASHI, S., SHIRANE, K., KABAYAMA, Y., SUYAMA, M., SASAKI, H. & ARIMA, T. 2018. Derivation of Human Trophoblast Stem Cells. *Cell Stem Cell,* 22**,** 50-63 e6.

OKAMOTO, K., OKAZAWA, H., OKUDA, A., SAKAI, M., MURAMATSU, M. & HAMADA, H. 1990. A novel octamer binding transcription factor is differentially expressed in mouse embryonic cells. *Cell,* 60**,** 461-72.

PACA, A., SEGUIN, C. A., CLEMENTS, M., RYCZKO, M., ROSSANT, J., RODRIGUEZ, T. A. & KUNATH, T. 2012. BMP signaling induces visceral endoderm differentiation of XEN cells and parietal endoderm. *Dev Biol,* 361**,** 90-102.

PAN, X., CANG, X., DAN, S., LI, J., CHENG, J., KANG, B., DUAN, X., SHEN, B. & WANG, Y. J. 2016. Site-specific Disruption of the Oct4/Sox2 Protein Interaction Reveals Coordinated Mesendodermal Differentiation and the Epithelial-Mesenchymal Transition. *J Biol Chem,* 291**,** 18353-69.

PAUKLIN, S. & VALLIER, L. 2015. Activin/Nodal signalling in stem cells. *Development,* 142**,** 607-19.

PEREA-GOMEZ, A., MEILHAC, S. M., PIOTROWSKA-NITSCHE, K., GRAY, D., COLLIGNON, J. & ZERNICKA-GOETZ, M. 2007. Regionalization of the mouse visceral endoderm as the blastocyst transforms into the egg cylinder. *BMC Dev Biol,* 7**,** 96.

PEREA-GOMEZ, A., VELLA, F. D., SHAWLOT, W., OULAD-ABDELGHANI, M., CHAZAUD, C., MENO, C., PFISTER, V., CHEN, L., ROBERTSON, E., HAMADA, H., BEHRINGER, R. R. & ANG, S. L. 2002. Nodal antagonists in the anterior visceral endoderm prevent the formation of multiple primitive streaks. *Dev Cell,* 3**,** 745-56.

PEY, R., VIAL, C., SCHATTEN, G. & HAFNER, M. 1998. Increase of intracellular Ca2+ and relocation of E-cadherin during experimental decompaction of mouse embryos. *Proc Natl Acad Sci U S A,* 95**,** 12977-82.

PLACHTA, N., BOLLENBACH, T., PEASE, S., FRASER, S. E. & PANTAZIS, P. 2011. Oct4 kinetics predict cell lineage patterning in the early mammalian embryo. *Nat Cell Biol,* 13**,** 117-23.

QIAN, D., JONES, C., RZADZINSKA, A., MARK, S., ZHANG, X., STEEL, K. P., DAI, X. & CHEN, P. 2007. Wnt5a functions in planar cell polarity regulation in mice. *Dev Biol,* 306**,** 121-33.

QUINN, J., KUNATH, T. & ROSSANT, J. 2006. Mouse trophoblast stem cells. *Methods Mol Med,* 121**,** 125-48.

REDMER, T., DIECKE, S., GRIGORYAN, T., QUIROGA-NEGREIRA, A., BIRCHMEIER, W. & BESSER, D. 2011. E-cadherin is crucial for embryonic stem cell pluripotency and can replace OCT4 during somatic cell reprogramming. *EMBO Rep,* 12**,** 720-6.

REED, S. E., STALEY, E. M., MAYGINNES, J. P., PINTEL, D. J. & TULLIS, G. E. 2006. Transfection of mammalian cells using linear polyethylenimine is a simple and effective means of producing recombinant adeno-associated virus vectors. *J Virol Methods,* 138**,** 85-98.

SCHLAFKE, S. & ENDERS, A. C. 1963. Observations on the Fine Structure of the Rat Blastocyst. *J Anat,* 97**,** 353-60.

SCHOLER, H. R., BALLING, R., HATZOPOULOS, A. K., SUZUKI, N. & GRUSS, P. 1989. Octamer binding proteins confer transcriptional activity in early mouse embryogenesis. *EMBO J,* 8**,** 2551-7.

SHELDAHL, L. C., PARK, M., MALBON, C. C. & MOON, R. T. 1999. Protein kinase C is differentially stimulated by Wnt and Frizzled homologs in a G-protein-dependent manner. *Curr Biol,* 9**,** 695-8.

SHEN, M. M. 2007. Nodal signaling: developmental roles and regulation. *Development,* 134**,** 1023-34.

SIMONS, M. & MLODZIK, M. 2008. Planar cell polarity signaling: from fly development to human disease. *Annu Rev Genet,* 42**,** 517-40.

SINGH, A. M., HAMAZAKI, T., HANKOWSKI, K. E. & TERADA, N. 2007. A heterogeneous expression pattern for Nanog in embryonic stem cells. *Stem Cells,* 25**,** 2534-42.

SLUSARSKI, D. C., CORCES, V. G. & MOON, R. T. 1997. Interaction of Wnt and a Frizzled homologue triggers G-protein-linked phosphatidylinositol signalling. *Nature,* 390**,** 410-3.

SRIDHARAN, R., TCHIEU, J., MASON, M. J., YACHECHKO, R., KUOY, E., HORVATH, S., ZHOU, Q. & PLATH, K. 2009. Role of the murine reprogramming factors in the induction of pluripotency. *Cell,* 136**,** 364-77.

STAMOS, J. L. & WEIS, W. I. 2013. The beta-catenin destruction complex. *Cold Spring Harb Perspect Biol,* 5**,** a007898.

STEFANOVIC, S., ABBOUD, N., DESILETS, S., NURY, D., COWAN, C. & PUCEAT, M. 2009. Interplay of Oct4 with Sox2 and Sox17: a molecular switch from stem cell pluripotency to specifying a cardiac fate. *J Cell Biol,* 186**,** 665-73.

STEFANOVIC, S. & PUCEAT, M. 2007. Oct-3/4: not just a gatekeeper of pluripotency for embryonic stem cell, a cell fate instructor through a gene dosage effect. *Cell Cycle,* 6**,** 8-10.

STERNECKERT, J., HOING, S. & SCHOLER, H. R. 2012. Concise review: Oct4 and more: the reprogramming expressway. *Stem Cells,* 30**,** 15-21.

SUN, L., LIU, T., ZHANG, S., GUO, K. & LIU, Y. 2017. Oct4 induces EMT through LEF1/beta-catenin dependent WNT signaling pathway in hepatocellular carcinoma. *Oncol Lett,* 13**,** 2599-2606.

SZABO, E., RAMPALLI, S., RISUENO, R. M., SCHNERCH, A., MITCHELL, R., FIEBIG-COMYN, A., LEVADOUX-MARTIN, M. & BHATIA, M. 2010. Direct conversion of human fibroblasts to multilineage blood progenitors. *Nature,* 468**,** 521-6.

TAKADA, R., SATOMI, Y., KURATA, T., UENO, N., NORIOKA, S., KONDOH, H., TAKAO, T. & TAKADA, S. 2006. Monounsaturated fatty acid modification of Wnt protein: its role in Wnt secretion. *Dev Cell,* 11**,** 791-801.

TAKAHASHI, K. & YAMANAKA, S. 2006. Induction of pluripotent stem cells from mouse embryonic and adult fibroblast cultures by defined factors. *Cell,* 126**,** 663-76.

TANAKA, S., KUNATH, T., HADJANTONAKIS, A. K., NAGY, A. & ROSSANT, J. 1998. Promotion of trophoblast stem cell proliferation by FGF4. *Science,* 282**,** 2072-5.

THIER, M., WORSDORFER, P., LAKES, Y. B., GORRIS, R., HERMS, S., OPITZ, T., SEIFERLING, D., QUANDEL, T., HOFFMANN, P., NOTHEN, M. M., BRUSTLE, O. & EDENHOFER, F. 2012. Direct conversion of fibroblasts into stably expandable neural stem cells. *Cell Stem Cell,* 10**,** 473-9.

THOMSON, J. A., ITSKOVITZ-ELDOR, J., SHAPIRO, S. S., WAKNITZ, M. A., SWIERGIEL, J. J., MARSHALL, V. S. & JONES, J. M. 1998. Embryonic stem cell lines derived from human blastocysts. *Science,* 282**,** 1145-7.

URIST, M. R. 1965. Bone: formation by autoinduction. *Science,* 150**,** 893-9.

VALE, W., RIVIER, J., VAUGHAN, J., MCCLINTOCK, R., CORRIGAN, A., WOO, W., KARR, D. & SPIESS, J. 1986. Purification and characterization of an FSH releasing protein from porcine ovarian follicular fluid. *Nature,* 321**,** 776-9.

VANDER ARK, A., CAO, J. & LI, X. 2018. TGF-beta receptors: In and beyond TGF-beta signaling. *Cell Signal,* 52**,** 112-120.

VELKEY, J. M. & O'SHEA, K. S. 2003. Oct4 RNA interference induces trophectoderm differentiation in mouse embryonic stem cells. *Genesis,* 37**,** 18-24.

VELTMAAT, J. M., ORELIO, C. C., WARD-VAN OOSTWAARD, D., VAN ROOIJEN, M. A., MUMMERY, C. L. & DEFIZE, L. H. 2000. Snail is an immediate early target gene of parathyroid hormone related peptide signaling in parietal endoderm formation. *Int J Dev Biol,* 44**,** 297-307.

VERHEIJEN, M. H. & DEFIZE, L. H. 1999. Signals governing extraembryonic endoderm formation in the mouse: involvement of the type 1 parathyroid hormone-related peptide (PTHrP) receptor, p21Ras and cell adhesion molecules. *Int J Dev Biol,* 43**,** 711-21.

WALDRIP, W. R., BIKOFF, E. K., HOODLESS, P. A., WRANA, J. L. & ROBERTSON, E. J. 1998. Smad2 signaling in extraembryonic tissues determines anterior-posterior polarity of the early mouse embryo. *Cell,* 92**,** 797-808.

WALLINGFORD, J. B. & HABAS, R. 2005. The developmental biology of Dishevelled: an enigmatic protein governing cell fate and cell polarity. *Development,* 132**,** 4421-36.

WANG, P., HAYDEN, S. & MASUI, Y. 2000. Transition of the blastomere cell cycle from cell size-independent to size-dependent control at the midblastula stage in Xenopus laevis. *J Exp Zool,* 287**,** 128-44.

WATSON, A. J. & BARCROFT, L. C. 2001. Regulation of blastocyst formation. *Front Biosci,* 6**,** D708-30.

WEHRLI, M., DOUGAN, S. T., CALDWELL, K., O'KEEFE, L., SCHWARTZ, S., VAIZEL-OHAYON, D., SCHEJTER, E., TOMLINSON, A. & DINARDO, S. 2000. arrow encodes an LDL-receptor-related protein essential for Wingless signalling. *Nature,* 407**,** 527-30.

WILLERT, K., BROWN, J. D., DANENBERG, E., DUNCAN, A. W., WEISSMAN, I. L., REYA, T., YATES, J. R., 3RD & NUSSE, R. 2003. Wnt proteins are lipid-modified and can act as stem cell growth factors. *Nature,* 423**,** 448-52.

WODARZ, A. & NUSSE, R. 1998. Mechanisms of Wnt signaling in development. *Annu Rev Cell Dev Biol,* 14**,** 59-88.

WRANA, J. L., ATTISANO, L., WIESER, R., VENTURA, F. & MASSAGUE, J. 1994. Mechanism of activation of the TGF-beta receptor. *Nature,* 370**,** 341-7.

XIAO, L., YUAN, X. & SHARKIS, S. J. 2006. Activin A maintains self-renewal and regulates fibroblast growth factor, Wnt, and bone morphogenic protein pathways in human embryonic stem cells. *Stem Cells,* 24**,** 1476-86.

YAMANAKA, Y., LANNER, F. & ROSSANT, J. 2010. FGF signal-dependent segregation of primitive endoderm and epiblast in the mouse blastocyst. *Development,* 137**,** 715-24.

YANG, D. H., SMITH, E. R., ROLAND, I. H., SHENG, Z., HE, J., MARTIN, W. D., HAMILTON, T. C., LAMBETH, J. D. & XU, X. X. 2002. Disabled-2 is essential for endodermal cell positioning and structure formation during mouse embryogenesis. *Dev Biol,* 251**,** 27-44.

YANG, Y. & MLODZIK, M. 2015. Wnt-Frizzled/planar cell polarity signaling: cellular orientation by facing the wind (Wnt). *Annu Rev Cell Dev Biol,* 31**,** 623-46.

YANNARELLI, G., PACIENZA, N., MONTANARI, S., SANTA-CRUZ, D., VISWANATHAN, S. & KEATING, A. 2017. OCT4 expression mediates partial cardiomyocyte reprogramming of mesenchymal stromal cells. *PLoS One,* 12**,** e0189131.

YAO, S., CHEN, S., CLARK, J., HAO, E., BEATTIE, G. M., HAYEK, A. & DING, S. 2006. Long-term self-renewal and directed differentiation of human embryonic stem cells in chemically defined conditions. *Proc Natl Acad Sci U S A,* 103**,** 6907-12.

YEH, J. C., OTTE, L. A. & FRANGOS, J. A. 2008. Regulation of G protein-coupled receptor activities by the platelet-endothelial cell adhesion molecule, PECAM-1. *Biochemistry,* 47**,** 9029-39.

YEOM, Y. I., FUHRMANN, G., OVITT, C. E., BREHM, A., OHBO, K., GROSS, M., HUBNER, K. & SCHOLER, H. R. 1996. Germline regulatory element of Oct-4 specific for the totipotent cycle of embryonal cells. *Development,* 122**,** 881-94.

YING, L., MILLS, J. A., FRENCH, D. L. & GADUE, P. 2015. OCT4 Coordinates with WNT Signaling to Pre-pattern Chromatin at the SOX17 Locus during Human ES Cell Differentiation into Definitive Endoderm. *Stem Cell Reports,* 5**,** 490-8.

YOSHIMATSU, Y., LEE, Y. G., AKATSU, Y., TAGUCHI, L., SUZUKI, H. I., CUNHA, S. I., MARUYAMA, K., SUZUKI, Y., YAMAZAKI, T., KATSURA, A., OH, S. P., ZIMMERS, T. A., LEE, S. J., PIETRAS, K., KOH, G. Y., MIYAZONO, K. & WATABE, T. 2013. Bone morphogenetic protein-9 inhibits lymphatic vessel formation via activin receptor-like kinase 1 during development and cancer progression. *Proc Natl Acad Sci U S A,* 110**,** 18940-5.

YU, J., VODYANIK, M. A., SMUGA-OTTO, K., ANTOSIEWICZ-BOURGET, J., FRANE, J. L., TIAN, S., NIE, J., JONSDOTTIR, G. A., RUOTTI, V., STEWART, R., SLUKVIN, II & THOMSON, J. A. 2007. Induced pluripotent stem cell lines derived from human somatic cells. *Science,* 318**,** 1917-20.

ZEINEDDINE, D., PAPADIMOU, E., CHEBLI, K., GINESTE, M., LIU, J., GREY, C., THURIG, S., BEHFAR, A., WALLACE, V. A., SKERJANC, I. S. & PUCEAT, M. 2006. Oct-3/4 dose dependently regulates specification of embryonic stem cells toward a cardiac lineage and early heart development. *Dev Cell,* 11**,** 535-46.

ZENG, X., TAMAI, K., DOBLE, B., LI, S., HUANG, H., HABAS, R., OKAMURA, H., WOODGETT, J. & HE, X. 2005. A dual-kinase mechanism for Wnt co-receptor phosphorylation and activation. *Nature,* 438**,** 873-7.

ZHAO, W., JI, X., ZHANG, F., LI, L. & MA, L. 2012. Embryonic stem cell markers. *Molecules,* 17**,** 6196-236.

ZHONG, Y., CHOI, T., KIM, M., JUNG, K. H., CHAI, Y. G. & BINAS, B. 2018. Isolation of primitive mouse extraembryonic endoderm (pXEN) stem cell lines. *Stem Cell Res,* 30**,** 100-112.

ZOHRABIAN, V. M., FORZANI, B., CHAU, Z., MURALI, R. & JHANWAR-UNIYAL, M. 2009. Rho/ROCK and MAPK signaling pathways are involved in glioblastoma cell migration and proliferation. *Anticancer Res,* 29**,** 119-23.

ABBREVIATIONS

Abb.	Full-form	Abb.	Full-form
2,4DQ	2,4-diaminoquinazoline	MAPC	Multipotent adult progenitor cell
AA	Activin A	MAPK	Mitogen-activated protein kinase
BMP	Bone morphogenetic protein	MET	Mesenchymal-epithelial transition
cAMP	Cyclic adenosine monophosphate	mRNA	Messenger RNA
cDNA	Complementary DNA	MSC	Mesenchymal stem cell
CHIR	CHIRON99021	Niclo	Niclosamide
CMV	Cytomegalovirus	PB	PiggyBac
DAPI	4′, 6-diamidino-2-phenylindole	PBS	phosphate-buffered saline
DMEM	Dulbecco´s Modified Eagle´s Medium	PCR	Polymerase chain reaction
DNA	Deoxyribonucleic acid	PDGF	Platelet-derived growth factor
Dox	Doxycycline	PE	Parietal endoderm
EF	Elongation factor	PrE	Primitive endoderm
EGF	Epidermal growth factor	pXEN	Primitive extraembryonic endoderm
EMT	Epithelial-mesenchymal transition	qRT-PCR	Quantitative reverse transcription-PCR
Epi	Epiblast	Ri	Rock inhibitor
ESC	Embryonic stem cell	RNA	Ribonucleic acid
FACS	Fluorescence-activated cell sorting	RNAi	RNA interference
FGF	Fibroblast growth factor	Rock	Rho-associated protein kinase
FN	Fibronectin	rtTA	Reverse tetracycline-controlled transactivator
FSK	Forskolin	S.D.	Standard deviation
GOI	Gene of interest	siRNA	Small interfering RNA
GSK	Glycogen synthase kinase	tetO	Tetracycline operator
HD	High density	TF	Transcription factor
hiPSC	Human induced pluripotent stem cell	TGFβ	Transforming growth factor beta
ICM	Inner cell mass	TRE	Tetracycline-responsive element
LD	Low density	VE	Visceral endoderm
LIF	Leukemia inhibitory factor	WT	Wild type

%	Percentage	H	Hours
µg	Micrograms	kDA	Kilo Daltons
µl	Microliters	M	Mol
µm	Micrometers	mg	Milligrams
µM	Micromoles	min	Minutes
°C	Degree Celsius	mL	Milliliters
E	Embryonic day	mM	Millimoles
g	Gram or G-force	ng	Nanograms

ACKNOWLEDGEMENTS

First of all, I would like to thank my supervisor and advisor Prof. Andreas Kurtz and Dr. Manfred Gossen for patient guidance, constructive advice and giving me the excellent research environment and opportunity to carry out this study. I am also grateful to Prof. Bert Binas for his knowledge, encouragement and inspiration.

Many thanks to my colleagues, Quang Vinh Phan, Jörg Contzen, Iris Fischer, Imran Ullah, Dr. Nancy Lynne Mah, Thi Thanh Thao Ngo, Lilas Batool, Enrico Fritsche and my office mate Hanieh Moradian for assistance and pleasant work atmosphere. And I wish Dr. Chinmaya Mahapatrato a good luck for new life in Berlin.

I am especially grateful to Su-Jun Oh (favorite Korean in Berlin) and Dr. Krithika Hariharan (favorite Indian in Berlin). Without your invaluable support and help, this work would not have been possible.

I consider myself very lucky to have been blessed with friendships in my life. Byeongcheol Song, Choisun Cha, Gulhee Lee, Garam Kim, Janghyo Hong, and Suyeon Park. I really appreciate for being constantly around me. I promise to continue to warrant your faith in me.

I would like to give a special thanks to my aunt Heidi Bae and lovely cousins Lotte Wang and Martin Wang. I am really grateful for your help and support. This means a lot to me.

Last but certainly not least, I am very grateful to my family who always supported, encouraged and prayed for me.

CURRICULUM VITAE

This CV has been removed for online publication.

DECLARATION / Selbständigkeitserklärung

Hiermit erkläre ich, dass ich die vorliegende Arbeit selbständig angefertigt und nur die hier aufgeführten Hilfsmittel verwendet habe. Ich versichere, dass ich die Arbeit weder in dieser noch einer anderen Form bei einer anderen Prüfungsbehörde vorgelegt habe und mich nicht anderweitig für ein Promotionsverfahren zur Erlangung des Titels Dr. rer. nat. angemeldet oder diesen Titel bereits erworben habe.

Berlin, den ……16. Dec. 2019…… ……

Dongjun Han